Interfacial and material aspects of powders with relevance to pharmaceutical tableting performance

Maria Badal Tejedor

Doctoral Thesis
Kungliga Tekniska Högskolan
Stockolm, Sweden 2017

Copyright © Maria Badal Tejedor
All rights reserved

Paper I © 2017 American Chemical Society
Paper II © 2017 N/A
Paper III © 2015 Elsevier
Paper IV © 2017 N/A

TRITA-CHE Report 2017:14
ISSN 1654-1081
ISBN 978-91-7729-293-7

Akademisk avhandling som med tillstånd av KTH i Stockholm framlägges till offentlig granskning för avläggande av teknologie doktorsexamen fredagen den 24 mars kl. 10.00 i sal F3, KTH, Lindstedtsvägen 26, Stockholm.

Cover Illustration: False-color SEM micrograph of ibuprofen particles processed by Carlos Aliaga Badal.

Abstract

The most common forms of drug administration are oral solid forms; in particular tablets which are not only convenient to administer but also easy to manufacture. However, problems associated with the adhesion of the powders to the tableting tools are common, resulting in tablets with defects that no longer fulfill the quality control standards. This phenomenon is known as *sticking* and even though it has been well documented and studied, it remains poorly understood and difficult to predict. The many factors that contribute to good performance of the powders make the problems that arise during tablet compaction, such as sticking, difficult to solve.

The goal of this study is to establish a relationship between the properties measured at the nanoscale to the overall tablet mechanical properties, tablet performance and powder pre-processing induced modifications. A further goal is to relate these properties to pharmaceutical tablet manufacture. By using atomic force microscopy (AFM) we aim to develop an analytical method to characterize the mechanical and adhesive properties of the pharmaceutical powders at the nanoscale. Other methodologies such as scanning electron microscopy (SEM), thermal analyses (DSC, TGA) and tablet strength test were also used. The materials that provide the focus of this study are three commonly used excipients, a known sticky drug and magnesium stearate (MgSt). Two different approaches offered by AFM for characterization were employed: sharp tip imaging and colloidal probe force measurements. Nano-mechanical properties of the materials were evaluated with a sharp tip cantilever showing that higher adhesion correlates with higher tablet cohesion and that both are significantly affected by the presence of MgSt. AFM characterization of the particle surface mechanical properties at the nanoscale was also used to detect the crystallinity and amorphicity levels

of the materials. New approaches to presenting such data that take into account the particle heterogeneity are revealed. It was also possible to track the dynamics of surface recrystallization using such an approach. Adhesive interactions between a steel sphere and sticky and non-sticky powders were performed with the colloidal probe technique. Sticky materials presented a higher adhesion against the steel surface after repeated contacts, and reveal the mechanism of stickiness for the drug investigated.

This work thus contributes to the provision of predictability of the performance of formulations at an early stage of the development process.

Sammanfattning

De vanligaste formuleringarna för läkemedelsadministrering är orala fasta formuleringar, i synnerhet tabletter. Tabletter är praktiska att administrera och relativt enkla att tillverka, men problem på grund av vidhäftning (adhesion) av pulver till tabletteringsverktygen är vanliga. Det leder till defekta tabletter som inte längre uppfyller kvalitetskraven. Fenomenet som är känt som *sticking* är väl dokumenterat och studerat, men förståelsen för fenomenet är otillräcklig och det är svårt att förutsäga när det kommer att uppstå. Eftersom det är många faktorer som påverkar pulvrens egenskaper, är det svårt att lösa de problem, t ex sticking, som uppstår under tabletteringen.

Målet med studien är att klarlägga förhållandet mellan egenskaper på nanonivå och tablettens mekaniska egenskaper, funktionalitet och förändringar som orsakas av processning av pulvret. Ett ytterligare mål är att relatera dessa egenskaper till tillverkning av läkemedelstabletter. För att kunna analysera pulvrens mekaniska egenskaper och vidhäftningsbeteende på nanonivå utvecklades en metod baserad på atomkraftsmikroskopi (AFM). Andra metoder, t.ex. svepelektronmikroskopi (SEM), termisk analys (differentiell svepkalorimetri (DSC), termogravimetrisk analys (TGA)) och test av tablettstyrka användes också. De material som är i fokus för studien är tre vanliga hjälpämnen (excipienter), ett läkemedel känt för sin klibbighet (ibuprofen) och magnesiumstearat (MgSt). Två AFM-metodiker för karaktärisering användes: *sharp tip imaging* (avbildning med en vass spets) och *colloidal probe* (kolloidal sond) kraftmätningar. Materialens nanomekaniska egenskaper, som utvärderades med en mikrobalk

(cantilever) med vass spets, visar att högre adhesion korrelerar med högre tablettkohesion (sammanhållande kraft) och att båda är signifikant påverkade av närvaron av MgSt. AFM-karakterisering av partikelytornas mekaniska egenskaper på nanonivå användes också för att detektera kristallinitets- och amorficitetsnivåerna i materialens yta och hur dessa egenskaper på verkades av malning. Studien visar nya sätt att presentera sådana data så att hänsyn tas till partikelheterogeniteten. Det var också möjligt att följa ytans återkristallisation över tid med detta tillvägagångssätt. Mätningar av den adhesiva växelverkan mellan en stålsfär och klibbiga eller icke-klibbiga pulver utfördes med colloidal probe tekniken. Klibbiga material gav en högre vidhäftning mot stålytan efter upprepad kontakt, och avslöjar därmed mekanismen bakom sticking hos det studerade läkemedlet. Studien bidrar till att skapa möjlighet att förutsäga formuleringars funktionalitet på ett tidigt skede i utvecklingsprocessen.

List of papers

I. Determination of interfacial amorphicity in functional powders

Maria Badal Tejedor, Niklas Nordgren, Michael Schuleit, Samaneh Pazesh, Göran Alderborn, Anna Millqvist-Fureby, Mark W. Rutland.
Langmuir, 2017, 33 (4), 920-926

II. Milling induced amorphisation and its effects on α-lactose monohydrate at the nanoscale

Maria Badal Tejedor, Niklas Nordgren, Michael Schuleit, Samaneh Pazesh, Mark W. Rutland, Göran Alderborn, Anna Millqvist-Fureby.
Manuscript

III. Tablet mechanics depend on nano and micro scale adhesion, lubrication and structure

Maria Badal Tejedor, Niklas Nordgren, Michael Schuleit, Anna Millqvist-Fureby, Mark W. Rutland.
International Journal of Pharmaceutics, 2015, 486 (1-2), 315-323

IV. AFM colloidal probe measurements to mimic punch-particle surface interactions during tableting

Maria Badal Tejedor, Niklas Nordgren, Michael Schuleit, Anna Millqvist-Fureby, Mark W. Rutland.
Manuscript

The author’s contribution to the papers:

I. All the experimental work and major part of the interpretation of the results and preparation of the manuscript.

II. All the experimental work and major part of the interpretation of the results and preparation of the manuscript.

III. All the experimental work and major part of the interpretation of the results and preparation of the manuscript.

IV. All the experimental work and major part of the interpretation of the results and preparation of the manuscript.

Abbreviations

AFM	atomic force microscopy
AMD	adhesion minimum depth
API	active pharmaceutical ingredient
DSC	differential scanning calorimetry
MCC	microcrystalline cellulose
MgSt	magnesium stearate
SEM	scanning electron microscopy
TGA	thermogravimetric analysis
QNM	quantitative nanomechanical mapping

Table of contents

To my parents,
Dionisio and Manuela

1 Introduction

1.1 Solid dosage forms

The preferred route for drug delivery is oral administration of a solid form. Solids are the most convenient dosage form to prescribe to patients and their manufacturing process is the most cost-effective [1]. Pharmaceutical solid forms comprise tablets and capsules. The most common form is the tablet, to be swallowed followed by disintegration and dissolution in the gastrointestinal tract. However, there are a variety of tablet types, designed to be swallowed or chewed and then disintegrated or effervescently dissolved in water prior to intake to suit different products and patient populations. The means by which the tablets will be disintegrated and dissolved, sets the requirements for the formulation and manufacturing [2].

The mechanical and chemical properties of the active pharmaceutical ingredient (API, also referred to in the thesis as “drug”) are important for tablet manufacturing. The API in powder form is usually mixed with powdered excipients to enable subsequent compressive formation of tablets of appropriate size. The excipient choice is also designed to control powder flowability, dose uniformity, compactability, long term stability, dissolution and subsequent drug release. The excipients are selected to compensate for the (generally) poor mechanical properties of the API, thus facilitating the manufacture of strong enough tablets with homogenous characteristics. Thus the physicochemical and mechanical attributes of the materials that comprise the tablet will not only affect the handling and performance of the powder during tableting, but also have a

great impact on the quality of the finished tablet and its oral administration [3, 4].
However, the powder properties may change during processing due to exposure to heat, humidity, solvents and mechanical stress. Powder modifications could not only affect the quality of the final product but may also result in manufacturing problems that delay and interrupt the tableting manufacturing [5]. Thus, it is essential to control and understand the properties of the powders to assure a reproducible and consistent performance of the blend [6, 7].

To enable more accurate prediction of the powder performance in the early stages of process design and pre-formulation, better understanding of the chemical and mechanical properties of the powders is needed [8]. Various analytical methods are used to measure and control the properties of the powders at different processing stages. It is important to address both surface and bulk characterization since they impact particle-particle and particle-tool adhesion, which affect powder flow and tableting performance.

1.2 Tablet manufacturing

1.2.1 Process operations

Prior to tableting there is a multi-stage process that involves different unit operations (Figure 1). The ultimate goal is to obtain a powder with the optimal properties in flowability and compressibility in order to produce consistent tablets in the tableting operation unit.

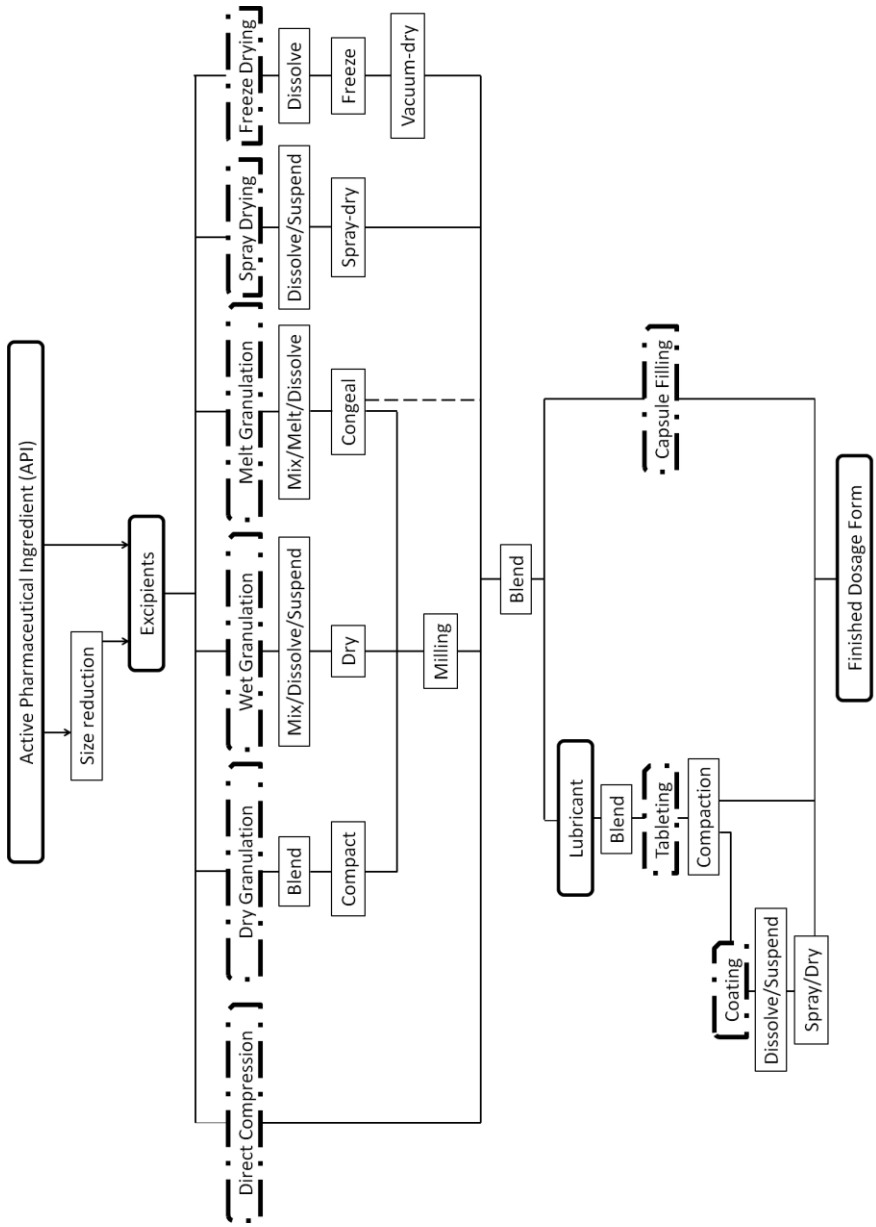

Figure 1. Oral solid dosage preparation process.

1.2.1.1 Size reduction/milling

The purpose of reducing the size of the particles of the powder is to obtain a more homogenous particle size distribution of the powder blend. A narrow distribution of the particles size and similar particle shapes prevents segregation problems and improves flow properties. This contributes to a uniform distribution of the drug during blending and die or capsule filling and decreases the energy input for powder handling during manufacturing. In addition, the enlargement of the surface area tends to increase the dissolution rate and consequent absorption of the drug into the body. Milling is one of the most common operations to perform particle size reduction. It usually involves a certain level of mechanical stress which can favor polymorphic transitions, dehydration or vitrification. These modifications induced during milling will be very dependent on the mechanical properties of the original solid material and the milling conditions [7-9].

1.2.1.2 Granulation

Granulation is a particle size enlargement process where particles are agglomerated to form larger units known as granules. Granulation is performed in order to overcome segregation problems of a mixture of different components due to density and particle size variations. It ensures a proper distribution of the drug in the granules with an increased bulk density. The size and shape of the granules are chosen to optimize the flowability of the powder and improve the compaction characteristics. Granulation is used to modify the surface properties in case of high cohesiveness of the powders. Further benefits include: i) reduction of the toxicity of a drug due to dilution in the granule matrix, ii) protection of

hygroscopic materials from water uptake and iii) densification of the mixture for more effective storage [8, 10]. There are different types of granulation processes which can be divided into “wet methods” and “dry methods”. They are described below:

Wet granulation

During wet granulation a liquid is used to agglomerate the powder. The liquid is usually incorporated into the agitated powder bed, where the granules are formed and subsequently dried to remove the solvent when the granulation process is finished. Solvent or heat sensitive drug substances are not suitable for wet granulation. Phase transformations of the drug are still likely to occur depending on the solubility of the drug in the liquid and the applied drying conditions [7, 11].

Dry granulation

Agglomeration of the powder mixture in dry granulation is achieved with two rotating rollers. The resulting material is in the form of ribbons which are milled under low shear stress to produce granules. This granulation process is adequate for moisture and temperature sensitive ingredients. Nevertheless, hardening of the material through dry granulation can reduce its compactability. Thus a binder is usually added to the powder mixture in order to compensate for the hardening and to improve the mechanical properties of the produced granules. Solid transformation mechanisms may also occur due to the mechanical stress applied during processing [7, 12, 13].

Melt granulation

In the melt granulation process the drug solubilizes in the partially or completely molten phase of the excipients. The melted material acts as a binder, dispersing the drug molecules, which is known to improve bioavailability. The sensitivity of the drug to temperature should be considered due to the high temperatures used in this process. Afterwards the molten phase is sprayed or extruded and subsequently cooled down. During the cooling stage the characteristics of the particles such as particle size and crystalline or amorphous phase formation can be controlled by the cooling rate [14, 15].

1.2.1.3 Spray drying

Spray drying is used to protect the drug by encapsulation or to form a controlled release system by coating of the drug. The spray-dried particles are obtained by droplet formation from a solution, suspension or emulsion where the drug or excipient is highly dispersed. The liquid droplets are sprayed into a chamber where a stream of hot air rapidly evaporates the solvent and particles are formed. The formation of a crystalline or amorphous phase of the spray dried drug or excipient upon drying depends on the nature of the material [16, 17]. Spray dried lactose for example is used in this work and it is considered completely amorphous.

1.2.1.4 Freeze drying

Freeze drying is an expensive process and is thus restricted to sensitive and/or valuable products. The dried material is obtained by sublimation of the ice in a frozen solution or dispersion. It can be obtained in

amorphous, crystalline or partially crystalline states and it is highly porous with low density. This is advantageous to improve solubility and reduce dissolution time even though it facilitates water uptake. Freeze drying is used when the drug is sensitive to temperature and cannot be dried by any other means [8, 18, 19].

1.2.1.5 Blending

An even distribution is required when there is more than one component in the powder or liquid mixture to assure a consistent drug content, especially when the drug load is low. The blending operation is performed before granulation in order to mix the drug with the solid materials or disperse it with the key components in the liquid that will be processed. Additional excipients such as lubricants, glidants and disintegrants are mixed with the granules prior to tableting at different blending times [20, 21].

1.2.1.6 Tableting

At the tableting stage the drug and excipients, either in powder form or already incorporated into the prepared granules, are pressed to form a tablet. Normally tablets are pressed in a rotatory tablet press that produces a large number of tablets per minute (10.000-20.000 tablets/min approx.) [22]. The tablets should fulfill certain quality attributes such as correct drug dosage, neat shape appearance, consistent weight and size, sufficient mechanical strength, product lifetime stability and user safety requirements [23]. In the next section the tableting process is described in more detail.

1.2.1.7 Coating

A film coating is usually applied to the exterior of the tablet. The coating confers the benefits of improved appearance, protection, taste masking, facilitates swallowing, color distinction and/or modified drug release. The coating layer is usually created by spraying polymer solution onto the tablets in a rotating drum. The solvent is removed under rapid drying conditions to avoid liquid-tablet interactions, leaving a thin layer of coating around the tablet [24-26].

1.2.2 Tableting

In the tableting process the powder blend is mechanically processed in order to transform the powder into a compact tablet. During compaction the powders are brought into close proximity so that the separation between particles approaches molecular scales. The intimate contact between the particles is achieved with a high pressure impact, generating a single solid unit.

The tablet formation process comprises three main stages as depicted in Figure 2:

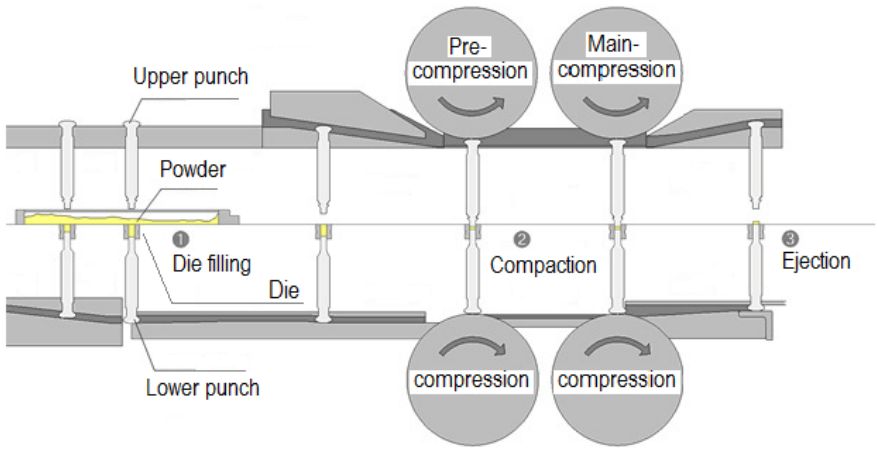

Figure 2. Tableting process flow. Adapted from [27].

First, the cavity of the die is normally filled by gravitational flow of the powder from a hopper (Fig. 2. ①). Later, a pre-compression force is applied after the upper punch enters into the die followed by the impact of the main compression force (Fig. 2. ②). The pre-compression force is typically of 1 kN and compression forces may vary within the range of 6 to 10 kN. The force can be applied in both directions if the lower punch moves upwards or it can be unidirectional when the lower punch is stationary. The contact times between the punch and the tablet depend on the tableting speed and are typically between 3 and 6 ms. During ejection the upper punch is displaced upwards and the lower punch is moved up towards the edge of the die, pushing the tablet unit out of the cavity (Fig. 2. ③) [28].

1.2.3 Problems associated with tableting

Tableting is a complex process where the physicochemical characteristics of the powders that constitute the blend play a very important role in the quality of the final product. Several technical problems are likely to occur if the powders have not been pre-conditioned to achieve the desired material properties and assure good performance at the tableting stage. Poor tablet quality and tabletability problems are discussed below:

Weight variation between the pressed tablet units concerns the equal distribution of the drug among the tablets. Weight variation is mainly due to poor flow of the powders resulting in inconsistent filling of the die. Weight variation is also attributed to powder segregation in the hopper prior compaction which is mostly influenced by particle size distribution and particle shape [28].

Tablet strength is a parameter that states the level of compactability of the materials. The fulfillment of certain requirements for tablet strength is a must to withstand potential stresses during any coating process, packing and distribution. How strongly the powders bind together, and the nature of the materials affects the disintegration and subsequent dissolution of the tablets, and consequently the release of the active substance. Tableting parameters such as applied force and tableting speed have a direct effect on the level of tablet strength. Material related properties such as powder binding, mechanical behavior of the powders under compaction or formulation influence the strength of the tablets [29].

Capping and lamination are noted as the separation of the tablet in layers; capping being more specific to the split of the top layer of the tablet (see Fig.3). This problem usually arises after compaction during the ejection process and it can be due to high friction forces, material elastic recovery, uneven distribution of the stress or stress concentration [30, 31]. The shape of the tooling and tableting force can control the distribution of the stress while a limited increase in lubrication seems to positively affect compaction, as does the use of excipients with good compactibility properties [32].

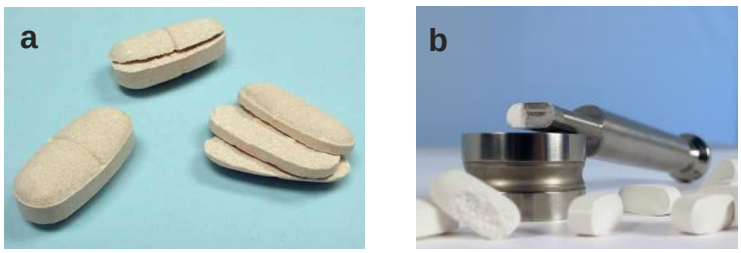

Figure 3. Examples of (a) capping and lamination [33] (b) sticking and picking [34].

Sticking and picking is a commonly encountered issue during tablet manufacturing that affects tablet quality and productivity. Sticking refers to the phenomenon of adhesion of the powders from the formulation blend to the surface of the tablet punches during compression. Picking is more specific to film formation by buildup of a particle layer on the punch that adheres to the tablet surface removing a fragment of the pressed tablet under decompression (see Figure 3). There are many factors that may contribute to trigger this complex phenomenon and it is still not well understood. The powder surface chemistry dominates both

particle-particle and particle-tools interactions in the latter case in combination with the surface chemistry of the tool surface. Thus it is important to balance the adhesion forces between the tools and the powder bed and the forces within the powder bed. Compactability of the powders as well as tableting process parameters help to promote the binding of the particles to each other avoiding sticking and picking. Many studies point to the active ingredient as being responsible though the evidence for this is not completely compelling. By changing the formulation components and their relative compositions it is sometimes possible to overcome the problem [28]. It is also possible to influence the extent of sticking and picking by tool design, choice of tool coating material and lubrication of the tools.

1.2.4 Pharmaceutical excipients

The main role of pharmaceutical excipients is to facilitate the manufacturing process and promote suitable product properties. The active pharmaceutical ingredient is thus protected in the formulation matrix that guarantees the quality of the tablet [35]. The total weight of excipients present in the tablet can be up to 90%, depending on the dosage of the drug. Although they are considered as inert ingredients having no pharmaceutical effect, they have the ability to influence stability, safety, release and bioavailability of the drug. Excipients can be categorized according to their function as in Table 1. (Note that some belong to more than one category and may fulfil several functions simultaneously [3, 36]).

Table 1. Commonly used excipients in tableting [2, 3, 5, 35].

Excipient category	Examples
Diluents	Lactose, mannitol, sorbitol, sucrose, microcrystalline cellulose, calcium salts, glucose, sodium sulfate, dextrin
Binders	Sugars, starch, gelatin, cellulose derivatives, polyvinyl pyrrolidone
Lubricants	Stearic acid, magnesium stearate, talc, sodium lauryl sulfate, sodium stearyl fumarate
Glidants	Silica, magnesium stearate, talc
Disintegrants	Crospovidone,starch, sodium starch gycolate, croscaramellose sodium, cellulose derivatives
Colorants	Natural pigments and synthetic dyes
Flavor modifiers	Mannitol, aspartame

Diluents

Diluents are excipients that provide bulk to the formulation and facilitate the handling. Preferably, diluents are inert, non-hygroscopic and hydrophilic. When they are used in direct compression, diluents are often pre-conditioned to improve flowability and compactibility. Many of the most commonly used diluents act also as fillers and binders [3].

Binders

Binders are added in the powder blend to increase adhesion between the powders and promote binding during compaction increasing the mechanical strength of the tablet. In direct compaction binders should have a high compactibility creating a large surface area to facilitate particle-particle bonding; they are therefore typically plastically

deformable. In the case of wet granulation binders are used in a solution. They are sprayed or poured into the powder blend and they homogeneously distribute improving the agglomeration of the particles to aid the granule formation. Larger size particles are obtained from granulation which directly improves flowability of the blend [3, 37].

Lubricants

Lubricants are used to reduce the friction between the die and the tablet upon ejection. An adverse effect of lubrication is the reduction of the adhesion within the powder bed because of the characteristically low shear strength. Lubricants are added prior to tableting in very low concentrations (less than 3%) and care is taken to not over mix the powder blend which would otherwise result in a thin film on all the particle surfaces. Such extensive mixing of the lubricant into the formulation could further affect dissolution and disintegration rates due to its hydrophobic nature. This is a more critical issue for the most commonly used lubricant, magnesium stearate, compared to other lubricants, due to its high hydrophobicity. Hydrophilic lubricants are not as efficient in lubrication even though they do not affect tablet dissolution and disintegration properties [3, 35].

Glidants

Flow properties of the powder blend are improved by addition of glidants. Glidants are very fine powders with a very low adhesive potential which helps to reduce friction. However, they share the same drawback as lubricants in that they negatively affect tablet strength by

reducing internal tablet adhesion forces. Some excipients act both as glidants and as lubricants.

Disintegrants

The main purpose of the disintegrants is to contribute to a rapid dissolution of the tablet in aqueous media. If the excipients present in the formulation are not water soluble or if rapid disintegration of the tablet is desired, then a disintegrant is used in the formulation. Disintegrants swell rapidly in the presence of water and employ a wicking mechanism when the tablet comes into contact with an aqueous fluid. This facilitates the disintegration and increasing the surface area for rapid tablet dissolution and consequent drug release [3, 5].

Colorants

The incorporation of colorants into the formulation is not always needed. The colorants are used for identification and to increase acceptability of the medication by the patients. They may also function as protective agents for light sensitive drugs and mask possible color changes of the powder blend, thus providing a homogeneous appearance to the batch. While they can be water soluble, the majority of colorants are not. Regulations are strict concerning this kind of excipient for toxicological reasons.[38]

Flavor modifiers

Most drugs have an unpleasant taste that is not easily tolerated by patients, especially young children. Due to stability reasons, flavors are not a formulation component that is easy to handle, though safety

considerations are usually mild since they are usually sourced from the food and drink industry and of natural origin. However, potential risks are related to the apparent similarities of the drug with confectionery, which could diminish patient awareness of the actual potency of the drug [8, 38].

1.2.5 Compaction mechanisms

The consolidation of the particulate systems occurs during compaction (Figure 4). Closer packing is initially achieved by bulk volume reduction. Particles rearrange by size and shape filling up the voids to reduce the air phase in the particulate system. When the particles are no longer able to rotate under the applied pressure, densification of the powder bed begins. Agglomerates and granules start to break before the primary particles start to deform. The particles deform as the pressure is increased, bringing them into closer proximity and interparticle bonds can thus be established. The type of deformation that the particles undergo depends on the physical properties of the material. Plastically deformable materials undergo a permanent deformation whereas elastic deformable components experience a reversible size reduction and shape change. The type and extent of the deformation depends not only on the mechanical properties of the material but also on the speed of the compression and the applied load; which is known as the viscoelastic behavior of the powder components. At higher loads, when the particles are no longer deformable they fracture. The critical stress value at which fracture occurs varies for different materials. Brittle materials experience more extensive fragmentation than deformable materials though typically there is a continuum between these extremes [8, 39].

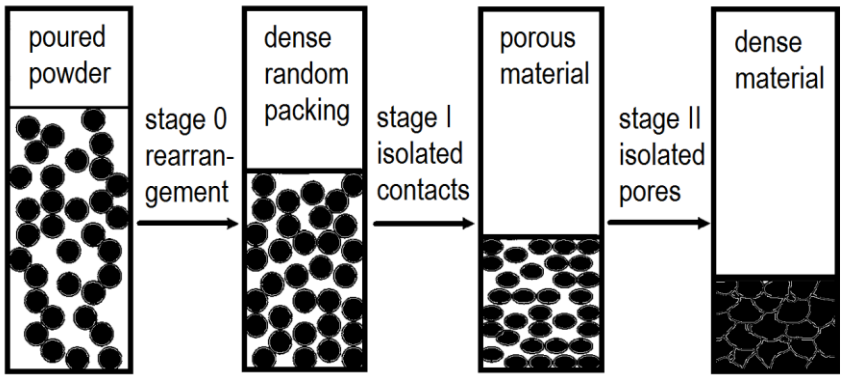

Figure 4. Compaction stages. Adapted from [28].

The manner in which the materials respond to compaction affects the properties of the tablet. The increase of the particle-particle contact area under compaction due to fracture and/or deformation promotes the formation of "bonds" between them. The contact area increase is irreversible in the case of plastic deformation. Prior to the onset of permanent deformation, any applied stress is elastically stored and the material returns to its initial shape if the compressive load is removed. Such elastic deformation does not facilitate bond formation, but rather creates stress points in the tablet structure due to material recovery when the compression force is removed. Fracture of the material under pressure reduces the particle size, increases the number of contact points and creates fresh particle surfaces [28, 40-42].

Processing conditions strongly influence the compaction mechanisms. Tableting speed, applied force and ejection force affect the mechanical response of the processed powder. The degree of fragmentation or the extent of the deformation of the materials will be determined by the

applied force under compression. The extent of adhesion between the tools and the materials determines the force needed to eject the tablet, which can potentially increase the stress in the tablet structure due to lateral friction forces that occur during the ejection stage [42, 43].

1.3 Adhesion mechanisms of pharmaceutical powders

The transformation of the dispensed powder into a tablet occurs during compaction due to interparticulate bonding at the contacts between particles. The dominant bonding mechanisms that hold the particles together upon removal of the applied load are solid bridges, mechanical interlocking (see Figure 5) and intermolecular forces. *Solid bridges* are formed when two regions come into contact at separations corresponding to molecular distances, creating a continuous solid phase. These are considered very strong bonds and also permit diffusion of molecules across the contact. An increase of the molecular mobility (due to melting, glass-rubber transitions or material solubility under local conditions of high pressure and heating) thus aids the formation of solid bridges. A physical contribution to binding particles together is *mechanical interlocking*. It depends on the shape and surface structure of the particles which might facilitate their remaining hooked together when the load is released. In contrast, *intermolecular forces* are present both between the particles and between the particles and the tools. Particle-tool surface interactions govern the processability of the powders during pre-conditioning and tableting operations. Both particle-particle and particle-tool adhesion mechanisms are important for the handling of the powders and the manufacture of a uniform tablet unit. Intermolecular forces

typically act over short distances binding particles together by attractive forces that include van der Waals forces, the strength of which decays with distance and depends on the dielectric properties of the materials. The bonding created through such intermolecular forces is relatively weak at individual contacts, but collectively significant in the overall contribution to the system. Electrostatic forces may also arise during dry processing resulting from the static charge of the particles. The force generated can be locally attractive or repulsive depending on the sign of the charge. However, these charges generally neutralize quickly over time due to the high diffusivity of the charge [4, 37, 39].

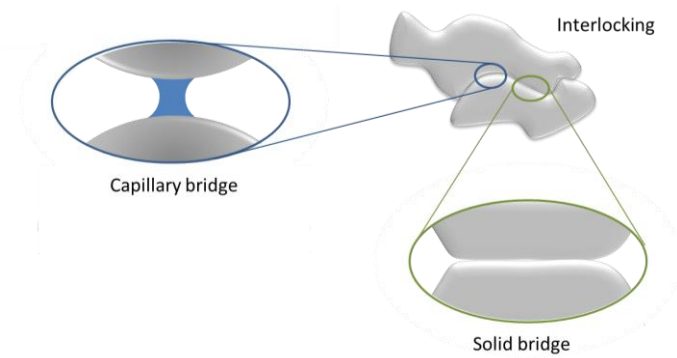

Figure 5. Some particle bonding mechanisms.

Another type of adhesive force is the *capillary force* which arises from the formation of capillary bridges between surfaces (see Figure 5). The liquid leading to the formation of capillary bridges can originate from moisture trapped in the structure of the hydrophilic materials or from the ambient humidity that condenses between two surfaces. Hydrophilic, *i.e.* more polar, surfaces facilitate the formation of liquid bridges due to the good wetting properties for water. The deformability of the liquid bridge means that very large displacements are required to separate the

particles and the range of the force is thus rather large compared to van der Waals forces [44, 45]. The presence of a certain amount of interstitial water can act as a binder, increase plastic deformation and reduce friction forces.

The surface energy is largely responsible for the strength of the adhesion and the affinity towards moisture. The surface energy is a characteristic of each material but can be modified during processing of the powders; that of a crystalline powder can for example be controlled through the crystallization process. Different crystallographic conformations (polymorphs and crystal habits) of the same molecule have been reported when the crystallization process is performed in different solvents. This leads to different orientations of the molecule in the crystal faces varying the surface energy of the particles and their mechanical behaviour [46]. Milling is a common pre-conditioning stage that involves high energy. The mechanical stress that the powders are exposed to during milling may induce both charge transfer and modifications of the surface structure of the particles. Shear forces contribute to the disruption of the molecular structure or temperature increase, affecting the overall surface energy and mechanical properties of the processed powders. Such changes in the surface energy and mechanical properties lead to changes in surface interactions, which in turn influence the performance of the powder blend [41, 47, 48].

The adhesion strength between surfaces is influenced by their morphological characteristics. Particle size, shape and surface roughness limit the contact area and proximity between two surfaces which are determinant factors for the adhesive force. Processing parameters such as

compaction load can sometimes improve the adhesion strength by increasing the contact area as described above [48].

As mentioned above, a lubricant is often added to the tablet formulation to prevent adhesion of the powders to the tools and minimize the die wall friction. Even though it is added as a very low amount it has a strong impact on tablet properties since the lubricant to some extent covers the particle surfaces and interferes with the particle binding mechanisms. Fracturing of the particles is especially important to overcome the coating effect of the lubricant and maintain the mechanical properties of the tablet [28, 39].

It is desirable that the powders develop adhesive forces within the blend which overcome the powder-tool adhesion forces upon unloading and thus avoid tablet defects due to sticking or picking [49].

1.3.1 Measuring adhesion with AFM

Particle-particle and particle-tool interactions govern the powder behavior during the majority of process operations; therefore the use of appropriate analytical tools is of relevance. Atomic force microscopy (AFM) offers the possibility to investigate the nature of these interactions [48]. AFM also allows surface topography evaluation at high resolution with simultaneous evaluation of the surface mechanical properties of the substrate and adhesive interactions between the substrate and the probe [50]. AFM has previously been applied to pharmaceutical systems, however the multiple possibilities that the technique offers have still not been fully exploited for the study of these systems [51-54].

1.4 Scope of the thesis

Picking and sticking are still common problems occurring during pharmaceutical tablet production despite having been recognized and reported on for some time. There is thus a need for a better understanding of the tableting process as well as for analytical tools to predict the material performance.

In this work we aim to better understand the adhesive interactions of particles that govern not only the tableting process but also the majority of the pre-processing operations during tablet manufacturing. The approach involves different analytical tools with a special focus on atomic force microscopy (AFM) which has a great potential to measure interfacial interactions and surface material properties at the nanoscale. The present work aims to develop analytical protocols with AFM that complement the material characterization toolbox.

In order to add value to the information gathered from the nanoscale material characterization and measured surface interactions, a relationship between the properties measured at the nanoscale to the overall tablet mechanical properties will be established. Therefore mechanical and chemical bulk properties of the powders were simultaneously evaluated with tablet tensile strength test, differential scanning calorimetry (DSC) and thermogravimetrical analysis (TGA). Visual examination of the powders and tablets was performed with scanning electron microscopy (SEM).

2 Materials

2.1 Excipients

Microcrystalline Cellulose

Microcrystalline cellulose (MCC) is widely used in tablet manufacture. It is an easily compressible excipient with good binding properties [55]. The cellulose polymer chain is formed of glucose units bound together. The three-dimensional conformation of the chains results in a partially crystalline structure. The polymer chains of cellulose are extracted from wood pulp, followed by purification to isolate the partially crystalline regions.

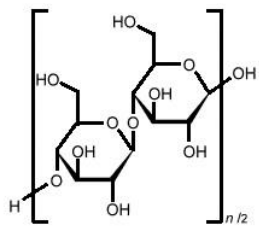

Figure 6. MCC chemical structure.

The microcrystalline cellulose (Cellulose Microcr. PH200, FMC) used in this work was a free flowing white powder of particle size on the order of 200 μm.

Lactose

Lactose is a common excipient used as filler in tableting. The lactose molecule is a disaccharide formed by galactose and glucose. It is obtained from the dairy industry as a by-product. Temperature control during the crystallization process can influence the mutarotation of the lactose

towards the so called α- or β- isomeric forms. Thus, crystalline lactose exists in different conformations. The α-lactose monohydrate is the most used lactose form which incorporates one water molecule per molecule of lactose in the crystal structure. Crystalline anhydrous α-lactose, stable and unstable (hygroscopic) form, are also known well as β-lactose, which does not contain water within its crystal structure [56]. Amorphous lactose displays random arrangement of the lactose molecules and is usually obtained by spray drying. Both α- and β-lactose are present in amorphous spray dried lactose. The hygroscopic nature of amorphous lactose facilitates recrystallization in the presence of a certain level of ambient moisture [57] (the dynamics of which are studied in paper 1).

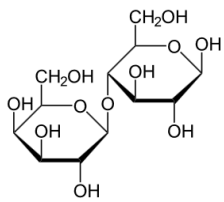

Figure 7. Lactose chemical structure.

The α-lactose monohydrate (DFE Pharma, Veghel, Netherlands) used in this work presents regular shaped crystals and a wide range of particle sizes (10-200 μm). Industrial spray dried lactose (Meggle, Germany) was also used. This product consists of lactose monohydrate crystals embedded in a matrix of amorphous lactose.

Mannitol

Mannitol is a commonly used filler and sweetener in tablet manufacture. It is classified as a sugar alcohol and it is derived from fructose. Sugar

alcohols have one –OH group attached to each carbon and they exist as a chain, unlike sugars, that tend to form rings.

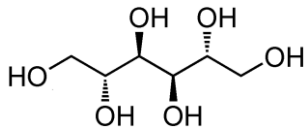

Figure 8. Mannitol chemical structure.

The mannitol (Mannitol 200SD, Merck) used in this work was in a powder form with oval shaped particles of approximately 200 μm in their largest dimension.

Magnesium Stearate (MgSt)

Magnesium stearate is incorporated in very low amounts (0.5-3%) in the tablet formulation as a lubricant. It is usually obtained from the reaction of sodium stearate with magnesium salts. MgSt is insoluble in water and is provided as a white powder of poor flow properties; the particles show a "plate-like" morphology.

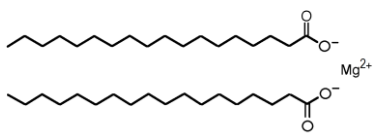

Figure 9. Magnesium Stearate chemical structure.

Magnesium stearate (Magnesium stearate Pharma, FACI) was used in this study in combination either with other excipients or a drug substance.

2.2 Drugs

Ibuprofen

Ibuprofen is an anti-inflammatory and analgesic drug and it is known for its sticking propensity upon tableting [58]. Therefore it is commonly used to study sticking phenomena. It displays optical activity in its two isomeric forms R-ibuprofen and S-ibuprofen; of which the latter is the most biologically active. It has a low melting point of 73°C and low water solubility (21 mg/l at 25°C). The water solubility improves at higher temperature and it is also soluble in many organic solvents.

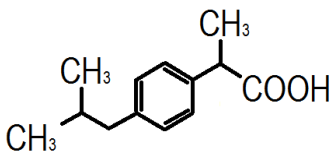

Figure 10. Ibuprofen chemical structure.

Ibuprofen (Ibuprofen 70, BASF) is used in this work. The drug was delivered as a white powder consisting of tetrahedrally shaped crystals.

2.3 Sample preparation

2.3.1 Spray drying

Spray drying is used extensively in order to dry a product from a solution. The lactose solution was dried using a laboratory spray dryer built at SP, Technical Research Institute of Sweden. The dryer consists of a jacketed two-fluid nozzle in co-current operation mode. In order to achieve droplet formation the feed solution is pumped at a flow rate of 5 ml/min through the 2 mm orifice of the nozzle using pressurized air. The droplets are

suspended in a 0.8 m^3/min air current inside the drying chamber (0.75 x 0.15 m). The inlet and outlet temperatures of the air flow are 150°C and 75°C respectively, and the jacket temperature is kept constant at 20°C. The collection of the powder is performed with a cyclone in which the powder enters and deposits gravitationally inside an attached vessel located below the cyclone.

The obtained amorphous lactose powder is then stored at room temperature in a desiccator at 0-5% relative humidity to avoid recrystallization of the lactose during storage.

2.3.2 Milling

Particle size reduction of α-lactose monohydrate was performed by collaborators at Uppsala University in a planetary ball mill (PM 100, Retsch, Germany). The ball mill consists of a milling jar of 12 cm^3 volume containing 50 balls of stainless steel each with a diameter of 5 mm. The rotation speed was set to 400 rpm and the milling times were 1 and 20 hours. The mill was sealed under the controlled ambient conditions of 30±5% relative humidity and 25±5 °C. However, in order to diffuse additional heat generated inside the chamber during the milling process, 5 minute pauses were made after every 20 minutes of milling. The milling chamber is sealed and an exchange of air inside does not occur until the chamber is opened.

Small amounts of milled lactose were collected after each milling cycle (1g of lactose; ball to powder mass ratio 25:1). The milled lactose was stored in a desiccator at room temperature and 0-5% relative humidity to preserve the potentially induced lactose transformations during milling for further evaluation [59].

2.3.3 Tableting

Tablets from the aforementioned excipients and drug were pressed using two different tableting machines:

- A manually operated laboratory tablet press (Specac, England) equipped with two flat punches of stainless steel of diameter 13 mm was used. Tablets were pressed at two different applied loads (75 MPa and 380 MPa) by manually ramping the load on the powder (400 mg) held within the die. The target load was maintained for 1 s and then released. The lower applied load was also maintained for 30 s in some experiments. Before mixtures of the materials were pressed into tablets, the components were mixed together in a vial using a vortex mixer (Ika, USA) for 30s.
- An automated tablet machine of a single punch (SKEAB, Korsh EK0) equipped with a flat punch of stainless steel with a diameter of 11 mm was also used. The tablets were pressed one at a time by manually filling the die with the powder (300 mg) before tablet compression. The loading, compression and ejection steps were automatically performed at a tableting speed of 43 rpm. Powder mixtures including more than one excipient/drug were blended using a turbula mixer (Turbula System Schatz, Basel, Switzerland) set to 96 rpm during 30 s prior to compression.

3 Methods

3.1 Atomic Force Microscopy

Atomic force microscopy is a highly versatile technique which offers the possibility of imaging a wide variety of samples at the micro- and nanoscale [60, 61]. New techniques have emerged over the years, for example enabling mapping of mechanical properties at the surface of a material. Another capability is to use the instrument to measure force and friction between various surfaces [62-64].

The general set up of the AFM instrument used (Multimode 8 AFM with a Nanoscope V controller, Bruker, Santa Barbara, CA) is shown in Figure 11. The sample is placed on a stage attached to a piezoelectric scanner which is capable of moving in the x, y and z (height) directions in response to applied voltages. A rectangular cantilever mounted in a holder is placed above the sample. A sharp tip or a spherical probe located at the end of the cantilever scans an area of the sample on a line by line basis. The deflection of the cantilever upon interaction with the sample is monitored using the reflection of a laser beam from the cantilever onto a position sensitive photodiode detector. The information collected by the photodiode is used to construct the topographical images or maps displaying surface properties of the sample [48].

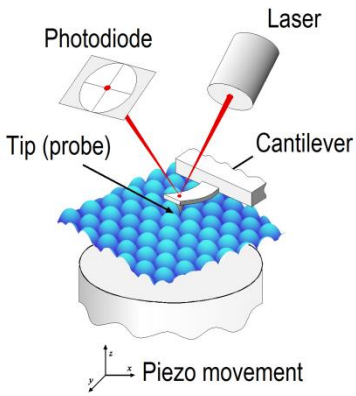

Figure 11. Schematic representation of an Atomic Force Microscope

3.1.1 Imaging

Topographical images can be captured using a cantilever with a sharp tip (approx. 10 nm radius) and employing a suitable imaging mode: for example contact mode, tapping mode or (less commonly) PeakForce® QNM (the latter is described in the next section 3.1.2). In contact mode, the tip is in permanent contact with the surface at a constant applied force that deflects the cantilever. The cantilever deflection is kept constant across the surface topography by the vertical movement of the piezo-scanner, which adjusts according to the feedback received from the photodetector (which monitors the changes of the cantilever deflection). The scanner movement is then converted into a topographic image. This technique is preferred when imaging hard and relatively flat surfaces for best possible image resolution. In tapping mode the tip oscillates close to its resonance frequency at constant amplitude and is briefly in contact with the surface at each oscillation cycle. Changes in the vertical scanner position in order to keep the

amplitude of oscillation constant are used to generate the topographic image. This technique provides better performance when imaging soft and brittle samples.

3.1.2 PeakForce® Quantitative Nanomechanical Mapping (QNM)

The recently developed PeakForce® QNM technique provides not only topographical information but may also be used to obtain contact-mechanical properties such as the DMT modulus [65, 66], adhesion, dissipation and surface deformation.

In PeakForce® QNM the scanner oscillates in the z direction at a set frequency and amplitude as it scans, and deflects the cantilever up to a predetermined maximum applied force (PeakForce). A force curve is generated at every contact between the tip and the sample (Figure 12). The contact mechanical parameters extracted from analysis of the force curves then provide a pixel value which can be used in map of those parameters.

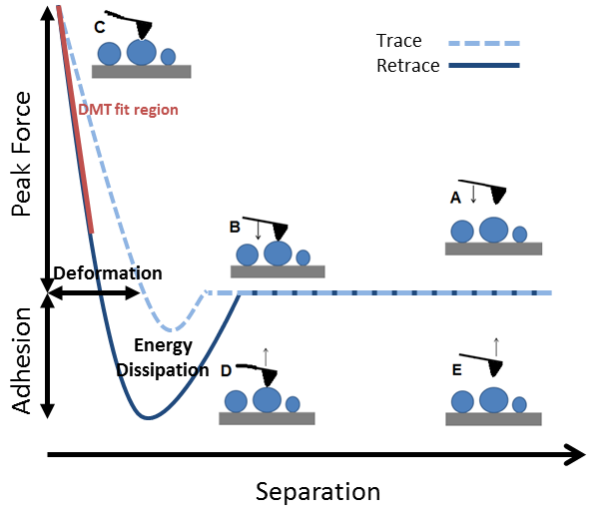

Figure 12. Representation of a pair of force curves generated with AFM.

Each pixel in the image is represented by data obtained from the force curves. The probe approaches the surface of the substrate until it achieves contact (Figure 12 A-B). A set force is applied (Figure 12 C) and then the probe is withdrawn. The probe and the substrate remain in contact until the force stored in the spring exceeds the adhesion force interacting between the probe and the sample (Figure 12 D-E). The magnitude of the adhesion is obtained from the value of the negative force minimum. If the approach and retraction curves do not overlap with each other, this indicates that plastic or viscoelastic deformation has occurred upon loading. The DMT modulus of the substrate can be extracted from the fit of contact mechanical theory to the contact region in the retraction curve. The area between the approach and the retraction curve provides information of the energy dissipation which is related to the degree of stiffness as well as the adhesion of the material. All the data generated at

the scanned surface area can be displayed as maps showing the spatial variation of the different parameters [67, 68]. Cantilevers with silicon-nitride tips were used for imaging, HQ-NSC 14/AlBS, Mikromasch (Estonia), with a tip radius of approximately 8 nm and a spring constant of 5±2 N/m.

3.1.3 The colloidal probe technique

In the colloidal probe technique [69] a particle of interest is attached to the end of a tipless cantilever using a micromanipulator mounted on an optical microscope. Smooth spherical particles are preferred in order to facilitate quantitative evaluation of the measurements since they provide a well-defined geometry of contact. Different probes would have different effective contact areas. Therefore in order to compare results obtained by using different probes the measured forces must be normalized. To facilitate this the Derjaguin approximation [70] is commonly used since it relates the normal force (F) to the energy per unit area between equivalent flat surfaces (W(D)) according to:

$$\frac{F}{R} = 2 \cdot \pi \cdot W(D)$$

where R is the radius of the particle interacting with a flat surface. In this thesis a steel probe is used to measure force and friction at the surface of different tablet components.

In the experiments of paper IV, single force measurements were performed using a ramp size of 1 μm and 1 μm/s velocity. Tip-less

cantilevers, HQ-NSC12-35/NoAl, Mikromasch (Estonia), with a spring constant of approximately 5±2 N/m were functionalized with a steel sphere (Figure 13). A maximum force of 24 nN was applied. Ambient conditions were constant during measurement (24±2°C and relative humidity of 45±5%).

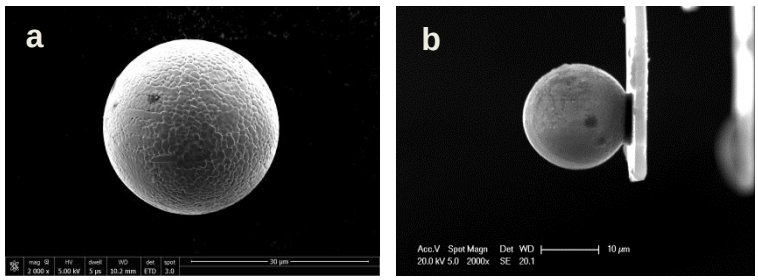

Figure 13. SEM images of (a) steel particle (30 µm scale bar) and (b) steel sphere glued to a tip-less cantilever (10 µm scale bar).

3.1.4 Force

Normal forces upon both approach and retraction are measured by controlling the movement of the piezoelectric scanner in the vertical direction. The obtained raw data are the vertical deflection of the cantilever and the z-piezo position. These variables are plotted against each other to identify three important regions in the curve (Figure 14a). In the zero deflection region the sample does not interact with the probe. At the zero separation (Z_0), the probe comes into contact with the sample. The region of the constant compliance (*i.e.* when the cantilever deflection and the piezoelectric scanner move at the same rate) can be used to arbitrarily define the zero separation. In order to transform the raw data into force vs. separation (Figure 14b), the measured deflection is multiplied by the inverse of the slope obtained from the constant

compliance region; so that volts are converted into meters. Then Hooke's law and the spring constant of the cantilever are applied in order to convert distance units into force units. Finally, the separation is calculated taking into account the zero separation (Z_0) and the movements of both the cantilever and the scanner [69, 71].

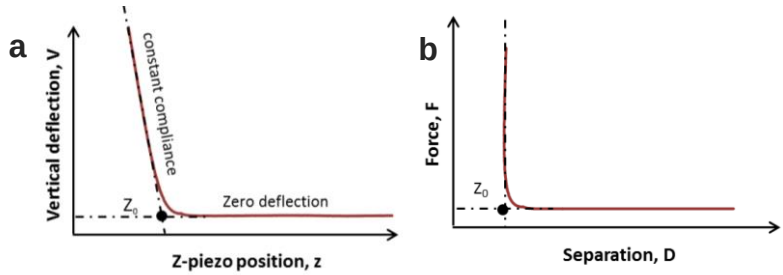

Figure 14. Graphical representation of the (a) raw data obtained using AFM and transformed into a (b) force vs. separation curve.

3.1.5 Friction

The friction is measured using lateral atomic force microscopy (LFM). In this mode the lateral movement, or twist, of the cantilever is monitored while dragging the probe along the surface in a reciprocating motion perpendicular to the long axis of the cantilever. The load is increased stepwise from below zero, (*i.e.* prior to contact) up to a maximum value and then reduced stepwise until the surfaces are out of contact. The output signals that reflect the lateral deflection, in the forward and backward directions, usually referred to as trace and retrace, are averaged giving an output voltage ΔV. Then the lateral deflection is converted to friction force (F_F) according to the following equation:

$$F_F = \frac{\Delta V \cdot k_\phi}{2 \cdot h_{eff} \cdot \delta}$$

Where k_ϕ is the torsional spring constant, h_{eff} is the effective height which corresponds to the diameter of the probe plus half the thickness of the cantilever, and δ is the lateral deflection sensitivity. The friction force is plotted as a function of the applied load to obtain the corresponding friction coefficient, μ, typically calculated from the slope of a linear region. [72, 73].

Force and friction were analyzed using AFM force IT v2.5.4 and AFM friction IT v2.5.4 software (ForceIT, Sweden).

3.1.6 Cantilever calibration

The normal and the lateral spring constants of the cantilevers used in this work were determined by the Sader method [74, 75] which is based on thermal vibrations and hydrodynamic damping of the cantilever. In order to obtain the resonance frequency and its quality factor, the thermal spectrum is fitted to a simple harmonic oscillator with added white noise. Then the resonance frequency and quality factor together with the length and width of the cantilever are used to determine the spring constant. This method is used for rectangular cantilevers. When preparing colloidal probes for this work, the cantilevers were calibrated before the particles were attached.

3.2 Scanning Electron Microscopy

The morphology of the samples was evaluated with a scanning electron microscope (FEI-XL, 30 series and Philips XL30). The sample is scanned

with an electron beam that penetrates several microns into the sample. The scattered electrons from the sample are then collected by a detector which provides the signal for the image. SEM was operated at different accelerated voltages (5-20 kV) under high vacuum using the secondary electron detector (SE), the backscattered secondary electron detector or a combination of the two. For imaging, the samples were attached to a double-sided carbon tape mounted on aluminum holders. In order to increase sample conductivity and reach high magnification without damaging the sample, these were gold coated (120s, 40 mA) using a Balzers SCD050 coater.

3.3 Profilometry

Profilometry is a non-contact optical method based on white light interferometry. A profilometer (Zygo new View 5010, Middlefield, CT, USA) was used to measure the surface roughness profiles of the pressed tablets. The sample surface area evaluated at each scan was of 440x330 μm, imaged with a 20x Mirau interference objective (Zygo) with a 0.8x zoom. The vertical movement of the light beam allows for a 3D measurement of the topography displayed in a height image. The vertical resolution is usually at the nanometer level, and the spatial resolution depends on the choice of optical set up. The advanced texture application in Metropro^{TM} 7.1.3 (Middlefield, CT, USA) analysis and control software was used to analyse the surface maps

3.4 Differential Scanning Calorimetry

Thermal events occurring during sample heating such as the glass transition, crystallization or melting were studied using Differential Scanning Calorimetry (Mettler Toledo DSC 1 STARe). The powder sample (4 mg) was placed in a hermetically sealed aluminum pan with a pinned lid inside a furnace together with an empty aluminum pan used as a reference. The temperature of the sample was raised from 20°C up to 240°C at a heating rate of 10 °C/min under N_2 flow (50 ml/min). Phase transitions of the powder sample are detected following the heat flow variations while the temperature increases.

3.5 Thermogravimetric analysis

Thermogravimetric analysis (TGA) was used to estimate the water content of the powder samples. The powder sample is heated up inside the small furnace of the thermogravimetric analyzer (Mettler Toledo, TGA2) under N_2 gas flow (20 ml/min). Sample weight loss is recorded as the temperature increases from 25°C to 240°C with a rate of 20°C/min.

3.6 Tablet strength

Tablet strength is used as a parameter to control the quality and uniformity of the produced tablets. The most widely used method to measure the strength of a tablet is the diametric compression test. A unidirectional force is applied along the tablet diameter by a mobile plate until tablet failure (Holland Tablet Hardness Tester C50). The applied

force needed to fracture the tablet is then measured. The test is useful to compare the "force at fracture" values of the different formulations [28].

3.7 Shear cell

The flow properties of the powder bed depend on many parameters such as particle shape and size, surface chemistry, moisture content of the powder and temperature. Since it is complicated to determine all these parameters and relate them to the flow properties of the powder, specific devices to test powder flow have been developed. The shear cell used (Ring Shear Tester RST-XS) is based on the magnitude of the applied load needed to deform a consolidated bulk solid until failure in order to quantitatively assess flowability. A certain volume of powder is placed in an annular cell covered with a cogged ring. Three increasing shear loads are gradually applied in the powder bed by rotating the metallic ring on the top of the powder. A flow function coefficient is calculated from the measured data as the major principal stress (σ_1) divided by the unconfined yield strength (σ_c) (ffc = σ_1/σ_c). Powders are classified as easy-flowing when no additional force except gravity is necessary to make them flow, while poor-flowing powders experience flow obstructions and consolidation making the flowing process difficult. The relationship between flow factors and powder flowability has been established considering free flowing for powders with factors larger than 10 and poor flowing for powders with factors lower than 2 [76, 77].

4 Results and discussion

4.1 Methodology development

4.1.1 Optimization of imaging parameters

In order to set up the AFM PeakForce® QNM measurements and collect accurate adhesive and mechanical information and good quality images from the scanned areas, optimization of the process parameters is needed. Due to the heterogeneity and the variable roughness of the scanned areas on both tablets and particles, different scan rates and scan sizes were used to allow for good tracking of the surface. A scan size of 50 μm was used to evaluate the surface of the tablets with a scan rate of 0.326 Hz. A reduced scan size of 2 μm was used to measure on the surface of the particles with a scan rate of 0.5 Hz. The applied PeakForce frequency was 2 kHz and the amplitude was 100 nm for all the measurements. The number of pixels per scan area was also constant during this study, 512 x 512.

An estimation of the number of contacts made between the tip and the sample per pixel was obtained for the aforementioned set of parameters at different scan rates. A certain scan rate in the direction of the x-axis results in different tip velocities depending on the size of the scan. The corresponding number of contacts per pixel at each tip velocity for two scan sizes, 50 μm and 10 μm, are presented in Figure 15. The adhesion measurements appeared to be comparable when they had the same number of contacts per pixel (Appendix I). This was achieved by using a constant scan rate for different scan sizes. By using the same scan rate at different scan sizes adhesion values appear different which may be

related to both the changing tip velocity and varying number of contacts per pixel (Appendix I).

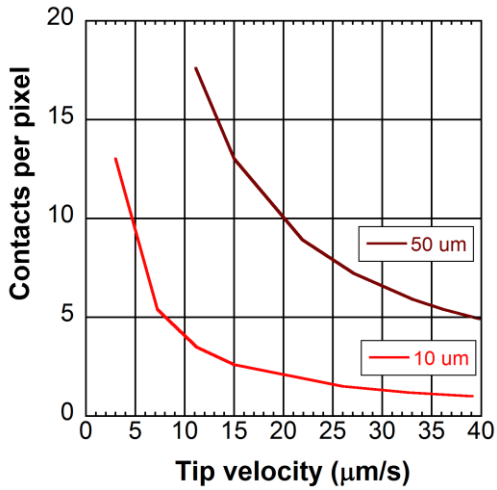

Figure 15. The number of contacts per pixel vs. tip velocity calculated for the scan sizes of 10 μm and 50 μm (512 x 512 pixels).

4.1.2 Characterization of surface amorphicity with AFM

The powders used in tableting may present either a crystalline or amorphous structure, which will affect the particle properties. Different structural conformations on the surface of the particles can affect the processability of the powders, thus AFM PeakForce® QNM was used to characterize the surface properties of crystalline and amorphous lactose and assess their relative amounts at the surfaces of particles. AFM PeakForce® QNM provides information on the topography, adhesion, deformation and energy dissipation of the scanned area of the sample, extracted from the force-distance curves (Figure 12) measured at each pixel. The dissipation is associated with the loss of energy and it is calculated from the hysteresis between the inward and the outward force curve at each contact of the tip. The extent of this difference depends on

both the viscoelastic deformation of the sample and the adhesion between the two surfaces. Crystalline and amorphous structural conformations differ in the spatial organization of the molecules. The lactose crystalline structure presents an organized three-dimensional structure that allocates one molecule of water per molecule of lactose in the crystal lattice. In contrast, amorphous lactose shows a random spatial distribution of the lactose molecules with intermolecular water content [78]. The different conformations give a different degree of spatial mobility to the lactose and water molecules; the later acting as a plasticizer [79, 80]. This affects the viscoelasticity of the material [81]. Therefore dissipation is a likely candidate to provide good imaging contrast when studying sample surface amorphicity. AFM was used to explore this possibility by first using α-lactose monohydrate as reference for the crystalline state and spray dried lactose as reference for the amorphous state. Some small regions of amorphous material were found in the crystalline samples and vice versa indicating that they were not completely homogeneous. Nonetheless, since these samples were used as references, their properties were assumed to represent the fully crystalline or amorphous extremes. (Both phases tend to coexist in pharmaceutical solids [82, 83]). Figure 16 shows 3D plots of the topographical features overlaid with a color map representing the energy dissipation. Darker colors represent low energy dissipation while lighter colors correspond to high energy dissipation. The earlier assumption regarding the appropriateness of dissipation as a discriminator was confirmed, since significant differences are observed for the evaluated lactose samples (Figure 16). Lower dissipation values were measured for the crystalline lactose while amorphous lactose presented high dissipation. In order to generate partially amorphous

particles, lactose powder was milled during 1h in a ball mill. Partially amorphized lactose was generated and it showed an intermediate behavior; well defined regions of low dissipation were detected among others of high dissipation values (Figure 16c).

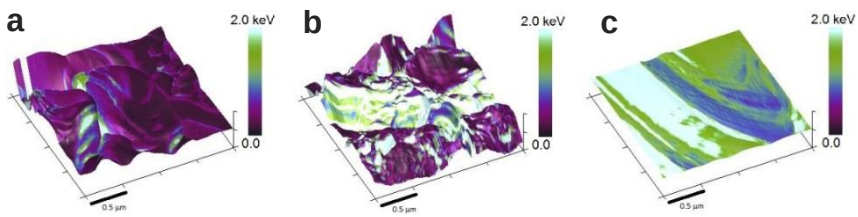

Figure 16. AFM PeakForce® QNM dissipation maps overlay the 3D topographical representation of (a) crystalline lactose, (b) partially amorphized lactose and (c) amorphous lactose. The vertical scale corresponds to the dissipation values in energy units. Scale bar of 0.5 µm. (Paper I)

In order to obtain a statistical representation of the surface properties multiple areas were analyzed from different particles of each sample. An average dissipation value was calculated with the software (Nanoscope Analysis 1.4, Bruker) for each area. This set of data is represented in a cumulative plot for each sample type in Figure 17. The accumulated fraction having their average value equal to or less than the dissipation bin value on the x axis is plotted using average dissipation bins of 250 eV. The same trend as for the individual AFM maps is observed for the whole set of data. Crystalline lactose accumulates the majority of the data at low dissipation while amorphous lactose data accumulation lies mostly above 1000 eV. The partially amorphised lactose cumulative data lies in between the two reference materials.

Even though the average dissipation is useful to evaluate sample amorphicity, in some cases it can be skewed by regions with significant

deviation from the mean value. Thus a bearing analysis indicating the percentage of the scanned area above a set threshold assigned to "amorphicity" may be useful. The crystalline-amorphous (C-A) boundary was assigned to 1000 eV on the basis of the trends observed in Figure 17. Approximately 80% of the values were lower than 1000 eV for crystalline lactose while for amorphous lactose 75% of the values were higher than 1000 eV.

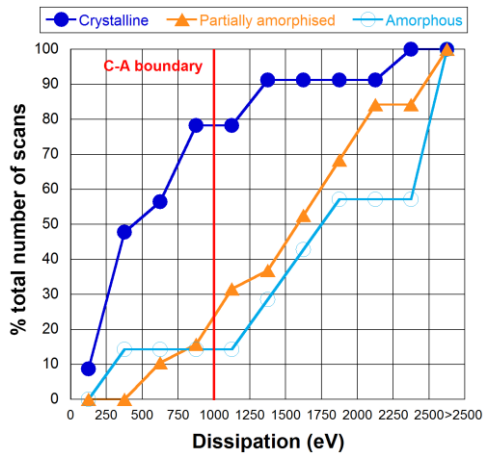

Figure 17. Cumulative distribution of the average energy dissipation from each area scanned with AFM. The vertical line indicates the crystalline-amorphous boundary at 1000 eV. (Paper I)

Bearing analysis was performed on each of the multiple scanned areas. The cumulative number of the scanned areas vs. the area percentage above the set threshold is represented in Figure 18. Nearly 90% of the scans from the crystalline lactose show 50% or lower area coverage by dissipation values of 1000 eV or above. On the other hand, for amorphous lactose only 30% of the scans have less than 50% of their area above the threshold. Partially amorphous lactose shows 50% of the scans with a 5-50% of dissipation coverage above the crystalline - amorphous

(C-A) boundary which means that the other 50% of the scans present 50-95% of dissipation values above the C-A set boundary. This confirms that crystalline and amorphous areas coexist on the surface of partially amorphous lactose, and provides a direct means for evaluation of the degree of surface amorphicity. It also clearly demonstrates that individual images cannot be used to provide statistically relevant estimates.

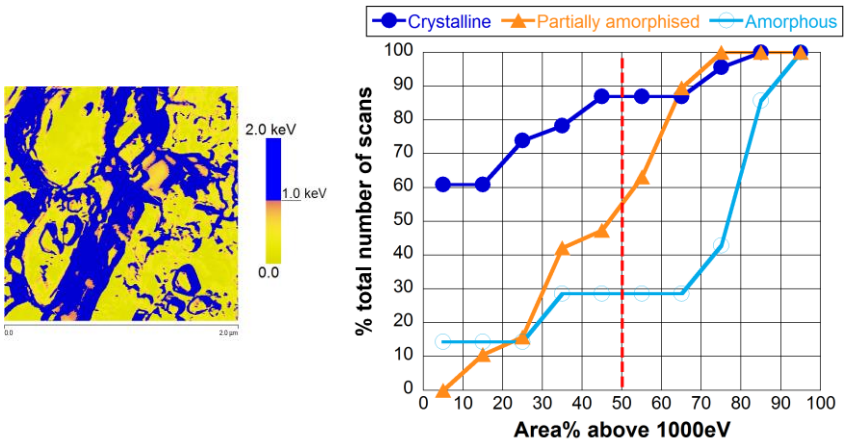

Figure 18. Energy dissipation map (left) of partially amorphous lactose obtained with AFM after the bearing tool was applied using a bearing depth of 1000 eV (2 µm scale bar). The blue areas cover 40% of the image and depict the areas of dissipation values above 1000 eV. The graph represents (right) the cumulative distribution of the scanned areas vs. the area coved by dissipation values lying above the C-A boundary for crystalline, partially amorphised and amorphous lactose samples. (Paper I)

Changes in the particles' surface properties can impact powder processability over time; for example through amorphous to crystalline state transformation. Recrystallization is a time dependent process accelerated by the ambient relative humidity and temperature [61, 84]. The transformation to the crystalline state is favored due to the less thermodynamically stable state of the amorphous form [85]. In paper I

SEM images and AFM images provided evidence of surface crystallization for amorphous samples exposed to ambient humidity. This effect was followed *in situ* using AFM at 25°C and a relative humidity of 55-60%. The evolution of the dissipation was tracked during 48 h and is plotted in Figure 19. The average dissipation of the first scans is above the C-A boundary indicating the amorphicity of the surface of the particle. After 2 hours of exposure the dissipation rapidly decreases to levels below the C-A boundary followed by a sharp decrease in dissipation within the next 2 h. Dissipation continues to decrease slowly over the ensuing 44 hours to values comparable to those of crystalline lactose. The variation in dissipation confirms the transition from the amorphous to crystalline state and the differences in mechanical properties of the two material structures. It thus both validates the approach and provides a direct measure of the kinetics of the surface rearrangement.

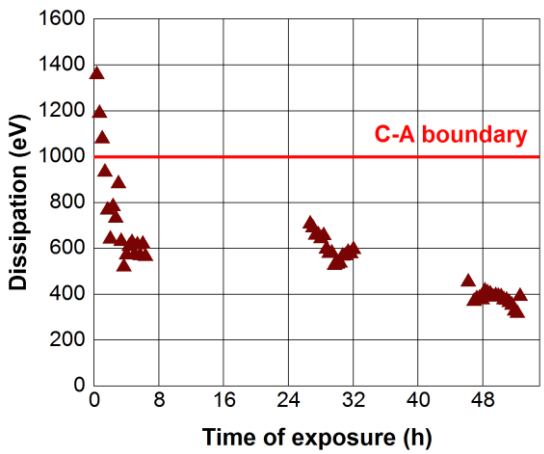

Figure 19. Continuous measurement with AFM at the same area of a particle of partially amorphous lactose under conditions of 55-60% RH and 25°C during 48 h. The scanned area was 2x2 µm size and the dissipation corresponds to the averaged energy dissipation form each of the scans collected over time. (Paper I)

4.2 Pre-processing: milling

For pharmaceutical powders milling is a common process usually performed prior to tableting and as discussed above, the mechanical stress induced during milling can induce changes in the material structure that will affect the subsequent properties [86]. Therefore it is important to characterize and quantify those changes which for example may be related to the sample amorphicity. Having established above that the amorphous and crystalline regions can be characterized and quantified by dissipation mapping, and the cumulative profiles thereof, it now remains to study the extent of the amorphisation with time and relate this to bulk measurements of amorphicity, as well as other physical changes that occur during milling. In addition to the two reference samples and the 1 hour milled sample used above, a further sample that had been milled for 20 h was employed.

Visual evaluation of the powders was done with SEM. Figure 20 depicts the particles shape and surface morphology at different magnifications. Figure 20a-a' shows α-lactose monohydrate, the lactose crystalline form, that presents particles of a polyhedral shape and with smooth surfaces. After 1 h and 20 h milling the particle size is reduced and the shape of the particles becomes rounded. Differences are observed on the surface of the particles. 1 h milled lactose particles (Figure 20b-b') show partially smooth surfaces with agglomeration of fragments generated during milling while 20 h milled lactose (Figure 20c-c') presents small protuberances over all the disrupted surface structure. Amorphous lactose particles (Figure 20d-d') are spherical with a highly smooth surface.

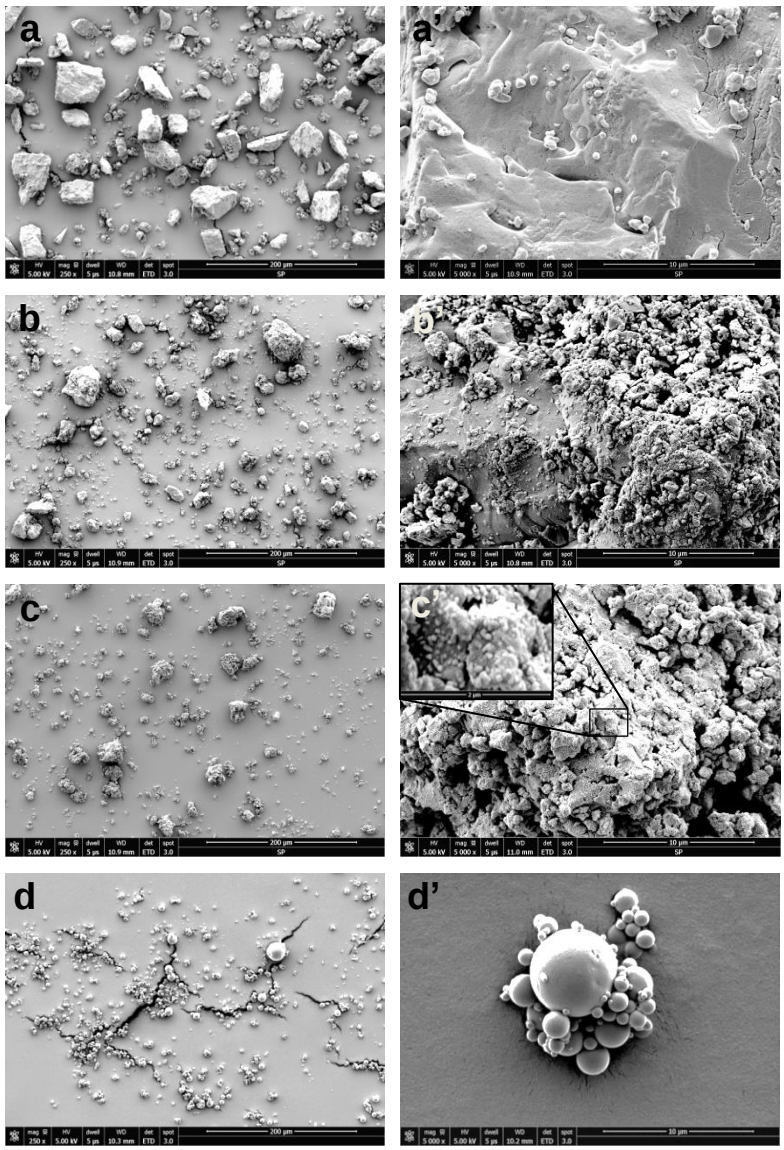

Figure 20. SEM images of (a-a') α-lactose monohydrate, (b-b') 1 h milled α-lactose, (c-c') 20 h milled α-lactose and (d-d') spray dried lactose. All the samples are shown at two magnifications with a scale bar of 200µm and 10µm. An additional image of larger magnification with a scale bar of 2 µm is inserted in c'. (Paper II)

SEM images reveal changes in particle size and surface morphology during milling which suggest changes of the mechanical properties of the particles. In addition, enlargement of the surface area after particle reduction is expected; this was measured with BET analysis (Table 2). A significant increase of the surface area is observed after milling with no major variation in surface area between short and prolonged milling times. The small protuberances observed with SEM after long milling maintain the higher value of the surface area as the particle size increases again with longer milling. It seems that agglomeration of the small fragments from the particle breakage after long milling leads to these observations. This unexpected, non-monotonic behaviour of the particles' area and size in response to milling suggests that other properties may warrant investigation.

Table 2. BET surface area of unmilled α-lactose monohydrate, 1h milled α-lactose and 20h milled α-lactose. Particle size measurements are from reference [a] performed by light scattering analysis. Apparent amorphicity is shown from reference [b]. (Paper II)

Sample	BET Surface Area (m^2/g)	Particle size (μm)[a]	Apparent amorphicity (%)
Unmilled lactose	0.5	30.2	0[b]
1h milled lactose	4	7.5	9.70±1.98
20h milled lactose	4.2	13.8	82.36±0.81[b]

[a][87], [b][59]

As discussed above, both surface amorphisation of the particles and propagation of this transformation into bulk can occur during milling [88]. The detection of the overall degree of amorphicity, which is dominated by the response of the bulk, can be detected with various analytical methodologies [86, 88, 89], however, characterization of the

particle surface state requires a more sensitive method for evaluation. The approach for quantifying particle surface amorphicity at the nanoscale described in section 4.1.2 has thus been employed (see paper I). It is based on the different dissipative responses exhibited by different material forms at the surface. Figure 21 presents cumulative plots of the average dissipation value for all the scans performed on each of the four materials. (Crystalline lactose, amorphous lactose, 1 h milled lactose and 20 h milled lactose). The cumulative trend of the 20 h milled lactose dissipation data is closer to the one measured for crystalline lactose, and does not *a priori*, indicate an increasing amorphisation with increasing milling time. This unexpected result indicates further material transformation at the surface after prolongued milling times. The extensively induced amorphization at short milling times is apparently reduced, which could be a result of either surface recrystallization or material evolution towards a different, more rigid amorphous conformation. Note that higher bulk amorphicity has been measured for longer milling times with Raman spectroscopy [59] (Table 2), which suggests a successful surface-bulk propagation of the amorphicity.

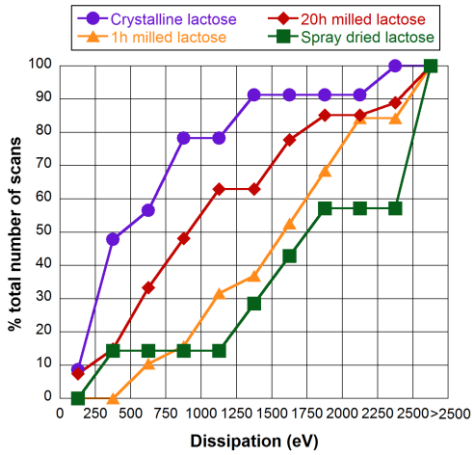

Figure 21. Cumulative distribution of the average energy dissipation for the scanned areas of α-lactose monohydrate, 1 h milled lactose, 20 h milled lactose and spray dried lactose. (Paper II)

Further analysis of the lactose to evaluate the bulk properties of the material, and to cast light on the apparent anomaly, was performed using DSC and TGA. DSC thermal profiles are represented in Figure 22a and TGA analysis in Figure 22b. The DSC analysis of α-lactose monohydrate shows the loss of the crystalline bound water with an endothermic peak at 148°C followed by the melting peak at 217°C. 1h milled lactose presents a similar profile with variations; partial amorphisation releases the crystalline bound water which can more easily leave the material over a broader temperature band. This is detected as an endotermic shoulder preceding the smaller peak for the remaining crystalline bound water. Part of the crystalline structure thus remains after milling for 1h. Further structural modifications are revealed during melting with a second melting peak appearing at 225°C in addition to the main α-lactose peak. However, no significant recrystallization event (a peak between e.g. 150°C and 200°C, indicating the presence of amorphous material) is

detected. This can be due to the low amorphicity level of the sample. Such recrystallization events appear for both spray dried lactose and prolonged milled lactose which confirms the highly amorphous structure of the two samples. Their thermal profiles are similar but the thermal events are shifted from one another. Spray dried lactose shows the loss of water and Tg combined in a broad endothermic transition starting at 70°C followed by the recrystallization peak at 185°C and the melting peak at 217°C. 20 h milled lactose shows a slight loss of the intramolecular water after the Tg event (120°C). Recrystallization occurs at 165°C and melting at 225°C. Thermal variations between the two amorphous lactose samples indicate differences in the amorphous structure likely reflected in material properties as observed with AFM. The melting temperature of the spray dried lactose coincides with the known α-lactose monohydrate melting temperature. In contrast, 20 h milled lactose melts at the same temperature as the *second* melting peak detected for 1 h milled lactose (225°C); this temperature is in between the melting temperatures of α-lactose monohydrate and β-lactose [90]. There is some support in the literature [91] for such a melting temperature for mechanically amorphized lactose, which suggests for example the existence of a cocrystal of α and β structure as a result of heating over 170°C. Spray dried lactose and 20 h milled lactose not only evolve differently upon heating resulting in a different melting temperature but also recrystallize at different stages. Therefore the history of the the two amorphous structures is reflected in the thermal pathways for the transitions during heating and they are very different.

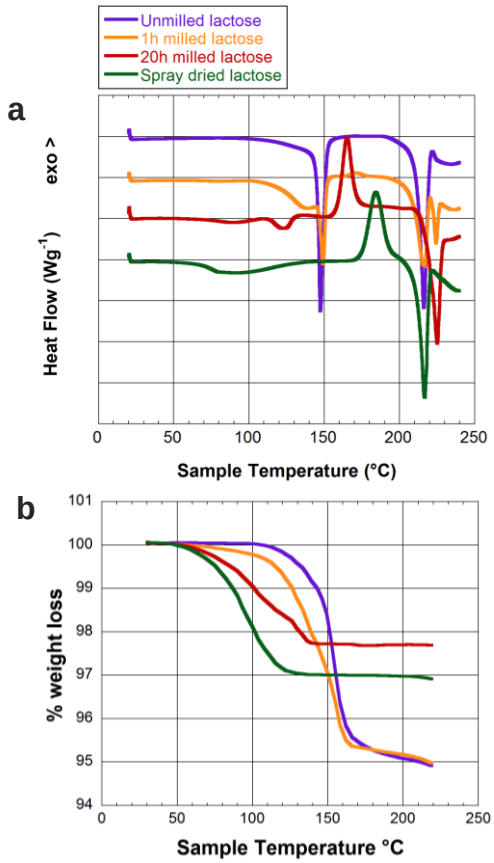

Figure 22. (a) DSC thermal analysis upon heating (10 °C/min) and (b) TGA representation of the weight loss vs. the temperature of the sample for α-lactose monohydrate, 1 h milled lactose, 20 h milled lactose and spray dried lactose. (Paper II)

Not only the nature of the material but also the water content of the sample can influence the mechanical response of the particle surface. Variations of the water content represented in weight loss percentange vs. sample temperature are shown in Figure 22b. Unmilled lactose (α-lactose monohydrate) and 1h milled lactose retain the initial water content of 5% w/w. Similar profiles but different paths followed during heating

indicate that the water binds differently in the two samples. Nearly all the water content is crystalline, bound to α-lactose monohydrate, indicated by the abrupt loss of weight. 1h milled lactose on the other hand stores water both in the remaining crystalline lattice and in the disrupted intramolecular structure and shows a more graducal weight decrease. The profiles observed for long milling lactose and spray dried lactose are similar showing 2% w/w and 3% w/w water content respectively, which is released at a different rate. The presence of water influences the mobility of the lactose molecules, decreasing the glass transition temperature [92, 93]. Thus it has implications in the softening of the material and its viscoelastic properties. The higher water content of the 1h milled lactose suggests a particle surface mechanical behavior similar to the one detected for the fully amorphous structure. Even though low bulk amorphicity levels are detected after 1h of milling [59], the tendency of the intramolecular water to remain in the amorphous structure, together with the location of the amorphous content at the surface, explain the amorphous-like reponse on the AFM measurements. Complete disruption of the lactose structure after prolonged milling and consequent water loss, helps to harden the material, blocking the molecular mobility. This results in a surface mechanical response similar to the unmilled lactose for AFM dissipation measurements. Another plausible explanation of the surface hardening of the 20 h milled lactose is the surface recrystallization at the very top layer of the particles. This may occur due to the increase of humidity inside the milling chamber triggered by the water released from the sample. Therefore significant differences in surface mechanical properties are detected with AFM between 20 h milled lactose and spray dried lactose in spite of the mostly amorphous bulk structure of the long

term milled sample [59], and the surface propeties, are clearly not represented by bulk measurements.

4.3 Tableting

4.3.1 Tablet press

A suitable balance between particle-tool and particle-particle adhesive forces is necessary to overcome sticking issues. The ability of different excipients to form tablets and their integrity were evaluated. Commonly used excipients such as MCC, commercial spray dried lactose, mannitol and MgSt (Figure 23) were pressed with a laboratory tablet press. Mixtures and tableting conditions were also considered for further tablet evaluation. Then tensile strength testing was applied to study the strength of the internal binding forces formed during compaction – often knows as tablet cohesion.

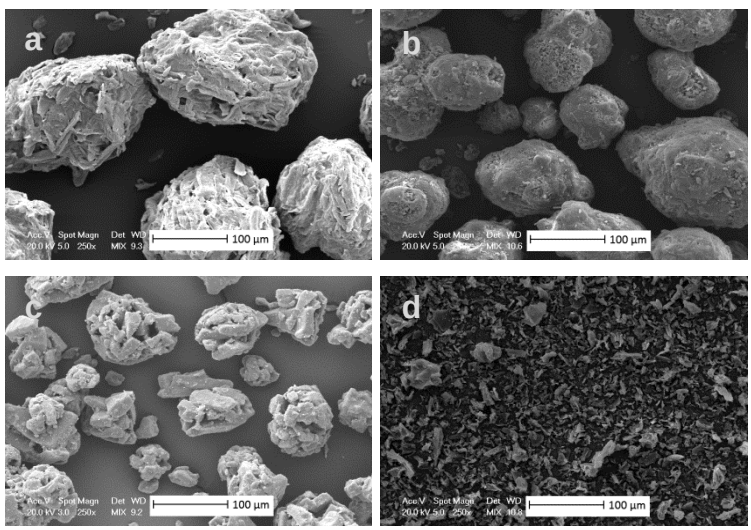

Figure 23. SEM images of (a) MCC, (b) mannitol, (c) lactose, (d) MgSt on its powder form. (Paper III)

Figure 24 shows that regardless of the choice of tablet component, higher applied force results in harder tablets. Lower compaction forces led to weaker tablet formation independently of the duration of the applied force. Increasing the applied load contributes to promoting binding by reducing the voids between the particles and to extend the contact area. The characteristics of the material are reflected in the different hardness values measured using the tablet hardness test for the pure excipients. Plastically deformable excipients like MCC, mostly undergo deformation, increasing the particles bonding areas. In particular, MCC has a fibre-like structure that contributes to the formation of an interlocked particulate structure upon withdrawal of the applied force after a limited elastic recovery. Brittle excipients tend to fracture under compaction creating smaller units which increase the interparticulate contact points. Lactose and mannitol behave as brittle materials, which is reflected in a tablet hardness much lower than MCC. Mixtures of equal amount of excipients in a two-component formulation results in a tablet with combined properties. The resulting tablet hardness is in between the tablet hardness of the two materials, but closer to that of lactose and mannitol. This suggests that fracture mechanics of lactose and mannitol dominate over the loadbearing properties of MCC.

The addition of a small amount (1%) of lubricant (MgSt) to both pure excipients and two-component formulations has a different effect depending on the compaction mechanics of the material. Magnesium stearate is a fatty acid bound to a metallic atom that spreads over the particles forming a thin film of variable thickness [94, 95]. Thus the tablet hardness of plastically deformable excipients such as MCC, is significantly weakened after such tablet lubrication. MgSt spreads over

the particle surface, reducing bonding between the particles. In the case of MCC, MgSt lubricates and makes the particles slip over each other, reducing the effect of interlocking. The fracture of brittle materials under compression leads to formation of fresh surfaces of higher energy not covered by MgSt. So particle-particle binding sites are made available and no significant change in tablet hardness is observed after addition of MgSt to either lactose or mannitol.

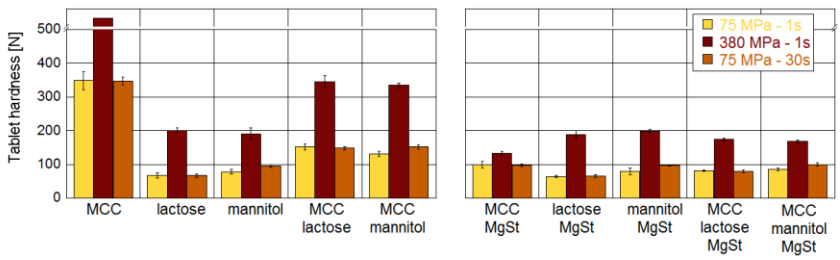

Figure 24. Tablet hardness of all the formulations pressed under different tableting conditions of applied force and time. (Paper III)

Tableting of the same set of formulations was also performed with a single punch tableting machine (Figure 25). Direct comparison with the previous measurements is not possible due to large differences in applied load and compaction rate. However variations in tablet hardness between samples follow the same trend observed when pressing the tablets with a laboratory press. MCC shows higher tablet hardness than lactose and mannitol. This is significantly reduced after adding MgSt which once again does not occur in case of lactose and mannitol. The only significant difference in trends using the different tableting machines would appear to be that lactose tablet hardness is lower in comparison to mannitol in the case of the punch. The two-component formulations show a

mechanical behavior which is clearly dominated by the brittle component. Therefore tablet hardness of the two-component formulations is not significantly affected by the addition of MgSt.

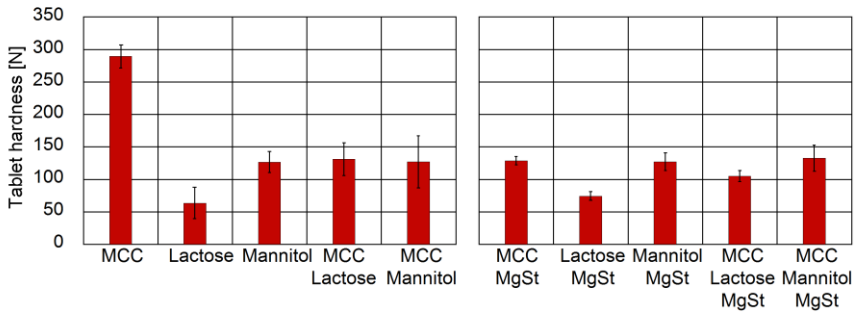

Figure 25. Tablet hardness of all the formulations pressed with a single punch tableting machine.

These results indicate that tablet properties greatly depend on material mechanical behavior under compaction. The replicate trends prove that both tableting procedures can be used to evaluate and compare the tableting response of the excipients during compression.

4.3.2 Tablet surface evaluation

Tablet surface features may vary depending on the applied compaction conditions. This variation is shown in Figure 26 with a representative example of SEM images used for evaluation of the surface of the pressed tablets. MCC presents a more closely packed structure when the tablet was pressed at a higher compaction load. Lower loads (independently of loading time) show a rougher surface with a less compact structure. The same observations are made for the other excipients (lactose and mannitol) and their corresponding mixtures (MCC+lactose and

MCC+mannitol) when they were pressed under the same conditions. Even though bonding strength depends on the mechanical and chemical properties of the materials, a higher applied load contributes to increase the particle contact area, thus increasing the probability of bonding.

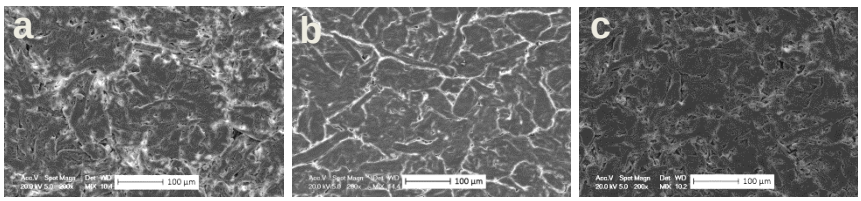

Figure 26. SEM images of MCC tablet surface pressed at different compaction conditions: (a) 75 MPa – 1s, (b) 380 MPa – 1s, (c) 75 MPa – 30s. (Scale bar 100 µm). (Paper III)

Further tablet surface evaluation was performed with AFM for the pure excipients and those lubricated with MgSt. Additional topographical features of the pressed tablets were observed on the nanoscale with AFM (Figure 27). MCC shows large and sharp features, likely as a result of its fibre-like particle structure. Addition of magnesium stearate seems not to smooth the tablet surface features at this level. Lactose and mannitol show a much smoother and more homogeneous surface, which in the case of lactose presents some small asperities. The presence of MgSt smoothens out the lactose tablet surface, but has no apparent impact on the topography of the tablet surface of mannitol.

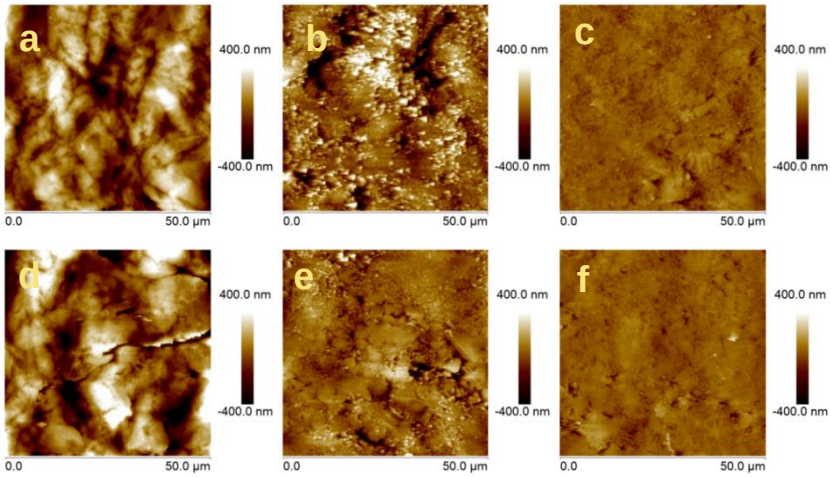

Figure 27. AFM topographical images of the surface of the tablets formulated with pure excipients: (a) MCC, (b) lactose, (c) mannitol and the excipients lubricated with MgSt: (d) MCC+MgSt, (e) lactose+MgSt, (f) mannitol+MgSt. (Paper III)

AFM measurements of tablet surface adhesion allow a comparative evaluation of the adhesion values. The color maps overlaid on top of the topography maps shown in Figure 28 represent the adhesion. Higher and more homogeneous adhesion values are observed for MCC in contrast to lactose and mannitol which present lower and comparable adhesion. Addition of MgSt to the pure excipients reduces adhesion for all three materials, but it is most pronounced in the case of MCC. For lactose and mannitol the AFM study indicates that addition of MgSt leads both to smoother surfaces (see paper III supporting information) and more homogeneous adhesion.

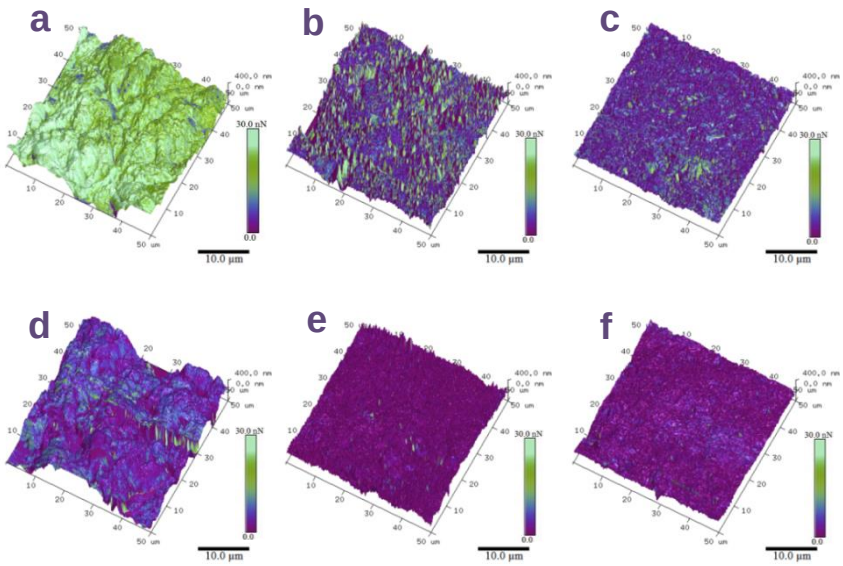

Figure 28. AFM adhesion maps overlap the 3D representation of surface topography. The adhesion levels are represented by the color scale where lower adhesion corresponds to darker color. The evaluated excipients were (a) MCC, (b) lactose, (c) mannitol and these formulated with MgSt: (d) MCC+MgSt, (e) lactose+MgSt, (f) mannitol+MgSt. (Paper III)

The adhesion trends observed in the AFM maps (Figure 28) are summarized in terms of the average adhesion for each evaluated system in Figure 29. Considering the high tabletability properties of MCC [55], the AFM measured adhesion could intuitively be associated to the material interparticulate forces if the hydrophilic tip is assumed to be representative of cellulose. Higher adhesion might indicate higher internal tablet cohesion. Thus MCC sticking propensity is low assuming that cohesive failure is a factor that promotes sticking. The larger spread in MCC adhesion data is attributed to the partial recovery of the MCC elastic component that creates irregular surface properties. Lactose and mannitol exhibit a similar behavior and show lower adhesion, thus, lower

tablet cohesion and consequently, the potential for a higher sticking propensity. The lubricating properties of MgSt also reduce tablet surface adhesion for all the excipients. Tablet surface adhesion is reduced to half of its value in case of lactose and mannitol while a larger reduction is noted for MCC. Therefore MgSt reduces the tablet cohesiveness to a different extent depending on the nature of the excipient. These observations confirm and explain the results obtained from the tablet tensile test (section 4.1.1) for the pure and lubricated excipients.

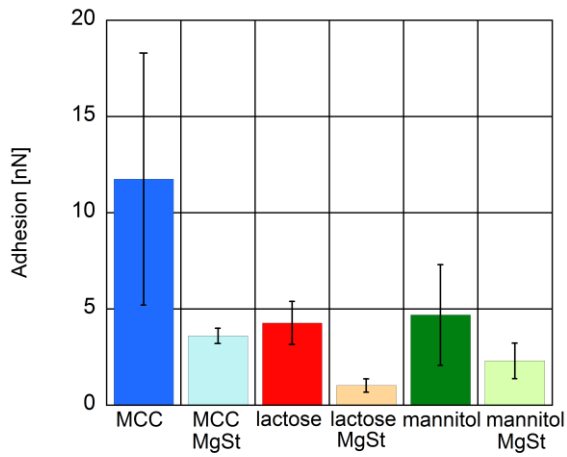

Figure 29. AFM average adhesion for each of the pure and lubricated excipients in a tablet form. The main adhesion of each scan was averaged with at least 7 scans obtained for each set of samples. (Paper III)

4.3.2.1 Ibuprofen tablet surface

The surface of the ibuprofen tablets (prepared under 380 MPa applied force with a manual laboratory tablet pressed) was studied with SEM directly after compaction and some months later. Figure 30 summarizes the observations of the ibuprofen surfaces with SEM. The crystals prior to tableting are shown in Figure 30a. After compaction, the surface of the

tablet (Figure 30b-c) presents a disrupted crystalline structure, which resembles material flow occurring during compaction and the individual crystals are largely absent. Figure 30d shows the surface of the tablet 9 months after it was pressed, and clearly indicates the presence of ibuprofen crystals which show a similar geometry to the original ibuprofen crystals (Figure 30a). Material defects may have been promoted during compaction which may have resulted in a rebuilding of the crystal structure over time on the surface of the pressed tablet [96].

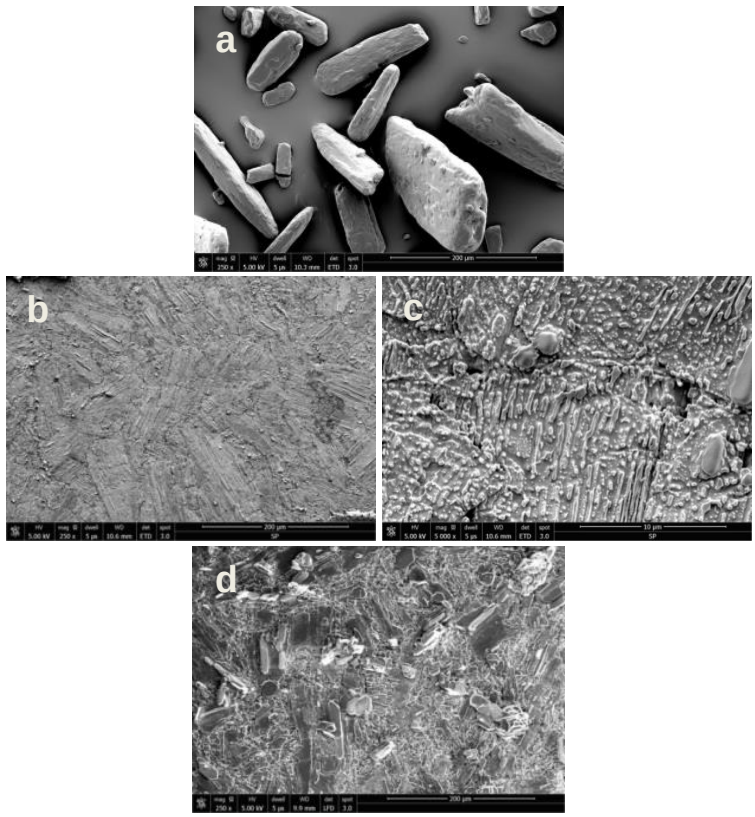

Figure 30. SEM images of (a) ibuprofen particles (200 µm scale bar), (b-c) tablet surface of ibuprofen (scale bars: b - 200 µm, c - 10 µm) and (d) tablet surface of ibuprofen 9 months later (200 µm scale bar).

4.3.3 Effects of the addition of lubrication agent (MgSt)

Even though magnesium stearate is commonly added in small amounts (1%-3%) into the formulation, it has a great impact on the performance and tablet quality. In previous sections (section 4.3.1, section 4.3.2 and paper III) it has been shown that tablet surface roughness is differently affected by MgSt depending on the mechanical properties of the excipients. MCC is extensively affected by the presence of MgSt while no major changes in surface roughness were observed for lactose and mannitol.

Thin layer formation of the lubricant on the surface of the MCC particles affects the elastic recovery of the particles after removal of the applied load. This results in a more leveled tablet surface of the lubricated MCC which was observed at larger scale with profilometry (Figure 31). This tends to suggest that the particles deform under load, but do not slide past each other to the same extent in the absence of the MgSt, *i.e.* the adhesive bonds are less disrupted.

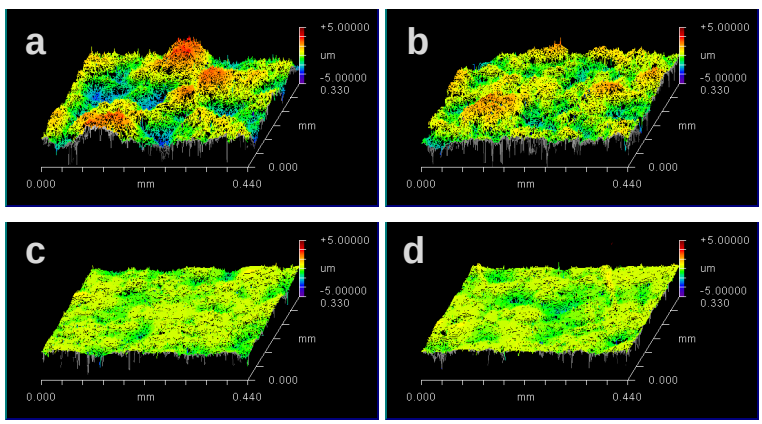

Figure 31. Profilometry profiles of the tablet surface of (a) MCC, (b) MCC+MgSt, (c) lactose and (d) lactose+MgSt. (Paper III)

Changes in tablet hardness and tablet surface properties induced by MgSt are also reflected in the internal tablet structure which was observed in cross-section after fracture in the tensile strength tests. The organization of the MCC particles varies in the presence of MgSt. Figure 32 shows a non-defined particle organization at the MCC tablet cross-section in contrast to the well-organized layered structure of the deformed MCC particles after MCC formulation with MgSt. No difference between the non-lubricated and lubricated tablets cross-section is observed for lactose or mannitol. This observation provides direct mechanistic evidence of action of MgSt depending on the material mechanical properties previously discussed, and further indicates the very different compaction and fracture mechanisms for the different excipients (section 4.1.1 and paper III).

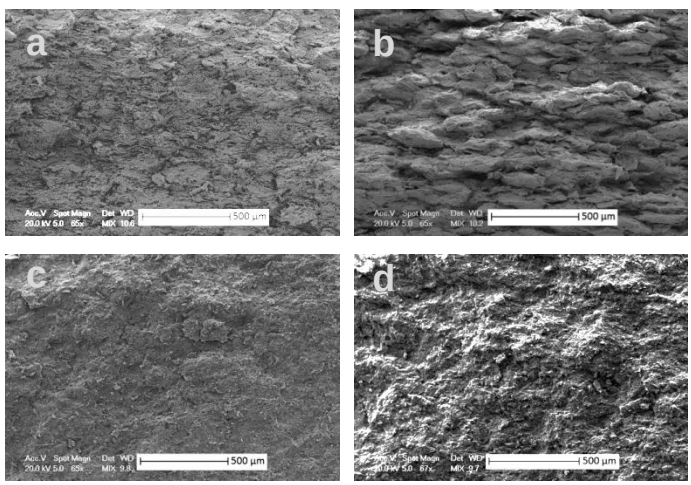

Figure 32. SEM images of the tablet cross-section (a) MCC, (b) MCC+MgSt, (c) lactose and (d) lactose+MgSt. (Paper III)

The effect of MgSt has also been evaluated in flowability studies performed with a shear cell for the excipients and ibuprofen. In contrast to the observations made for tableting, the presence of MgSt did not affect the flow of the powders (see Appendix II).

4.3.4 Experiments simulating punch-particle interactions

Adhesion of the powders to the tableting tools arises from interactions of particles to the steel surface in preference to the tablet bulk. The probability of the powder attaching to the tools will partially depend on the magnitude of the adhesive forces built up during compaction between the contact surfaces. AFM colloidal probe was used as an analytical technique to emulate the particle-steel surface interactions. The cantilever was functionalized with a steel probe (Figure 13) and brought into contact individually with three excipients of differing tabletability performance [97] and a model sticky drug (ibuprofen) [58]. Typical force-separation curves of MCC, lactose monohydrate, spray dried lactose and ibuprofen are presented in Figure 33. Overall, two different types of curves are detected and referred to as short distance/sharp retraction and long distance/extended retraction. MCC, lactose monohydrate and spray dried lactose show a short distance/sharp behavior for 78% of the performed measurements. This is characterized by the jump out separation distance of 10-20 nm and a well-defined point of immediate detachment between the two surfaces. However, ibuprofen shows a long distance/extended retraction profile characterized by a much longer jump out separation distance than 20 nm and a sluggish physical separation between the steel and the particle surface. This type of behavior is observed in 65% of the performed measurements on ibuprofen.

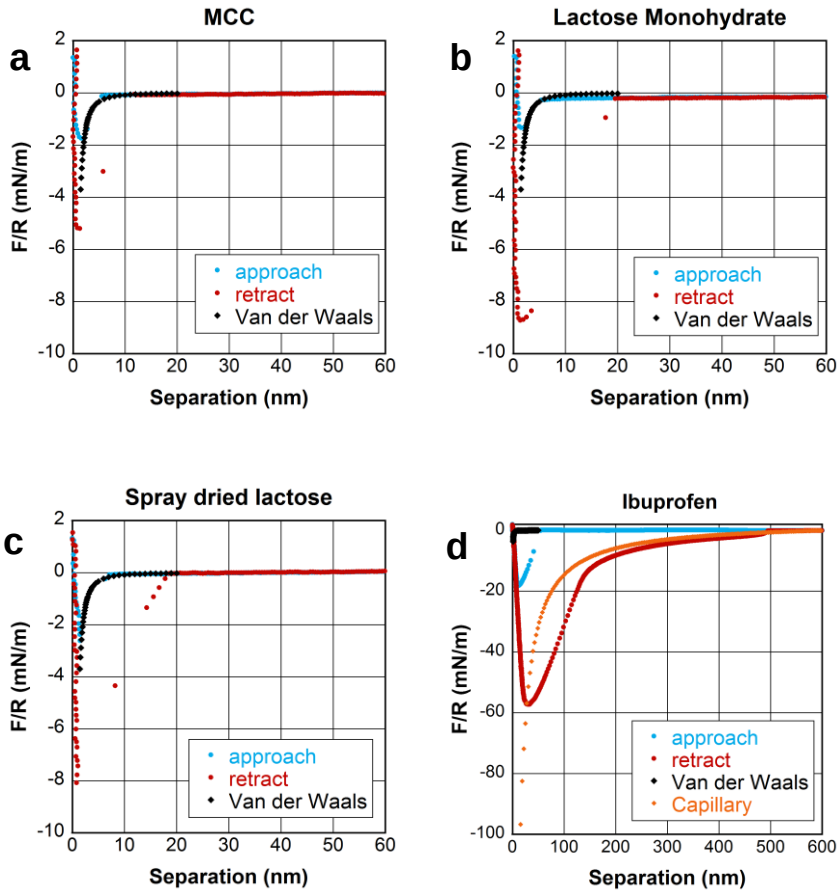

Figure 33. Representative examples of force-separation profiles measured with AFM colloidal probe for (a) MCC, (b) lactose monohydrate, (c) spray dried lactose and (d) ibuprofen. Note that larger order of magnitude is used for ibuprofen. A fitting of model curves for van der Waals and capillary attraction forces are represented in each of the graphs. (Paper IV)

Several types of forces can act at the particle-steel interface. Lifshitz attractive forces are weak and they act over short range; these are ubiquitous forces, always present between two interacting surfaces. The MCC, lactose monohydrate and spray dried lactose force curves are well explained by such an interaction, due to the low attraction force acting in

a short jump into contact from a distance of 5 nm and detachment force lower than 10mN/m. A fit of Lifshitz forces is shown in each of the graphs. Ibuprofen adhesion upon retraction is of 60 mN/m, six times larger than for the other evaluated excipients. The attraction force acts over a longer distance of 50 nm. The explanation of these longer ranged forces on ibuprofen is challenging. Charge transfer might occur during repeated contacts of two interfaces promoting the increase of charge on the surface [98, 99]. This phenomenon would depend on the surface and dielectric properties [100]. An increase of charge would result in higher adhesion between the two contact surfaces which would be manifested in an equally long ranged force upon approach. The less hydrophilic nature of the ibuprofen would tend to favour the possibility of charging. Capillary forces may also arise if sufficient water condenses to form a water bridge. Forces due to capillary condensation are strong and act over large distances. These are dependent on the hydrophilic properties of the material and the topography of the surface. While the ibuprofen force profile on separation can be well fitted to an electrostatic force profile the equivalent long ranged attractive force is missing on approach. In general ambient humidity levels above 20% RH will dissipate charge and such coulombic forces are thus not generally observed. On the other hand, ambient humidity may also contribute to the formation of capillary forces favored in case of hydrofilic surface properties. Ibuprofen is not a highly hydrofilic crystal on any of its crystal faces [58], in contrast to the evaluated excipients, so the question arises as to why the capillary force is only observed for the most hydrophobic surface. The answer lies in surface roughness. Capillary condensates will from around the local asperity contacts of the hydrophilic materials but for surfaces roughnesses

greater than the Kelvin radius this does not affect adhesion [101, 102]. For smooth surfaces (roughness below Kelvin radius – of the order of a nm at 40% RH) the condensate can flood the contact zone. For condensation to occur the net charge in the surface energy of the solid surfaces upon inmersion in water needs to outweigh the entropy penalty of condensing the water below the saturation vapour pressure. This criterion is met if the contact angle of water on the surfaces is les than 90°. The formation of a condensate on smooth surfaces can thus increase adhesion even for not highly hydrophilic surfaces. In this case the steel oxide is hydrophilic and the contact angle of ibuprofen is significantly less than 90°. Thus capillary condensation is likely to occur on ibuprofen, and the relatively smooth and deformable surface means that the contact zone can be flooded. Both the approach and separation force curves are consistent with such a capillary force, and a good fit is obtained to the separation curves using constant volume approximations (see paper IV and [103, 104]).

Figure 34 shows an example of a set of force curves collected sequentially at one spot on an ibuprofen particle. The increased number of contacts leads to an increased adhesion minimum depth (AMD). An increase of the attractive force and the jump-in distance between the two surfaces is also detected. This type of observation could conceivably be explained by the increased contact area after repeated contact. This possibility is discarded since there is no evidence of deformation in the constant compliance regions of the curves. Contact electrification and charging of the material by the generation of a larger effective change after repeated contact [98, 99] could also be consistent with the outward

curves but as argued above, not with the inward curves. Once again the presence of a capillary condensate is entirely consistent with these observations. “Harvesting” of moisture between contact surfaces [101, 105] due to fast condensation kinetics in comparison to evaporation lead to a slightly larger condensate on each subsequent contact. Attractive forces on approach grow due to the deformable droplet remaining on one or both surfaces after separation of each contact. The formation of the capillary neck leads each time to a larger adhesive force. The possibility of *both* electrostatic and capillary forces acting simultaneously is not considered since the condensate would immediately dissipate charge.

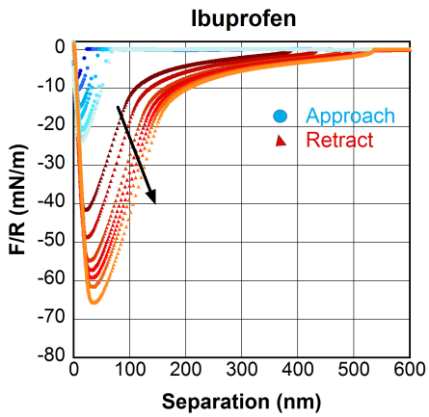

Figure 34. An example of several separation-force curves measured simultaneously with AFM colloid probe on ibuprofen. A total number of 22 curves were collected at the same spot. Curves number 2, 5, 8, 10, 13, 16 and 20 are represented in this graph. The arrow indicates increasing time. (Paper IV)

A summary of the average values of the average minimun depth (AMD) for all the evaluated particles (three different spots on three different particles: a total number of 9 different spots) from each material is shown in Figure 35. The values are obtained from averages of at least 25 force measurements performed continuously on the same spot. The excipients,

MCC, lactose monohydrate and spray dried lactose, show much lower, and comparable, AMDs than ibuprofen. Even though larger variation was observed for ibuprofen, the AMD is still significantly higher in all the performed measurements. This shows the higher affinity of ibuprofen to the steel surface which might indicate the higher propensity of the drug to adhere to the punch during tableting. The explanation might lie in the smoothness of the surface of the ibuprofen, allowing flooding of the contact. In contrast, the excipients are rougher although more hydrophilic. So capillary condensation confined to the asperity contacts will not increase adhesion. The sticking propensity of the drug can thus be diminished when it is incorporated into the formulation due to the presence of less sticky materials such as MCC, lactose monohydrate or spray dried lactose. However the build up of water on the steel punch associated with condensates may also lead to sticking of the other excipients in a tableting context.

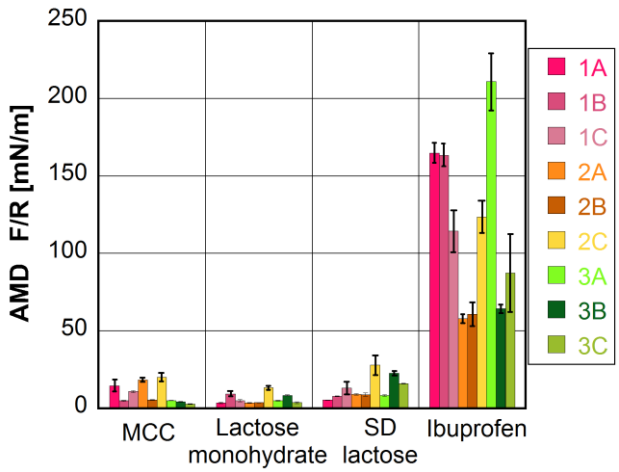

Figure 35. Average of the adhesion minimum depth (AMD) measured with AFM colloidal probe for each of the evaluated contact areas: three different spots (A, B, C) over three different particles (1, 2, 3) of each material. (Paper IV)

The AMD over time indicated as number of contacts is summarized in Figure 36. The linear fit of the evolution of AMD for all the areas evaluated for each sample is averaged and represented as a function of the continuously increasing number of contacts (supporting information paper IV). An increase in adhesion force overtime is observed for ibuprofen (already exemplified for an individual measurement in Figure 34) while adhesion remains constant over repeated number of contacts for MCC and lactose monohydrate. A nearly constant behavior is also observed for spray-dried lactose. This observation could be related to the repeated compaction impacts during tableting where the sticking phenomenon might happen after several compaction cycles. In tableting, it is the steel surface which is repeatedly brought into contact with different ibuprofen particles. Therefore this might suggest that moisture build-up on the steel surface could help to strongly attract fines from the powder, and those remain on the steel surface building up a particle layer. This would further promote sticking and picking during the tableting process [106]. The different behavior between the excipients and ibuprofen observed over time clearly exemplifies the affinity of the sticky and non-sticky materials towards the steel. Thus the higher the measured adhesion with AFM colloidal probe, the higher the sticking propensity of the material to the tableting tools.

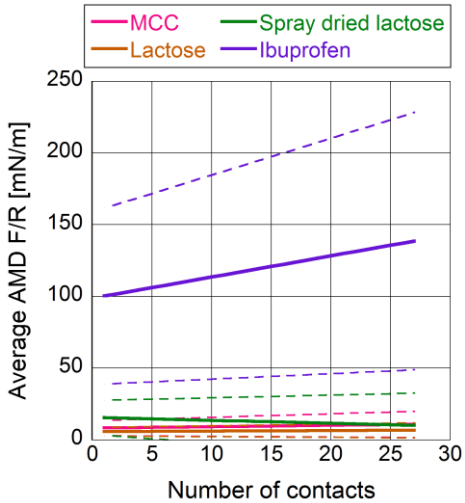

Figure 36. Relative evolution of the AMD as function of the increased number of contacts (from 1 to 25 min.) performed continuously on the same spot for each sample. The dashed lines indicate standard deviation. (Paper IV)

The colloidal probes used to perform the measurements were imaged with SEM after measurements on Ibuprofen (Figure 37). While the probe used to carry out the experiments shown here is free of any material residue after completion of the measurements (Figure 37a), an example of material transfer due to possible material pick up and transport in a water film is observed in Figure 37b.

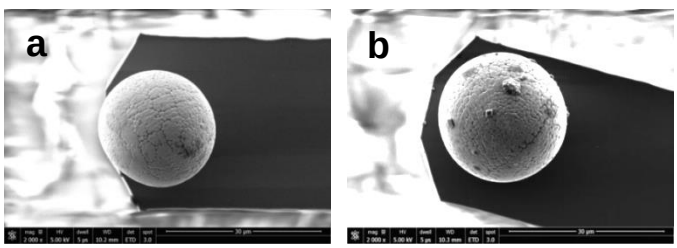

Figure 37. SEM images of (a) clean probe after measurements and (b) contaminated probe after measurements on ibuprofen showing the possible material transfer. (Paper IV)

4.4 Friction measurements

Friction measurements have also been performed between the samples above and the steel colloidal probe (Figure 38). Such measurements could be used to model tablet ejection and the movement of the particles against the punch during compaction. In fact the friction measurements are most useful in supporting the interpretations of the mechanistic information of the force studies above. This is because friction is intimately connected to adhesion, and the trends observed below mainly reflect the dynamics of the capillary condensate harvesting. Typically friction studies involve measurement of friction (through twist of the exhaustively calibrated cantilever) in response to systematic changes in the applied load. In fact the capillary harvesting leads to an increasing effective load (due to the increasing adhesion) irrespective of whether the contact is loaded or unloaded. The figures below demonstrate the typical hysteresis of the friction-load relationships that is measured during capillary harvesting. Note that they also demonstrate the full spectrum of behaviour condensation at the local asperity level (Figure 38a) to full contact flooding (Figure 38d). Thus while it is clear that the friction behaviour of the different excipients is distinguishable, the major benefit to this work is the unambiguous support for the capillary condensation mechanisms of the large adhesion measured with ibuprofen.

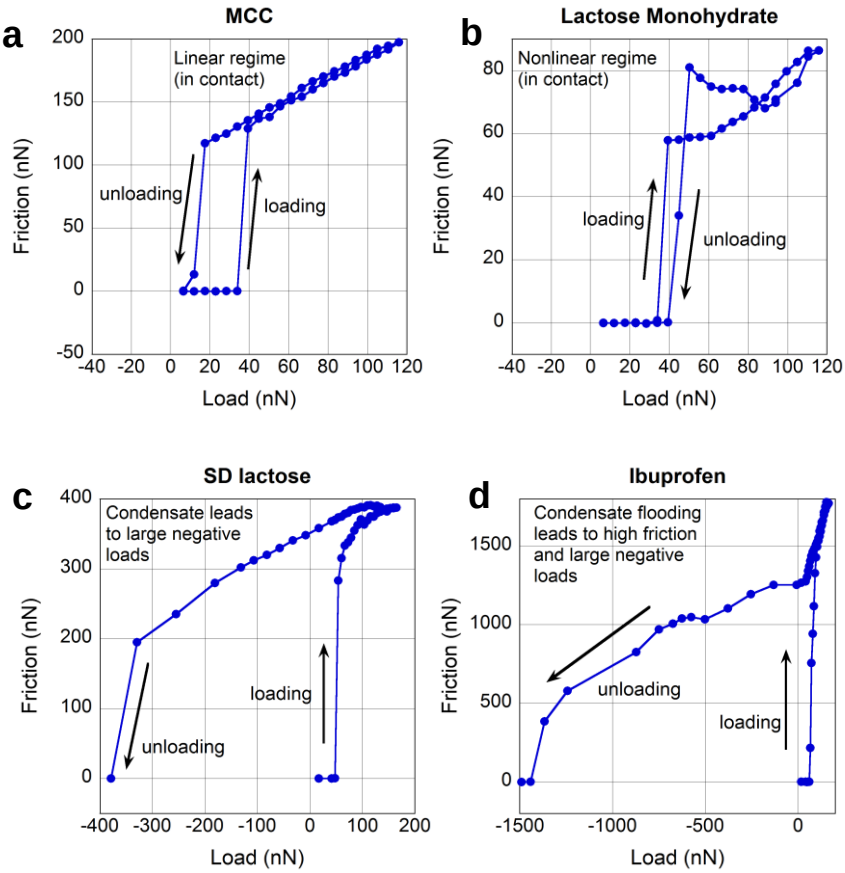

Figure 38. (a) Friction load relationship MCC-steel. No capillary condensate evidence. Linear anhysteretic friction-load relationship. (b) Lactose-steel friction data. The contact regime is non-linear due to a gradual increase in adhesion contributing to the effective load as a result of harvesting at asperity contacts. When the sliding direction is reversed the harvesting continues and the adhesion increases faster than the load is decreased leading to apparent negative friction coefficients. (c) Spray dried lactose-steel. In this example the capillary becomes more established (closer to a flooded state) due to harvesting. The friction forces become very large due to the large extra load that builds up due to capillary adhesion. This means that upon unloading, large negative loads reflect the force require to break the condensate. (d) Ibuprofen-steel friction data. Basically as for (c) but complete flooding of contact zone leads to very high friction and negative loads. (Supporting Information Paper IV)

5 Conclusion

Material performance during tableting depends as much on the bulk properties of the powders as on the surface properties of the particles, which can differ significantly from each other. The use of several analytical approaches such as microscopy, thermal and bulk mechanistic evaluation of the materials and AFM PeakForce® QNM, a nanoscale surface sensitive technique, have proved to provide valuable information to gain a better insight in prediction of powder tableting performance.

Tablet hardness is dominated by the particle-particle contact adhesion. The presence of MgSt strongly affects tablets hardness depending on the fracture mechanics of the materials under compression. It was observed that MgSt spreads on the surface of the particles preventing particle-particle bonding in the case of deformable materials. In contrast, brittle materials that fracture within the particles rather than at the contacts are unaffected by the presence of lubricant. This probably also depends on the fact that many particle contacts are formed between fresh, uncoated surfaces as a result of particle fracture during compaction. MgSt also contributes to smooth the surface of the tablet by reducing the mechanical interlocking of the particles which otherwise display elastic recovery after compression. Tablet hardness is important since it also reflects the balance of adhesive forces that arise between the particles and the tools during tableting.

A high adhesive propensity of a sticky drug (ibuprofen) towards the steel surface in contrast to the low adhesive interaction of the non-sticky

(excipients) powders was measured with AFM colloidal probe technique. The evidence for water bridge formation with subsequent harvesting is compelling. The relatively smooth surface of the crystals faces is thought to promote capillary bridge formation despite the less hydrophilic character of ibuprofen. This mechanistic effect observed with AFM at the nanoscale could be a key factor leading to sticking during tableting.

Crystalline to amorphous transformations are common during milling. AFM PeakForce® QNM is presented as a novel approach to evaluate the particle surface amorphicity. The recrystallization of surface amorphicity could be followed in real time using this approach, which both validates the approach and provides a direct means of following the dynamics. In combination with bulk measurements AFM imaging reveals that bulk and surface properties are largely unrelated to one another – it is the surface properties that contribute for example to adhesion, so caution should be applied in interpreting bulk measurements. The concept of amorphicity vs. crystalline is also by no means clear. Increased milling can lead to both an increase in particle size (though with uncompromised surface area, due to the small particles retaining their integrity during agglomeration) and a big change in the surface properties of the materials. Moreover, milling leads to a different amorphous structure of the lactose suggested by the shifted crystallization pathway observed upon heating in comparison to spray dried lactose.

Understanding of the mechanistic response as well as the particle-particle surface interactions of the materials is the first stage for further evaluation of the performance of the powders during tableting.

6 Acknowledgements

I would like to express my gratitude to everyone that has contributed to the completion of this thesis. During my PhD I had the honour to be guided by four supervisors. Each one contributed with their expertise and their own vision to approach the research problems that we have faced during the past years - that has been really valuable to deliver this thesis.
I would like to thank my academic supervisor, Professor Mark Rutland, for his guidance in the most rigorous and scientific way. I would also like to thank Dr. Anna Fureby, my supervisor at SP, who encouraged me to make my decision to start with this project. I am thankful to her for sharing her knowledge throughout this work. I am thankful to Dr. Niklas Nordgren, my supervisor at SP and AFM specialist, for introducing me to all the complex aspects of the AFM technique and for giving me support and guidance. Thanks for your enthusiasm and your willingness to help.
Special gratitude to my industrial supervisor, Dr. Michael Schuleit, that regardless of how far his office was from ours, he had always been actively involved in the project sharing with us his invaluable industrial experience. Thanks for your overall support and encouragement!

I would like to express my gratitude to Novartis Pharma AG for the financial support of my thesis project. In addition, Novartis had always been showing a clear interest in our research project. In particular, I would like to thank Dr. Gururajan Bindhu who has actively participated in our meetings bringing his hands-on experience in tableting and formulation. Thanks to him and Baskim Ajdini for assisting me during my stays in Novartis in Basel.

SP Process and Development gave me the opportunity to perform several tests and experiments in their facilities. Special thanks to Bo Lassen who kindly helped me around the facility.

Part of this work was the result of collaboration with Uppsala University. I am thankful to Prof. Göran Alderborn and Samaneh Pazesh for our fruitful discussions that provided us with valuable feedback.

I would like to thank my section manager, Fredrik Johansson, for allowing me to become a member of YKI and my group manager, Per Wessman, for ensuring a nice working environment. A warm thanks to Lubica Macakova for mentoring me when I joined the former YKI back in 2010, fresh from university. Thanks for teaching me and showing me how to work in the lab.

Despite being far from Spain I could feel a bit closer to home when I shared my time with the spanish speaking people at SP, always cheerful and helpful. Thanks to my PhD office colleagues, present and past, Hanna, Marine and Lukas, for your help and amusing discussions; Akanksha at KTH, for sharing in parallel with me our PhD chapter. And to the new PhD students, good luck with your projects!

To my friends in Stockholm, στα κορίτσια μου! Evi, Vicky, Olga, Lorena, Mary, Xenia, Apostolia and Nafsika. Thanks for your care, the laughs, the trips, the weekends and much more. Returning to work on Mondays was always easier after having spent good time with you. And thanks to my friends in Zaragoza, specially Vero and Brezo, always there no matter the time and the distance.
To Giannis, for everything I have learned from you, the long discussions and good advices.

Finally, my deepest gratitude to my family for all the fun, care, love and support over the years. Last but most important, thanks to my parents for their unconditional support and endless love.

7 References

1. Conway, B.R., *Solid Dosage Forms*, in *Pharmaceutical Manufacturing Handbook*. 2007, John Wiley & Sons, Inc. p. 233-265.
2. Bittorf, K.J., T. Sanghvi, and J.P. Katstra, *Design of Solid Dosage Formulations*, in *Chemical Engineering in the Pharmaceutical Industry*. 2010, John Wiley & Sons, Inc. p. 673-702.
3. Gad, S.C., *Pharmaceutical Manufacturing Handbook Production and Processes*. Pharmaceutical Development Series. 2008, Hoboken: Hoboken : Wiley.
4. Çelik, M., *Pharmaceutical powder compaction technology*. 2016: CRC Press.
5. Fishburn, A.G., *Chapter 6 - Solid Formulations*, in *An Introduction to Pharmaceutical Formulation*. 1965, Pergamon. p. 81-116.
6. Andrews, G.P., *Advances in Solid Dosage Form Manufacturing Technology*. Philosophical Transactions: Mathematical, Physical and Engineering Sciences, 2007. 365(1861): p. 2935-2949.
7. Zhang, G.G.Z., et al., *Phase transformation considerations during process development and manufacture of solid oral dosage forms.* Advanced Drug Delivery Reviews, 2004. 56(3): p. 371-390.
8. *Pharmaceutics : the science of dosage form design*. 2. ed.. ed, ed. M.E. Aulton. 2002, Edinburgh: Edinburgh : Churchill Livingstone.
9. Seibert, K.D., P.C. Collins, and E. Fisher, *Milling Operations in the Pharmaceutical Industry*, in *Chemical Engineering in the Pharmaceutical Industry*. 2010, John Wiley & Sons, Inc. p. 365-378.
10. *Granulation*, in *Applications of Fluidization to Food Processing*. 2007, Blackwell Science Ltd. p. 139-184.
11. Emady, H., K. Hapgood, and R. Smith, *Granulation and Tabletting*, in *Production, Handling and Characterization of Particulate Materials*, G.H. Merkus and M.H.G. Meesters, Editors. 2016, Springer International Publishing: Cham. p. 107-136.
12. Mangal, H., M. Kirsolak, and P. Kleinebudde, *Roll compaction/dry granulation: Suitability of different binders.* International Journal of Pharmaceutics, 2016. 503(1-2): p. 213-219.
13. Kleinebudde, P., *Roll compaction/dry granulation: pharmaceutical applications.* European Journal of Pharmaceutics and Biopharmaceutics, 2004. 58(2): p. 317-326.
14. Shah, S. and A.M. Repka, *Melt Extrusion in Drug Delivery: Three Decades of Progress*, in *Melt Extrusion: Materials, Technology and Drug Product Design*, A.M. Repka, N. Langley, and J. DiNunzio, Editors. 2013, Springer New York: New York, NY. p. 3-46.

15. Patil, H., R.V. Tiwari, and M.A. Repka, *Hot-Melt Extrusion: from Theory to Application in Pharmaceutical Formulation.* AAPS PharmSciTech, 2016. 17(1): p. 20-42.
16. Van'T Land, C.M., *Spray Drying*. 2012, Hoboken, NJ, USA: Hoboken, NJ, USA: John Wiley & Sons, Inc. 133-162.
17. Sloth, J., et al., *Spray Drying of Suspensions for Pharma and Bio Products: Drying Kinetics and Morphology.* Industrial & Engineering Chemistry Research, 2009. 48(7): p. 3657-3664.
18. Oetjen, G.-W. and P. Haseley, *Pharmaceutical, Biological and Medical Products*, in *Freeze-Drying*. 2007, Wiley-VCH Verlag GmbH & Co. KGaA. p. 295-344.
19. Oetjen, G.-W. and P. Haseley, *Foundations and Process Engineering*, in *Freeze-Drying*. 2007, Wiley-VCH Verlag GmbH & Co. KGaA. p. 1-75.
20. Barling, D., D.A.V. Morton, and K. Hapgood, *Pharmaceutical dry powder blending and scale-up: Maintaining equivalent mixing conditions using a coloured tracer powder.* Powder Technology, 2015. 270, Part B: p. 461-469.
21. Yijie, G., F.J. Muzzio, and M.G. Ierapetritou, *Scale-up strategy for continuous powder blending process.* Powder Technology, 2013. 235: p. 55-69.
22. *Pharmaceutical Dosage Forms : Tablets, Volume 3 : Manufacture and Process Control (3rd Edition)*. 2008, New York, NY, USA: CRC Press.
23. Liu, Z., et al., *Modeling and Optimization of a Tablet Manufacturing Line.* Journal of Pharmaceutical Innovation, 2011. 6(3): p. 170-180.
24. Suzzi, D., S. Radl, and J.G. Khinast, *Local analysis of the tablet coating process: Impact of operation conditions on film quality.* Chemical Engineering Science, 2010. 65(21): p. 5699-5715.
25. Dubey, A., et al., *Improvement of Tablet Coating Uniformity Using a Quality by Design Approach.* AAPS PharmSciTech, 2012. 13(1): p. 231-246.
26. Boehling, P., et al., *Analysis of large-scale tablet coating: Modeling, simulation and experiments.* European Journal of Pharmaceutical Sciences, 2016. 90: p. 14-24.
27. Seisakusho, K. *What is rotatory press?* 2005 [cited 2017 February 09]; Available from: http://www.kikusui.com/en/pro_info/tabpress.asp.
28. Pitt, K. and C. Sinka, *Chapter 16 Tabletting*, in *Handbook of Powder Technology*, M.J.H. A.D. Salman and J.P.K. Seville, Editors. 2007, Elsevier Science B.V. p. 735-778.
29. Juban, A., et al., *Predictive model for tensile strength of pharmaceutical tablets based on local hardness measurements.* International Journal of Pharmaceutics, 2015. 490(1-2): p. 438-445.

30. Sinka, I.C., et al., *Measurement of density variations in tablets using X-ray computed tomography.* International Journal of Pharmaceutics, 2004. 271(1): p. 215-224.
31. Klinzing, G.R., et al., *Temperature and density evolution during compaction of a capsule shaped tablet.* Computers and Chemical Engineering, 2010. 34(7): p. 1082-1091.
32. Dudhat, S.M., C.N. Kettler, and R.H. Dave, *To Study Capping or Lamination Tendency of Tablets Through Evaluation of Powder Rheological Properties and Tablet Mechanical Properties of Directly Compressible Blends.* AAPS PharmSciTech, 2016.
33. Slashme. *Tablet failure*. 2007 [cited 2017 February 10]; Available from: https://commons.wikimedia.org/wiki/File:Tabletfailure.jpg#filelinks.
34. Boughton, P. *Quality by design in tableting*. 2015 [cited 2017 February 10]; Available from: http://www.scientistlive.com/content/quality-design-tableting.
35. Haywood, A. and B.D. Glass, *Pharmaceutical excipients – where do we begin?* Australian Prescriber, 2011. 34(4): p. 112-114.
36. Narang, S.A. and H.S. Boddu, *Excipient Applications in Formulation Design and Drug Delivery*, in *Excipient Applications in Formulation Design and Drug Delivery*, S.A. Narang and S.S.H. Boddu, Editors. 2015, Springer International Publishing: Cham. p. 1-10.
37. Mattsson, S., *Pharmaceutical binders and their function in directly compressed tablets: Mechanistic studies on the effect of dry binders on mechanical strength, pore structure and disintegration of tablets.* 2000.
38. Fishburn, A.G., *Chapter 5 - Colours, Flavours and Preservatives*, in *An Introduction to Pharmaceutical Formulation*. 1965, Pergamon. p. 61-80.
39. Alderborn, G. and C. Nystrom, *Pharmaceutical Powder Compaction Technology*. 1996.
40. Hiestand, E.N., *Mechanical Properties of Compacts and Particles that Control Tableting Success.* Journal of Pharmaceutical Sciences, 1997. 86(9): p. 985-990.
41. Mohan, S., *Compresion physics of pharmaceutical powders: A review.* International Journal of Pharmaceutical Sciences and Research, 2012. 3(6): p. 1580-1592.
42. Banker, G.S., J. Siepmann, and C. Rhodes, *Modern pharmaceutics*. 2002: CRC Press.
43. Tye, C.K., C. Sun, and G.E. Amidon, *Evaluation of the effects of tableting speed on the relationships between compaction pressure, tablet tensile strength, and tablet solid fraction.* Journal of Pharmaceutical Sciences, 2005. 94(3): p. 465-472.
44. Podczeck, F., *Particle-particle adhesion in pharmaceutical powder handling*. 1998: World Scientific.

45. Mittal, K.L. and R. Jaiswal, *Particle adhesion and removal*. 2015: John Wiley & Sons.
46. Ålander, E. and Å. Rasmuson, *Agglomeration and adhesion free energy of paracetamol crystals in organic solvents.* American Institute of Chemical Engineers. AIChE Journal, 2007. 53(10): p. 2590.
47. Wildfong, P.L.D., et al., *Towards an understanding of the structurally based potential for mechanically activated disordering of small molecule organic crystals.* Journal of Pharmaceutical Sciences, 2006. 95(12): p. 2645-2656.
48. Etzler, F.M. and M.N. Uddin, *Powder Technology and Pharmaceutical Development: Particle Size and Particle Adhesion.* KONA Powder and Particle Journal, 2013. 30(0): p. 125-143.
49. Badal Tejedor, M., et al., *Tablet mechanics depend on nano and micro scale adhesion, lubrication and structure.* International Journal of Pharmaceutics, 2015. 486(1–2): p. 315-323.
50. Hopf, J. and E.M. Pierce, *Topography and Mechanical Property Mapping of International Simple Glass Surfaces with Atomic Force Microscopy.* Procedia Materials Science, 2014. 7: p. 216-222.
51. Chow, E.H.H., D.-k. Buar, and W. Jones, *New opportunities in crystal engineering the role of atomic force microscopy in studies of molecular crystals.* Chemical Communications, 2012. 48(74): p. 9210-9226.
52. Zhang, J., et al., *Determination of the Surface Free Energy of Crystalline and Amorphous Lactose by Atomic Force Microscopy Adhesion Measurement.* Pharmaceutical Research, 2006. 23(2): p. 401-407.
53. Weiss, C., P. McLoughlin, and H. Cathcart, *Characterisation of dry powder inhaler formulations using atomic force microscopy.* International Journal of Pharmaceutics, 2015. 494(1): p. 393-407.
54. Moribe, K., et al., *Structural evaluation of probucol nanoparticles in water by atomic force microscopy.* International Journal of Pharmaceutics, 2012. 427(2): p. 365-371.
55. Thoorens, G., et al., *Microcrystalline cellulose, a direct compression binder in a quality by design environment—A review.* International Journal of Pharmaceutics, 2014. 473(1–2): p. 64-72.
56. Wong, S.Y. and R.W. Hartel, *Crystallization in Lactose Refining—A Review.* Journal of Food Science, 2014. 79(3): p. R257-R272.
57. Price, R. and P.M. Young, *Visualization of the crystallization of lactose from the amorphous state.* Journal of Pharmaceutical Sciences, 2004. 93(1): p. 155-164.
58. Rasenack, N. and B.W. Müller, *Ibuprofen crystals with optimized properties.* International Journal of Pharmaceutics, 2002. 245(1): p. 9-24.

59. Pazesh, S., et al., *Considerations on the quantitative analysis of apparent amorphicity of milled lactose by Raman spectroscopy.* International Journal of Pharmaceutics, 2016. 511(1): p. 488-504.
60. Yoshida, A., *Non-Invasive Imaging of F-Actin Dynamics in Living Cells by Atomic Force Microscopy*. 2015. p. 453a-453a.
61. Mahlin, D., et al., *Moisture-Induced Surface Crystallization of Spray-Dried Amorphous Lactose Particles Studied by Atomic Force Microscopy.* Journal of Pharmaceutical Sciences, 2004. 93: p. 29-37.
62. Rutland, M.W., et al., *Surface force measurements between cellulose surfaces using scanning probe microscopy.* Colloids and Surfaces A: Physicochemical and Engineering Aspects, 1997. 123: p. 369-374.
63. Nordgren, N. and M.W. Rutland, *Tunable nanolubrication between dual-responsive polyionic grafts.* Nano letters, 2009. 9(8): p. 2984.
64. Álvarez-Asencio, R., et al., *Nanomechanical properties of human skin and introduction of a novel hair indenter.* Journal of the Mechanical Behavior of Biomedical Materials, 2016. 54: p. 185-193.
65. Derjaguin, B.V., V.M. Muller, and Y.P. Toporov, *Effect of contact deformations on the adhesion of particles.* Journal of Colloid And Interface Science, 1975. 53(2): p. 314-326.
66. Muller, V.M., B.V. Derjaguin, and Y.P. Toporov, *On two methods of calculation of the force of sticking of an elastic sphere to a rigid plane.* Colloids and Surfaces, 1983. 7(3): p. 251-259.
67. Butt, H.-J., B. Cappella, and M. Kappl, *Force measurements with the atomic force microscope: Technique, interpretation and applications.* Surface Science Reports, 2005. 59(1): p. 1-152.
68. Cappella, B. and G. Dietler, *Force-distance curves by atomic force microscopy.* Surface Science Reports, 1999. 34(1–3): p. 1-104.
69. Ducker, W.A., T.J. Senden, and R.M. Pashley, *Direct measurement of colloidal forces using an atomic force microscope.* Nature, 1991. 353(6341): p. 239.
70. Derjaguin, B., *Untersuchungen über die Reibung und Adhäsion, IV.* Kolloid-Zeitschrift, 1934. 69(2): p. 155-164.
71. Ralston, J., et al., *Atomic force microscopy and direct surface force measurements (IUPAC Technical Report).* Pure and Applied Chemistry, 2005. 77(12): p. 2149-2170.
72. Karapetian, S.S. and Y.I. Korostelin, *The dependence of the friction coefficient on the crystal structure of solids: Physical principles.* Wear, 1983. 85(2): p. 133-141.
73. Bunker, M.J., et al., *A nanoscale study of particle friction in a pharmaceutical system.* International Journal of Pharmaceutics, 2006. 325(1 2): p. 163.
74. Sader, J.E., J.W.M. Chon, and P. Mulvaney, *Calibration of rectangular atomic force microscope cantilevers.* Review of Scientific Instruments, 1999. 70(10): p. 3967-3969.

75. Pettersson, T., et al., *Comparison of different methods to calibrate torsional spring constant and photodetector for atomic force microscopy friction measurements in air and liquid.* Rev Sci Instrum, 2007. 78(9): p. 093702.
76. Jager, P.D., T. Bramante, and P.E. Luner, *Assessment of Pharmaceutical Powder Flowability using Shear Cell-Based Methods and Application of Jenike's Methodology.* Journal of Pharmaceutical Sciences, 2015. 104(11): p. 3804-3813.
77. Schulze, D., *Powders and Bulk Solids: Behavior, Characterization, Storage and Flow*. Behavior, Characterization, Storage and Flow. 2008, Berlin, Heidelberg: Springer Berlin Heidelberg: Berlin, Heidelberg.
78. Ward, S., et al., *Identifying and Mapping Surface Amorphous Domains.* Pharmaceutical Research, 2005. 22(7): p. 1195-202.
79. Ermolina, I. and G. Smith, *Dielectric spectroscopy of low-losses sugar lyophiles: III: The influence of moisture on the dielectric response of freeze-dried lactose.* Journal of Non-Crystalline Solids, 2011. 357(2): p. 671-676.
80. Walstra, P., *Physical chemistry of foods*. 2002: CRC Press.
81. Hancock, B.C. and G. Zografi, *Characteristics and significance of the amorphous state in pharmaceutical systems*. 1997: Journal of pharmaceutical sciences. p. 1-12.
82. Bates, S., et al., *Analysis of Amorphous and Nanocrystalline Solids from Their X-Ray Diffraction Patterns.* Pharmaceutical Research, 2006. 23(10): p. 2333-2349.
83. Shalaev, E. and G. Zografi, *The concept of 'structure' in amorphous solids from the perspective of the pharmaceutical sciences*, in *Amorphous Food and Pharmaceutical Systems*, H. Levine, Editor. 2002, The Royal Society of Chemistry. p. 11-30.
84. Wang, G.D., J.Y.Y. Heng, and D.R. Williams, *Dilatometry of powder compacts — Characterizing amorphous-crystalline transformations.* Powder Technology, 2013. 236: p. 12-16.
85. Sestak, J., *Glassy, Amorphous and Nano-Crystalline Materials Thermal Physics, Analysis, Structure and Properties*. Hot Topics in Thermal Analysis and Calorimetry, Volume 8, ed. J. Mares and P. Hubik. 2010, Dordrecht: Dordrecht : Springer.
86. Gaisford, S., *Isothermal microcalorimetry for quantifying amorphous content in processed pharmaceuticals.* Advanced Drug Delivery Reviews, 2012. 64(5): p. 431-439.
87. Pazesh, S. and G. Alderborn, *Comminution-amorphisation relationships during ball milling of lactose at different stress* in *European Journal of Pharmaceutics and Biopharmaceutics*. 2017. p. Submitted.
88. Willart, J.F., V. Caron, and M. Descamps, *Transformations of crystalline sugars upon milling.* Journal of Thermal Analysis and Calorimetry, 2007. 90(1): p. 125.

89. Vollenbroek, J., et al., *Determination of low levels of amorphous content in inhalation grade lactose by moisture sorption isotherms.* International Journal of Pharmaceutics, 2010. 395(1): p. 62-70.
90. Angberg, M., *Lactose and thermal analysis with special emphasis on microcalorimetry*. Thermochimica Acta, 1995. 248: p. 161-176.
91. Willart, J.F., et al., *Athermal character of the solid state amorphization of lactose induced by ball milling.* Solid State Communications, 2004. 132(10): p. 693-696.
92. Bhattacharya, S. and R. Suryanarayanan, *Local mobility in amorphous pharmaceuticals—characterization and implications on stability*. 2009: Hoboken. p. 2935-2953.
93. Hancock, B.C. and G. Zografi, *The Relationship Between the Glass Transition Temperature and the Water Content of Amorphous Pharmaceutical Solids.* Pharmaceutical Research, 1994. 11(4): p. 471-477.
94. Roblot-Treupel, L. and F. Puisieux, *Distribution of magnesium stearate on the surface of lubricated particles.* International Journal of Pharmaceutics, 1986. 31(1–2): p. 131-136.
95. van der Watt, J.G., *The effect of the particle size of microcrystalline cellulose on tablet properties in mixtures with magnesium stearate.* International Journal of Pharmaceutics, 1987. 36(1): p. 51-54.
96. Dudognon, E., et al., *Solid-solid transformation in racemic Ibuprofen.* Pharmaceutical research, 2013. 30(1): p. 81.
97. Mousa Al-Ibraheemi, Z., et al., *Deformation and Mechanical Characteristics of Compacted Binary Mixtures of Plastic (Microcrystalline Cellulose), Elastic (Sodium Starch Glycolate), and Brittle (Lactose Monohydrate) Pharmaceutical Excipients.* Particulate Science and Technology, 2013. 31(6): p. 561.
98. Eve, J.K., et al., *A study of single drug particle adhesion interactions using atomic force microscopy.* International Journal of Pharmaceutics, 2002. 238(1): p. 17-27.
99. Bunker, M., et al., *Direct Observation of Single Particle Electrostatic Charging by Atomic Force Microscopy.* Pharmaceutical Research, 2007. 24(6): p. 1165-1169.
100. Naik, S., et al., *An experimental and numerical modeling study of tribocharging in pharmaceutical granular mixtures.* Powder Technology, 2016. 297: p. 211-219.
101. Feiler, A., P. Jenkins, and M. Rutland, *Effect of relative humidity on adhesion and frictional properties of micro- and nano-scopic contacts.* Journal of Adhesion Science and Technology, 2005. 19(3): p. 165-179.
102. Rabinovich, Y.I., et al., *Capillary forces between surfaces with nanoscale roughness.* Advances in Colloid and Interface Science, 2002. 96(1): p. 213-230.

103. Biggs, S., et al., *Direct measurements of the adhesion between a glass particle and a glass surface in a humid atmosphere.* Journal of Adhesion Science and Technology, 2002. 16(7): p. 869-885.
104. Israelachvili, J.N., *Intermolecular and Surface Forces*. 3rd ed.. ed. Intermolecular and Surface Forces. 2010, Burlington: Burlington : Elsevier Science.
105. Feiler, A.A., et al., *Effect of capillary condensation on friction force and adhesion.* Langmuir : the ACS journal of surfaces and colloids, 2007. 23(2): p. 517.
106. Paul, S., et al., *Mechanism and Kinetics of Punch Sticking of Pharmaceuticals.* Journal of Pharmaceutical Sciences, 2016.

Apendix I

AFM parameters

Different scan rates were set to test the quality of the image and mechanical data in a reference area of the scanned sample. For each of the set scan rates at different scan sizes the AFM software sets a tip velocity. The correspondence between different scan sizes and tip velocities at 50 µm and 10 µm scan size is presented in the following table:

Table 1. Scan rate that corresponds to each tip velocity for the scan sizes of 50 µm and 10 µm.

50 µm scan size		**10 µm scan size**	
Tip velocity(µm/s)	*Scan rate (Hz)*	*Tip velocity(µm/s)*	*Scan rate (Hz)*
39.9	0.359	39.1	1.76
36.2	0.326	35.5	1.60
33.1	0.298	32.6	1.46
27.1	0.244	26.0	1.17
21.9	0.198	15.0	0.676
15.0	0.135	11.2	0.502
11.1	0.0999	7.23	0.326
		3.00	0.135

An increase of the adhesion was observed at an increased number of contacts per pixel when scanning the same area (50 µm) – which indicates that a certain caution should be emloyed.

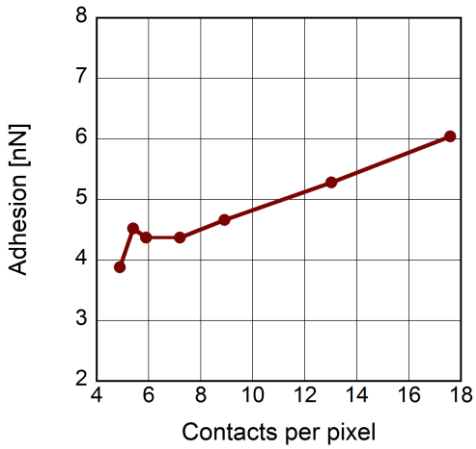

Figure 1. Adhesion values vs. contacts per pixel calculated for a 50 µm scan size.

Apendix II

Flowability

Free flowing powders facilitate the filling of the die during tableting avoiding weight variation of the pressed tablets. Flowability is influenced by the size, shape and surface properties of the particles. The figure shows the flowability of several excipients and ibuprofen which are in the focus of the present study. Flowability is characterized numerically using the flow function coefficient ratio ($ff_c = \sigma_1/\sigma_c$). The powders categorized as free flowing present a ff_c equal or higher than 10 such as MCC, commercial spray dried lactose and mannitol. Ibuprofen show less flowability although still showing easy flowing properties with a ff_c close to 10. Poor flowing powder present a ff_c lower or equal to 2. The more cohesive powder is α-lactose monohydrate which ff_c is slightly higher than 2. The addition of a small portion (1%) of lubricant (MgSt) to the powders does not affect their flowing behavior.

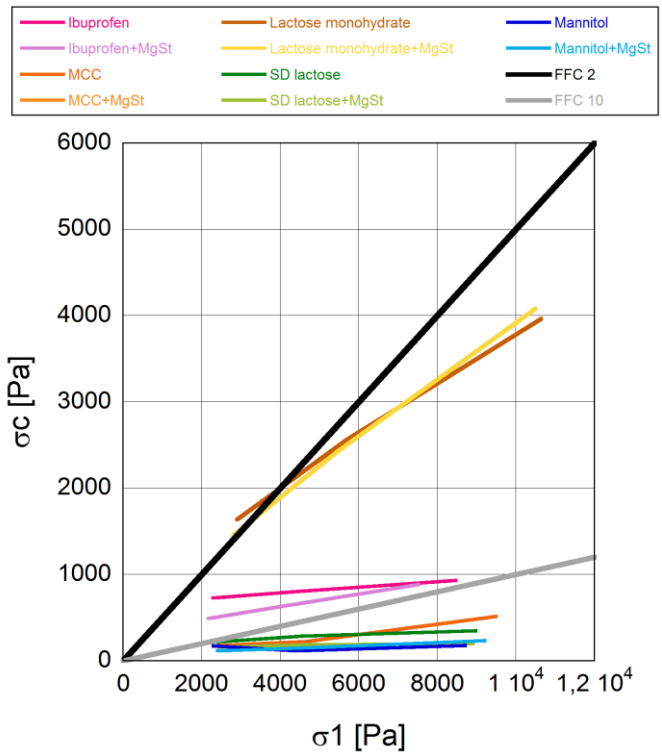

Figure 1. Shear cell measurements in pure ibuprofen, α-lactose monohydrate, MCC, commercial spray dried lactose, mannitol and these mixed with 1% MgSt. The unconfined yield strength (σ_c) is represented vs. the consolidation stress (σ_1).

Paper I

LANGMUIR

Article

pubs.acs.org/Langmuir

Determination of Interfacial Amorphicity in Functional Powders

Maria Badal Tejedor,[†,‡] Niklas Nordgren,[†] Michael Schuleit,[§] Samaneh Pazesh,[∥] Göran Alderborn,[∥] Anna Millqvist-Fureby,[†] and Mark W. Rutland*[,†,‡]

[†]SP Chemistry, Materials and Surfaces, SP Technical Research Institute of Sweden, Box 5607, SE-114 86 Stockholm, Sweden

[‡]Division of Surface and Corrosion Science, KTH Royal Institute of Technology, Drottning Kristinas väg 51, SE-100 44 Stockholm, Sweden

[§]Novartis Institutes for Biomedical Research, GDC, Novartis Pharma AG, Novartis Campus, 4002 Basel, Switzerland

[∥]Department of Pharmacy, Uppsala University, Uppsala, Sweden

ABSTRACT: The nature of the surfaces of particles of pharmaceutical ingredients, food powders, and polymers is a determining factor for their performance in for example tableting, powder handling, or mixing. Changes on the surface structure of the material will impact the flow properties, dissolution rate, and tabletability of the powder blend. For crystalline materials, surface amorphization is a phenomenon which is known to impact performance. Since it is important to measure and control the level of amorphicity, several characterization techniques are available to determine the bulk amorphous content of a processed material. The possibility of characterizing the degree of amorphicity at the surface, for example by studying the mechanical properties of the particles' surface at the nanoscale, is currently only offered by atomic force microscopy (AFM). The AFM PeakForce QNM technique has been used to measure the variation in energy dissipation (eV) at the surface of the particles which sheds light on the mechanical changes occurring as a result of amorphization or recrystallization events. Two novel approaches for the characterization of amorphicity are presented here. First, since particles are heterogeneous, we present a methodology to present the results of extensive QNM analysis of multiple particles in a coherent and easily interpreted manner, by studying cumulative distributions of dissipation data with respect to a threshold value which can be used to distinguish the crystalline and amorphous states. To exemplify the approach, which is generally applicable to any material, reference materials of purely crystalline α-lactose monohydrate and completely amorphous spray dried lactose particles were compared to a partially amorphized α-lactose monohydrate sample. Dissipation data are compared to evaluations of the lactose samples with conventional AFM and SEM showing significant topographical differences. Finally, the recrystallization of the surface amorphous regions in response to humidity was followed by studying the dissipation response of a well-defined surface region over time, which confirms both that dissipation measurement is a useful measure of surface amorphicity and that significant recrystallization occurs at the surface in response to humidity.

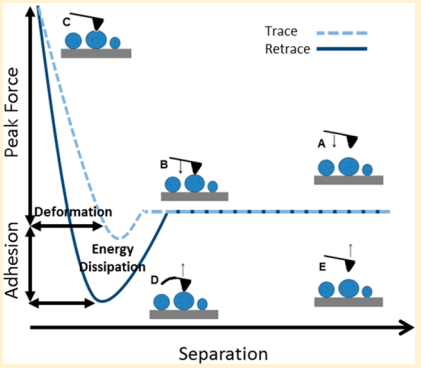

INTRODUCTION

Powder surface properties determine the handling and processing behavior of the powder blend during the manufacturing of for example solid pharmaceutical forms, food, and polymer powders. Unpredictable behavior of the powders due to changes in particle surface properties results in deviations from the final product requirements and poor performance of the powder, thus increasing manufacturing costs.[1,2] Preprocessing of the powders is usually performed to improve powder flowability, avoid powder segregation, and improve, for instance, tableting compaction and stability of the pharmaceutical forms; however, particle surface modifications can occur as an undesired event during some of the preprocessing stages.[3] The materials suffering from undesired surface modifications such as changes in surface energy, transformation from crystalline to amorphous structure, variations in particle physicochemical properties, and surface roughness may alter their cohesiveness and adhesive behavior, hygroscopicity, and mechanical properties under compaction.[4,5] These result in modification of the powder flow, compatibility, and long-term stability properties.[1,2] Thus, it is important to control and evaluate particle surface properties of the processed powders so as to avoid low quality finished solid forms and unexpected problems during manufacturing.

Preprocessing designed to control, for example, the particle size can often require large energy inputs leading to significant amorphization at the surface and bulk.[6] Such changes in material surface and bulk properties affect product manufacturing and the characteristics of the final product. The lower energy state of the crystalline structure favors recrystallization of the amorphous material, adding a certain instability into the system at specific relative humidity and temperature conditions.[7] This is not desirable considering that crystalline and amorphous structural conformations of the same substance

Received: November 2, 2016
Revised: December 22, 2016
Published: January 3, 2017

© 2017 American Chemical Society

DOI: 10.1021/acs.langmuir.6b03969
Langmuir 2017, 33, 920−926

have shown different dissolution rates, flowability properties, tablet tensile strength, and stability, with additional risk of lump formation during storage.[8] Therefore, quantification of the amorphous content and understanding of the amorphization mechanisms are highly relevant and have been reviewed in previous studies.[9−11]

Different analytical techniques have been used to evaluate the amorphous content of a particulate material. Some examples are differential scanning calorimetry and isothermal microcalorimetry, which show the thermal events of the powders upon heating which are related to the nature of the molecules and their spatial conformation.[12] Other methods are near-infrared spectroscopy (NIR), Raman spectroscopy, and solid-state NMR for which analytical methodologies based on mathematical models have been developed.[13,14] Another method employed is dynamic vapor sorption that uses the sorption or recrystallization events of the amorphous phase at optimal ambient conditions in order to quantify the degree of amorphicity.[15]

These methods, however, probe bulk amorphicity, rather than the degree of amorphicity at the surface, which is likely to be most important for powder behavior. Notable among the characterization techniques sensitive to surface changes in particle amorphicity is inverse gas chromatography;[16] however, other surface-sensitive techniques have rarely been applied for characterization of surface amorphicity of powders. An exception is the technique of atomic force microscopy (AFM): a surface-sensitive microscopy technique able to measure material surface properties at the nanoscale.[17−19]

The present study develops an approach for evaluating particle surface amorphicity using AFM. A commonly used excipient, α-lactose monohydrate, has been used in three different forms: crystalline, partially amorphized, and completely amorphous (spray-dried). Unprocessed crystalline and spray-dried lactose thus serve as references for fully crystalline and amorphous lactose. The nanomechanical information provided by the PeakForce QNM AFM technique and the topography of the particles visualized with both AFM and SEM were used to analyze the samples, and to follow the recrystallization of amorphous material in response to humidity.

EXPERIMENTAL SECTION

Materials. The material used in the present study is α-lactose monohydrate which is a commonly used excipient in oral dosage formulations. α-Lactose monohydrate was purchased from DFE Pharma (Veghel, Netherlands). The partially amorphized sample was produced by milling for 1 h according to a method described earlier.[20] After milling the sample was stored in a desiccator over P_2O_5 in order to maintain a dry atmosphere below 5% relative humidity to prevent material changes caused by ambient humidity over time. Amorphous lactose was prepared by spray drying a 10% (w/w) aqueous solution of α-lactose monohydrate using a Büchi Mini Spray Dryer B-290 advance (Büchi Labortechnik AF, Glawil, Switzerland). The feed was pumped with a rate of 4 mL/min, and the flow of dry air was set to 40 L/min with an inlet and outlet temperature of 170 and 98 °C, respectively. The collected powder was stored in a desiccator under 0−5% relative humidity controlled with P_2O_5.

Scanning Electron Microscopy. The morphology of the powder samples was examined by scanning electron microscopy (FEI-XL, 30 series) in high vacuum with an accelerated voltage of 5 kV. Before imaging, the samples were sprinkled on a double-sided tape mounted on an aluminum holder and blown out with nitrogen gas to remove the excess of powder. To allow evaluation at high magnifications without damaging the sample, they were gold coated (120 s, 40 mA) using a Balzers SCD050 coater.

Atomic Force Microscopy. Surface analyses of the nanomechanical properties of the particulate samples were conducted using a Multimode 8 atomic force microscope equipped with a Nanoscope V controller (Bruker, Santa Barbara, CA) operated in PeakForce QNM (Quantitative Nanomechanical Property Mapping) mode. The cantilevers used were of type HQ-NSC 14/AlBS, Mikromasch (Estonia), with a silicon nitride tip (radius of approximately 8 nm). The spring constants of the cantilevers were calibrated using the technique of Sader.[21,22] A maximum force (i.e., PeakForce) of 24 nN was applied at each oscillation. Each oscillation is represented by a set of force profiles (normal force as a function of apparent separation) collected from the approach and the retraction paths between the sample and the tip during loading and unloading, respectively. The area between the loading and unloading curves is a measure of the surface energy dissipation (eV).

The settings used during the measurements were a scan rate of approximately 0.5 Hz and a PeakForce tapping frequency of 2 kHz at scan size of 2 × 2 μm. The dissipation at each scan is an average value of the dissipation data collected at each force cycle along the whole scanned area. The dissipation is averaged at each pixel and each scan consists of 512 × 512 pixels. Multiple particles were analyzed for each sample type, and the images were collected at three different surface locations for each particle. Further evaluation of the scanned areas was performed by using the bearing analysis tool available in the Nanoscope Analysis 1.4 (Bruker) software. This tool allows for calculating the area percentage of values above a set threshold in the scan.

The powder samples were sprinkled on a double-sided sticky tape mounted on a metallic holder for AFM evaluation. The excess of loose powder sitting on the tape was blown off with N_2. The particles or group of particles selected for AFM evaluation were of a minimum dimension of 50 μm. This is due to optical limitations to land the tip (cantilever width of 30 μm) on the particle surface.

The size of spray dried lactose particle is smaller than the width of the cantilever; therefore, it was only feasible to approach the cantilever toward a group or agglomerate of particles. In some cases the scans would transcend edges between particles, and these scans were not used due to uncertainty concerning image artifacts. So data were collected only from scans where the evaluated area belonged to a single particle. The scans were of 2 μm size which necessarily exclude the finest particles.

The measurements were performed under controlled ambient conditions (temperature 25 ± 1 °C and relative humidity 20 ± 2%) in order to avoid recrystallization of the lactose during the experiment. However, in order to investigate the potential effects of surface recrystallization at higher relative humidity, continuous PeakForce QNM imaging was conducted in the same area over a 48 h period under controlled relative humidity of 55−60%.

RESULTS AND DISCUSSION

The surface features of the unprocessed, partially amorphized, and spray dried lactose particles are displayed in the SEM micrographs (Figure 1). The crystalline sample (α-lactose monohydrate, Figure 1a) presents regular shaped particles with smooth surfaces that show scattered micrometer size particles adhered on top.

The partially amorphized displayed a more rounded morphology. The surfaces of the particles appeared to be covered by small fragments of material resulting from the amorphization processing (Figure 1b). The appearance of some of these fragments is sharp and edged particles while others display a more rounded morphology. The spray dried particles (amorphous particles) show an almost perfect spherical shape and a very smooth surface (Figure 1c).

Topographical differences may result in differences in mechanical properties that can be simultaneously evaluated by using AFM. The characteristic topographical features

DOI: 10.1021/acs.langmuir.6b03969
Langmuir 2017, 33, 920−926

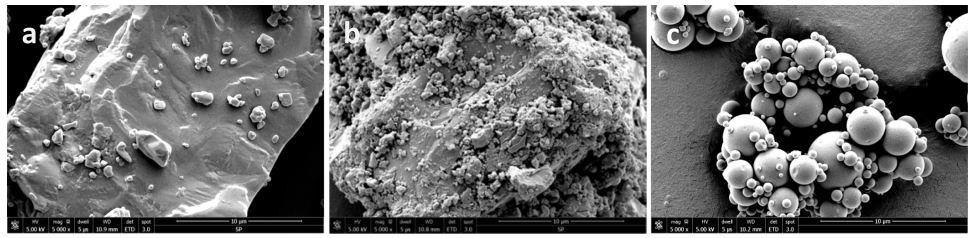

Figure 1. SEM images of α-lactose monohydrate: (a) crystalline, (b) partially amorphized, and (c) amorphous. The micrographs are taken at the same magnification with a scale bar of 10 μm.

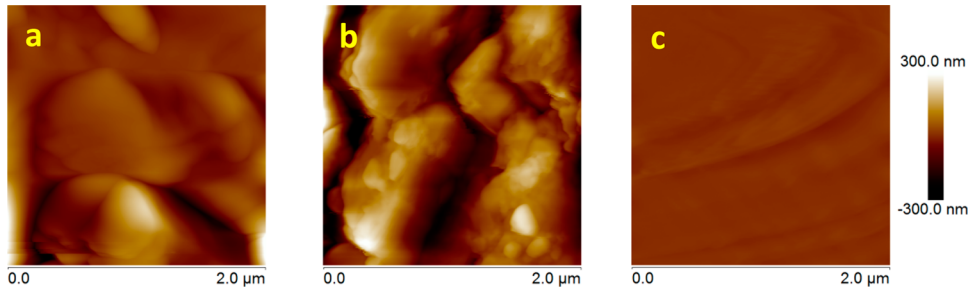

Figure 2. AFM topography images: (a) crystalline, (b) partially amorphized, and (c) amorphous lactose.

observed in the SEM images were also found using AFM imaging at about 5 times higher magnification. Representative examples of topographical AFM images for the three different systems are displayed in Figure 2. The evaluated areas for the crystalline α-lactose monohydrate with AFM showed bulky features with a smooth surface (Figure 2a). The surface of the partially amorphized particles becomes rougher and smaller features appear (Figure 2b). For the purely amorphous lactose (Figure 2c), a much smoother surface was observed in comparison to the other two systems and without any of the protrusions characteristic of the former.

The three-dimensional organization of the molecules results in various topographical features. The α-lactose molecules are fixed in a defined crystal lattice, which results in angular particles with relatively flat and smooth surfaces. The amorphous character of the spray-dried lactose allows for smoothly shaped particles, where the particle morphology is determined by the droplet size and lactose concentration in the spray dryer.[23]

Crystalline and amorphous structural conformations at the molecular level allow for a potentially different degree of freedom for displacement of the molecules when an external force is applied[18] and is known to affect the physical and chemical properties of the materials, for example, the viscoelastic properties.[3] The water content and its distribution differ between both structures contributing to the mobility of the lactose molecules which has implications for the material viscosity.[24,25] In the case of the α-lactose monohydrate, the major part of the water content is incorporated into the crystal lattice by 1:1 association of a water molecule to each lactose molecule leading to a less moisture sensitive and rigid structure. In the amorphous form of the lactose the total water content is distributed within the randomly organized molecular structure allowing higher mobility. This is reflected in the thermodynamic behavior of the two different forms.[26] A higher spatial mobility of the molecules into a nonorganized structure would imply variations in deformation as a response to an external applied load. Previous studies have used the elastic modulus to report the differences in deformation of pharmaceutical excipients in its crystalline and amorphous form.[18,27] These measurements showed lower values of the elastic modulus for the amorphous than for the crystalline samples. Therefore, at the same applied force a larger deformation is more likely to occur for the amorphous form of a material than in its crystalline state. The loss of energy during an AFM surface force measurement is referred to as the energy dissipation; this is related to both the surface deformation and adhesion properties of the sample. The origin of the mechanical properties discrimination inferred by "dissipation" is the hysteresis of the force measurements collected at each pixel and the stability of this deviation on each approach and retraction cycle between the tip and the sample (see graphical abstract). The magnitude of the hysteresis between the approach and retraction curve at positive (repulsive) force values depends on the viscoelastic deformation of the system. The adhesion component at negative force also contributes to the dissipation which for plastic deformation can also be dependent on the increase of the contact area. Note that according to the definition of dissipation used here, dissipation is not necessarily associated with irreversible deformation of the sample, and in general this is related to the magnitude of the peak force. Thus, when dissipation presents larger values, those are mostly related to a larger deformation component.[28] Therefore, by measuring the energy dissipation, the particle surface amorphous content could potentially be estimated.

In order to explore this possibility PeakForce QNM analyses were performed (Figure 3). The magnitude of the energy dissipation data is represented using a color code which is overlaid on top of the topographical 3D images. Darker colors correspond to lower energy dissipation values while higher energy dissipation is presented with lighter color. The highest dissipation values are shown in light blue. In order to evaluate whether energy dissipation is a useful parameter for studying surface amorphicity, certain assumptions about the samples have to be made. As a reference for evaluation of the partially amorphous sample, model samples for the crystalline and the amorphous states of the lactose were used—the crystalline α-lactose monohydrate and the amorphous spray-dried sample.

DOI: 10.1021/acs.langmuir.6b03969
Langmuir 2017, 33, 920−926

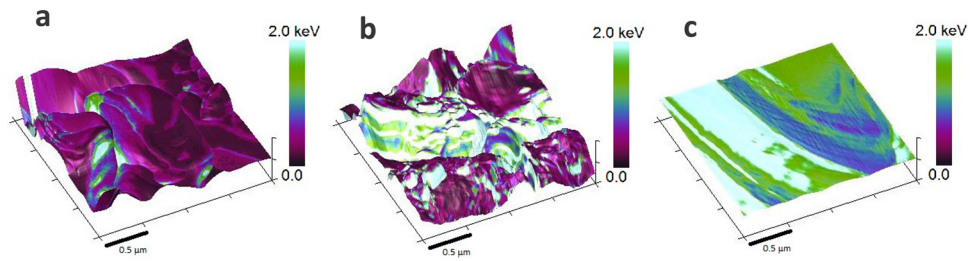

Figure 3. AFM PeakForce QNM dissipation maps overlay the 3D plot representation of the AFM surface topography: (a) crystalline lactose, (b) partially amorphized lactose, and (c) amorphous lactose. The vertical scale refers to the dissipation values and has units of energy.

The assumptions of fully crystalline and amorphous compositions are made even though in pharmaceutical solids both forms may coexist even in small portions for predominantly crystalline or amorphous structures.[3] The assumptions appear broadly justified since significant differences in energy dissipation on the reference samples were observed (Figure 3). The energy dissipation of the partially amorphized samples however fell between the measured dissipation on the crystalline and amorphous samples. There were also well-defined regions in each of the various scans measured on the partially amorphized sample showing low-energy dissipation and high-energy dissipation values. The energy dissipation values in those regions were comparable to the ones measured on the crystalline and the amorphous references.

To evaluate the degree of amorphicity *per image*, it is rather straightforward to perform a bearing analysis in terms of a threshold value that is identified as being characteristic of the difference of the two regions. Figure 4 is an example of such an

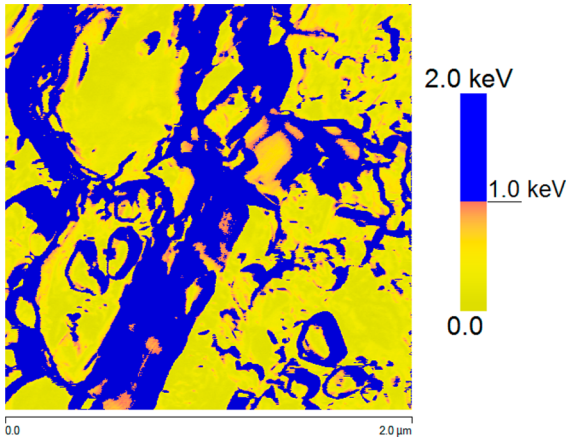

Figure 4. Dissipation map obtained using AFM PeakForce QNM of the partially amorphous sample after which the bearing analysis tool has been applied using a bearing depth of 1000 eV. The blue regions depict dissipation values above 1000 eV covering 40% of the image.

area where the threshold value of 1000 eV has been chosen (on the basis of examining multiple images such as those seen in Figure 3). In this image it can be seen that 40% of the image has a dissipation which has been assigned to "amorphicity".

While such images clearly show the differences in dissipation between the various samples, they are not in themselves sufficient to provide a statistically significant description of the surface properties. A larger number of images on a number of particles must be taken to obtain such a description. These data then need to be portrayed in a clear and intuitive manner, to allow evaluation of the degree of amorphicity. Such a portrayal of the data is shown in Figure 5 where the same trend is observed when comparing the full set of dissipation data

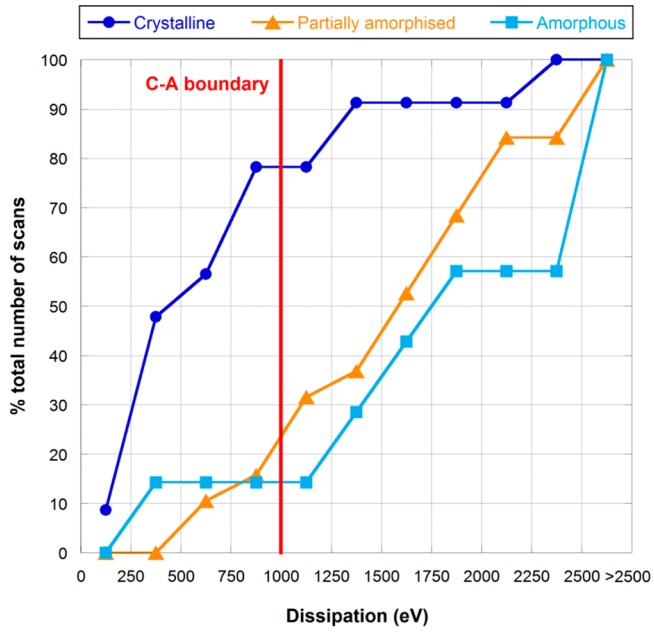

Figure 5. Cumulative distribution of the AFM scanned areas in terms of the average dissipation value for each scan. The vertical line indicates the crystalline−amorphous boundary or threshold value.

collected with AFM from the three different samples. The graph is constructed as follows. The average dissipation of each scan is determined. Since the average dissipation is observed to vary between 0 and 2750 eV in these experiments, each scan is assigned to a bin within this range where the bin width has been arbitrarily selected as 250 eV. The cumulative number of scanned areas vs the binned average dissipation is then plotted. Crystalline α-lactose monohydrate shows a steep increase for the cumulative number of scans at low dissipation values since most of the scans return a low dissipation (reflecting the crystalline nature as discussed above). An opposite trend is observed for the amorphous reference since the majority of scans have a high average dissipation value. Partially amorphous lactose shows a clear intermediate behavior. This provides a means of quantitatively evaluating the different materials in terms of dissipation behavior.

This average dissipation value of the scanned area is useful for evaluating the amorphicity, but in some cases the average can be skewed if, for example, regions of very high dissipation are encountered. In this case it may be preferable to rather use the percentage area of the scan above the amorphicity threshold, instead of the average value, as obtained from

DOI: 10.1021/acs.langmuir.6b03969
Langmuir 2017, 33, 920−926

Figure 5 where the crystalline−amorphous (C−A) boundary was set to 1000 eV. Thus, the level of surface amorphicity for the evaluated sample is estimated by the area percentage with dissipation values above the C−A boundary; the larger the area percentage above the C−A boundary, the higher the level of amorphicity.

Figure 6 shows the cumulative number of the scanned areas vs the area percentage above the C−A boundary for the same

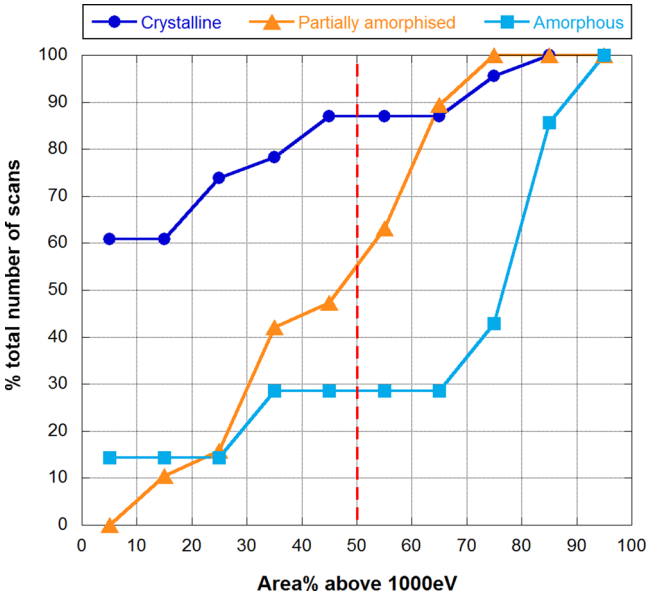

Figure 6. Cumulative distribution of the AFM scanned areas in function of the total area percentage of the scans covered by dissipation values lying above the set C−A threshold for crystalline α-lactose monohydrate, partially amorphized lactose, and amorphous lactose samples.

three samples. Almost 90% of the scans collected from the crystalline lactose present a level of below 50%, and 75% of the collected scans fall below 30% amorphicity (according to the C−A threshold definition). In contrast, only 30% of the scans from the amorphous samples showed amorphicity areas below 50% (and only 15% of the evaluated areas had amorphicity below 30%). For partially amorphized lactose, 50% of the scans showed a level of amorphicity between 5 and 50%, which implies that the other 50% of the data has amorphicity levels in the range of 50−95%. This clearly reflects the distribution of crystalline and amorphous regions and provides a straightforward means of evaluating the degree of surface amorphicity.

It is known that amorphicity reduces due to recrystallization in the presence of humidity. Thus, a further demonstration of the usefulness of dissipation as a measure of surface amorphicity would be if this process could be followed by AFM imaging. In fact, this would have the additional benefit of confirming that the dissipation approach outlined above does in fact reflect the surface amorphicity.

Visual identification is possible through changes from the initial amorphous structure into a well-defined cubic, needle, or tetrahedral shapes characteristic of the crystalline phase. This transition occurs because of the less thermodynamically stable state of the amorphous material, turning into a more stable form of a lower enthalpy.[29] Recrystallization is a time-dependent process where ambient conditions such as temperature and humidity are important to favor the transition.[30] Previous studies have shown that 25 °C temperature and 48% relative humidity are critical points to trigger recrystallization of amorphous lactose.[31] In the present study samples of the partially amorphous lactose were exposed for 48 h to both 50% and 75% relative humidity. The SEM images from the particles before and after exposure are shown in Figure 7. No sharply defined angular forms could be distinguished across the topography of the particles before exposure (Figure 7a) or after exposure at 50% RH for 48 h (Figure 7b). However, storage of the sample at 75% RH for 48 h appeared to trigger recrystallization which resulted in the formation of cubic structures over the surface of the particles (Figure 7c).

The effect of exposure to elevated humidity was thus followed *in situ* in the AFM. The relative humidity was restricted to 55−60% due to the risk of condensation in the electronics of the AFM. The evolution of the dissipation data for 48 h on a single region was tracked over time by continuous PeakForce QNM imaging (Figure 8). Image drift was unavoidable during this continuous imaging period. Thus, only dissipation data which could confidently be assigned to the same region is plotted in Figure 8. The average dissipation of the first scans is above the C−A boundary which indicates the amorphicity of the particle surface and is in fact reminiscent of the very amorphous samples. A sharp decrease in dissipation (to below the C−A threshold) is observed during the first 2 h, and this steep decrease in dissipation continues during the subsequent 2 h. This observation is consistent with earlier studies of humidity-induced changes in amorphicity.[32,33] The dissipation decreases more slowly during the remaining time. After 48 h exposure to elevated RH, the dissipation value is comparable to that characteristic of the crystalline lactose sample. The changes in dissipation over time under favorable ambient conditions for recrystallization confirm the transition from amorphous to crystalline state and the corresponding differences in mechanical properties and thus also that the average dissipation is a highly useful means of quantifying the degree of amorphicity and its temporal evolution.

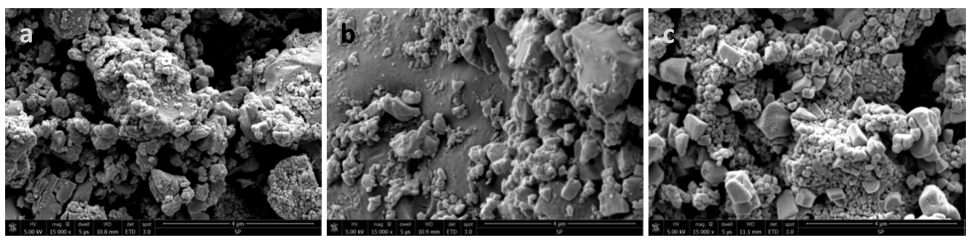

Figure 7. Particle of partially amorphized α-lactose monohydrate: (a) fresh from storage in the desiccator at 0−5% RH, (b) after exposure to 50% RH conditions for 48 h, and (c) after exposure to 75% RH for 48 h.

DOI: 10.1021/acs.langmuir.6b03969
Langmuir 2017, 33, 920−926

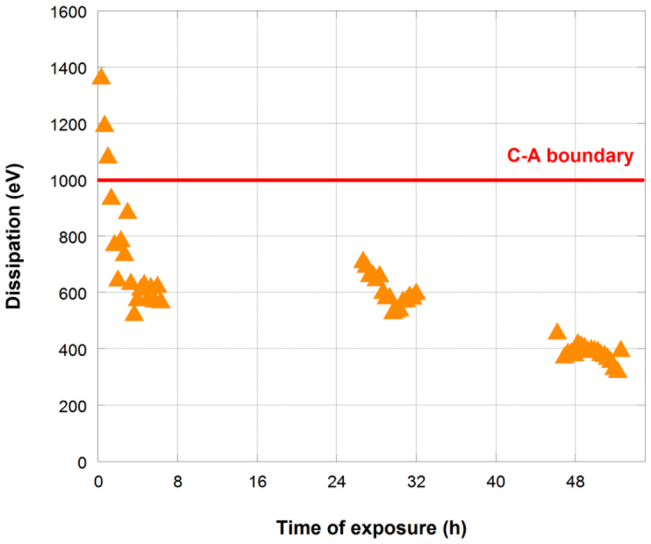

Figure 8. Continuous measurement on the same area of a particle of the partially amorphized sample under conditions of 55−60% RH and 25 °C for 48 h. The size of the evaluated area is 2 × 2 μm and the dissipation values correspond to the average dissipation for each of the collected dissipation maps on the surface of the particle over time.

CONCLUSION

Amorphicity can be observed using SEM, through the morphology of the particles, though surface amorphicity is difficult to identify and impossible to quantify. AFM topography images can distinguish between known regions of amorphicity and crystallinity, but conventional imaging of this nature is of limited used in directly quantifying the degree of surface amorphicity, due to the difficulty of relating topography in a quantitative manner to surface amorphicity. The use of the so-called dissipation parameter of the QNM imaging mode, which is sensitive to a combination of differences in adhesion and material properties, has proven to be useful means of quantifying surface amorphicity because crystalline and amorphous regions vary rather systematically in these properties. It is also clear that individual particles cannot be considered representative of the sample as a whole, and a number of particles and regions need to be probed to provide statistically significant descriptions.

Cumulative distributions of dissipation data, either of average dissipation per scan, or the area per scan above a certain threshold provide a convenient means to graphically compare sample data, particularly when clear, well-defined reference samples are available. The technique is somewhat laborious and is unlikely to be embraced as a routine means of characterizing powder samples in a processing environment or tableting plant. It does, however, provide an unambiguous forensic diagnostic tool for trouble shooting. We demonstrate here that it is useful for characterizing surface amorphicity; however, the approach is generally portable across any sample that consists of a bimodal distribution of surface manifestations, which differ in material properties.

Finally, due to the robustness of the dissipation parameter for characterizing amorphicity, it can also be used *in situ* to study recrystallization processes in real time and therefore provides dynamical information. While other techniques undeniably provide the opportunity to follow sample amorphicity in real time, the surface amorphicity is likely to be the most important parameter governing particle adhesion, flow, and subsequent tablet strength. Thus, the dissipation parameter allows the surface and bulk recrystallization rates to be isolated from one another.

AUTHOR INFORMATION

Corresponding Author

*E-mail mark@kth.se; Tel +46768640081 (M.W.R.).

ORCID

Maria Badal Tejedor: 0000-0001-5894-7123

Notes

The authors declare no competing financial interest.

REFERENCES

(1) Shi, L.; Sun, C. Overcoming Poor Tabletability of Pharmaceutical Crystals by Surface Modification. *Pharm. Res.* **2011**, *28* (12), 3248−3255.

(2) Ghoroi, C.; Gurumurthy, L.; McDaniel, D. J.; Jallo, L. J.; Davé, R. N. Multi-faceted characterization of pharmaceutical powders to discern the influence of surface modification. *Powder Technol.* **2013**, *236*, 63.

(3) Hancock, B. C.; Zografi, G. Characteristics and significance of the amorphous state in pharmaceutical systems. *J. Pharm. Sci.* **1997**, *86*, 1−12.

(4) Sebhatu, T.; Alderborn, G. Relationships between the effective interparticulate contact area and the tensile strength of tablets of amorphous and crystalline lactose of varying particle size. *Eur. J. Pharm. Sci.* **1999**, *8* (4), 235−242.

(5) Fichtner, F.; Mahlin, D.; Welch, K.; Gaisford, S.; Alderborn, G. Effect of Surface Energy on Powder Compactibility. *Pharm. Res.* **2008**, *25* (12), 2750−2759.

(6) Wildfong, P. L. D.; Hancock, B. C.; Moore, M. D.; Morris, K. R. Towards an understanding of the structurally based potential for mechanically activated disordering of small molecule organic crystals. *J. Pharm. Sci.* **2006**, *95* (12), 2645−2656.

(7) Zelkó, R.; Szakonyi, G. The effect of water on the solid state characteristics of pharmaceutical excipients: Molecular mechanisms, measurement techniques, and quality aspects of final dosage form. *Int. J. Pharm. Invest.* **2012**, *2* (1), 18.

(8) Craig, D. Q. M.; Royall, P. G.; Kett, V. L.; Hopton, M. L. The relevance of the amorphous state to pharmaceutical dosage forms: glassy drugs and freeze dried systems. *Int. J. Pharm.* **1999**, *179* (2), 179−207.

(9) Ermolina, I.; Darkwah, J.; Smith, G. Characterisation of Crystalline-Amorphous Blends of Sucrose with Terahertz-Pulsed Spectroscopy: the Development of a Prediction Technique for Estimating the Degree of Crystallinity with Partial Least Squares Regression. *AAPS PharmSciTech* **2014**, *15* (2), 253−260.

(10) Brittain, H. G. Effects of mechanical processing on phase composition. *J. Pharm. Sci.* **2002**, *91*, 1573−1580.

(11) Boldyrev, V. Mechanochemical modification and synthesis of drugs. *J. Mater. Sci.* **2004**, *39* (16), 5117−5120.

(12) Buckton, G.; Darcy, P.; Greenleaf, D.; Holbrook, P. The use of isothermal microcalorimetry in the study of changes in crystallinity of spray-dried salbutamol sulphate. *Int. J. Pharm.* **1995**, *116* (1), 113−118.

(13) Taylor, L.; Zografi, G. The Quantitative Analysis of Crystallinity Using FT-Raman Spectroscopy. *Pharm. Res.* **1998**, *15* (5), 755−761.

(14) Gombás, Á.; Antal, I.; Szabó-Révész, P.; Marton, S.; Erõs, I. Quantitative determination of crystallinity of alpha-lactose monohydrate by Near Infrared Spectroscopy (NIRS). *Int. J. Pharm.* **2003**, *256* (1), 25−32.

(15) Sheokand, S.; Modi, S. R.; Bansal, A. K. Dynamic Vapor Sorption as a Tool for Characterization and Quantification of Amorphous Content in Predominantly Crystalline Materials. *J. Pharm. Sci.* **2014**, *103* (11), 3364−3376.

(16) Ticehurst, M. D.; York, P.; Rowe, R. C.; Dwivedi, S. K. Characterisation of the surface properties of α-lactose monohydrate

DOI: 10.1021/acs.langmuir.6b03969
Langmuir 2017, 33, 920−926

with inverse gas chromatography, used to detect batch variation. *Int. J. Pharm.* **1996**, *141* (1), 93−99.
(17) Zhang, J.; Ebbens, S.; Chen, X.; Jin, Z.; Luk, S.; Madden, C.; Patel, N.; Roberts, C. Determination of the Surface Free Energy of Crystalline and Amorphous Lactose by Atomic Force Microscopy Adhesion Measurement. *Pharm. Res.* **2006**, *23* (2), 401−407.
(18) Ward, S.; Perkins, M.; Zhang, J.; Roberts, C.; Madden, C.; Luk, S.; Patel, N.; Ebbens, S. Identifying and Mapping Surface Amorphous Domains. *Pharm. Res.* **2005**, *22* (7), 1195−202.
(19) Badal Tejedor, M.; Nordgren, N.; Schuleit, M.; Rutland, M. W.; Millqvist-Fureby, A. Tablet mechanics depend on nano and micro scale adhesion, lubrication and structure. *Int. J. Pharm.* **2015**, *486* (1−2), 315−323.
(20) Pazesh, S.; Lazorova, L.; Berggren, J.; Alderborn, G.; Gråsjö, J. Considerations on the quantitative analysis of apparent amorphicity of milled lactose by Raman spectroscopy. *Int. J. Pharm.* **2016**, *511* (1), 488−504.
(21) Sader, J. E.; Chon, J. W. M.; Mulvaney, P. Calibration of rectangular atomic force microscope cantilevers. *Rev. Sci. Instrum.* **1999**, *70* (10), 3967−3969.
(22) Pettersson, T.; Nordgren, N.; Rutland, M. W.; Feiler, A. Comparison of different methods to calibrate torsional spring constant and photodetector for atomic force microscopy friction measurements in air and liquid. *Rev. Sci. Instrum.* **2007**, *78* (9), 093702.
(23) Elversson, J.; Millqvist-Fureby, A.; Alderborn, G.; Elofsson, U. Droplet and Particle Size Relationship and Shell Thickness of Inhalable Lactose Particles During Spray Drying. *J. Pharm. Sci.* **2003**, *92*, 900−910.
(24) Ermolina, I.; Smith, G. Dielectric spectroscopy of low-losses sugar lyophiles: III: The influence of moisture on the dielectric response of freeze-dried lactose. *J. Non-Cryst. Solids* **2011**, *357* (2), 671−676.
(25) Walstra, P. *Physical Chemistry of Foods*; CRC Press: 2002.
(26) Trasi, N.; Boerrigter, S.; Byrn, S. Investigation of the Milling-Induced Thermal Behavior of Crystalline and Amorphous Griseofulvin. *Pharm. Res.* **2010**, *27* (7), 1377−1389.
(27) Perkins, M.; Ebbens, S. J.; Hayes, S.; Roberts, C. J.; Madden, C. E.; Luk, S. Y.; Patel, N. Elastic modulus measurements from individual lactose particles using atomic force microscopy. *Int. J. Pharm.* **2007**, *332* (1), 168−175.
(28) Hoffmann, P. M.; Jeffery, S.; Pethica, J. B.; Özgür Özer, H.; Oral, A. Energy dissipation in atomic force microscopy and atomic loss processes. *Phys. Rev. Lett.* **2001**, *87* (26), 265502.
(29) Sestak, J. *Glassy, Amorphous and Nano-Crystalline Materials Thermal Physics, Analysis, Structure and Properties*; Springer: Dordrecht, 2010.
(30) Wang, G. D.; Heng, J. Y. Y.; Williams, D. R. Dilatometry of powder compacts — Characterizing amorphous-crystalline transformations. *Powder Technol.* **2013**, *236*, 12−16.
(31) Burnett, D. J.; Thielmann, F.; Sokoloski, T.; Brum, J. Investigating the moisture-induced crystallization kinetics of spray-dried lactose. *Int. J. Pharm.* **2006**, *313* (1−2), 23−28.
(32) Price, R.; Young, P. M. Visualization of the crystallization of lactose from the amorphous state. *J. Pharm. Sci.* **2004**, *93* (1), 155−164.
(33) Mahlin, D.; Berggren, J.; Alderborn, G.; Engström, S. Moisture-Induced Surface Crystallization of Spray-Dried Amorphous Lactose Particles Studied by Atomic Force Microscopy. *J. Pharm. Sci.* **2004**, *93*, 29−37.

DOI: 10.1021/acs.langmuir.6b03969
Langmuir 2017, 33, 920−926

Paper II

Milling induced amorphisation and its effects on α-lactose monohydrate at the nanoscale

Maria Badal Tejedor[a,b], Samaneh Pazesh[c], Niklas Nordgren[a], Michael Schuleit[d], Mark W. Rutland[a,b], Göran Alderborn[c], Anna Millqvist-Fureby*[a].
[a]SP Technical Research Institute of Sweden, Box 5607, SE-114 86 Stockholm, Sweden.
*Anna.Fureby@sp.se; Mobile: +46 768640046
[b]KTH Royal Institute of Technology, Division of Surface and Corrosion Science, Drottning Kristinas väg 51, SE-100 44 Stockholm, Sweden.
[c]Department of Pharmacy, Uppsala University, Uppsala, Sweden.
[d]Novartis Pharma AG, Novartis Institutes for Biomedical Research, GDC, Novartis Campus, 4002 Basel, Switzerland.

Abstract

Preprocessing of pharmaceutical powders is a common procedure to condition the materials for a better manufacturing performance. Good flowability and tabletability properties are essential to avoid problems during tablet manufacturing. Nonetheless preprocessing unit operations do not always fulfill the desired goal but may also induce undesired material properties modifications. Material induced amorphization when conditioning particle size through milling is an example. Surface and bulk modifications on the material structure will change material properties affecting the processability of the powder. Hence it is essential to control the material transformations that occur during milling. Topographical and mechanical changes in surface properties can be a preliminary indication of further material transformations. Therefore an initial surface evaluation of the α-lactose monohydrate after short and prolonged milling times has been performed in the present study.

Unprocessed α-lactose monohydrate and spray dried lactose were evaluated in parallel to the milled samples as reference examples of the crystalline and amorphous lactose structure. Morphological differences between unprocessed α-lactose, 1h and 20h milled lactose and spray dried lactose were detected from SEM and AFM images. Additionally, AFM was used to simultaneously characterize particle surface amorphicity by measuring energy dissipation. Extensive surface amorphicity was detected after 1h of milling while prolonged milling times showed only a moderate particle surface amorphization. Bulk material characterization performed with DSC indicated a partial amorphicity for the 1h milled lactose and a fully amorphous thermal profile for the 20h milled lactose. The temperature profiles however, were shifted somewhat in the comparison to the amorphous reference, particularly after extended milling. This suggests a surface-bulk propagation of the amorphicity during milling in combination with a different amorphous structural conformation to that of the amorphous spray dried lactose. This might reflect a crystalline-like surface behavior of the 20h milled lactose. Water loss during milling was measured with TGA showing lower water content for the lactose amorphized through milling

compared to spray dried amorphous lactose. The hardened surface may be due to either surface crystallization of lactose or to a low-water glass. Thus, bulk characterization confirms the amorphization phenomena induced through milling which differs from the amorphous structure formed by spray drying.

(Keywords: tableting, milling, lactose, amorphisation, recrystallization, mechanical properties, atomic force microscopy, differential scanning calorimetry, TGA)

1. Introduction

Tableting performance is influenced by the chemical and mechanical properties of the formulation ingredients. In order to assure a good tableting performance, the powders are preprocessed under different processes such as granulation, drying, milling and blending, to achieve an optimal particle size, particle size distribution, stability, good flowability and a homogeneous mixture between the formulation components. However, the excipients or active ingredients might suffer from undesired structural changes which alter their surface properties during the different pre-conditioning steps (Gaisford, 2012). An example of this phenomenon is surface amorphisation due to milling – a common processing step prior to tableting in order to generate the desired particle size. High shear friction, crushing and collision forces in combination with arise in temperature during milling contribute to the amorphisation of the particles (Willart and Descamps, 2009). The modifications induced through milling have been extensively studied in both drugs and excipients (Curtin et al., 2013; Willart et al., 2007). While amorphisation might be considered a side effect of the milling process, it is by no means always undesirable, for example the benefit of the amorphous state in increasing the dissolution rates for some poorly soluble drugs has been reported (Kawabata et al., 2011). On the other hand, problems related to the instability of the amorphous phase have also been investigated, raising issues about the long term stability of the drug (Caron et al., 2013; Trasi et al., 2010). The reversible amorphous state of sugar based excipients can result in lump formation among the particles when recrystallization occurs; for example while the powder is stored under the temperature and relative humidity conditions of the manufacturing facility before it is incorporated into the process. A controlled degree of amorphicity in some excipients has shown an increase in tablet tensile strength while an extended level of amorphicity has led to a reduction in the tablet strength (Paterson et al., 2005). Thus particle surface and bulk amorphisation can influence tableting performance leading to sticking and picking problems if adhesion and cohesion forces within the tablet become weaker (Badal Tejedor et al., 2015). Furthermore, particle surface amorphicity might impact the flowability of the powder which is important for the handling and processing operations to maintain reasonable blending times and high compaction speeds. An inconsistent powder flow affects the quality of the tablets in terms of content and tablet weight uniformity (Fitzpatrick et al., 2007; Prescott and Barnum, 2000). Therefore uncontrolled particle amorphisation could have a detrimental effect on the final properties of the powder

(Vromans et al., 1987). The unintended modification of the properties of the particles after milling introduces an uncertainty into the later performance of the powders. Therefore, in order to understand powder behavior it becomes important to study the changes in surface and bulk properties of the particles induced by milling (Gaisford, 2012; Hancock and Zografi, 1997). Moreover, improved understanding of the propagation of the amorphous content will influence the design of the milling process.

Milling induced amorphisation of particulate solids has been reported by several reserachers. It has been suggested that the solid state amorphisation upon milling occurs during prolonged processing times, while the first stages of milling lead to particle comminution without amorphisation(Caron et al., 2011). However, the possibility of surface only amorphisation, leading to a low overall level of amorphicity, was not discussed. Surface amorphisation during milling through melt mediated solid transformation has been proposed by (Hckerfelt et al., 2009) and Pazesh et al (Pazesh et al., 2013). Here, the solid transformation is due to friction developed at the inter-particle contacts during the particle flow, thus it can be ascribed to a surface process. One of the bulk amorphisation mechanisms suggested in the literature is mechanical activation where the mechanical energy transferred through impact is stored in form of defects in the material. Friction and fracture of the particles contribute to disorder the initial crystalline structures (Lei et al., 2012). However, this process of activation is reversible resulting in recrystallization followed by a release of energy from the system (Hüttenrauch et al., 1985).

The potential impact of even partial amorphisation of the material on processing and product performance calls for careful characterization of the powders (Çelik, 2011). Different analytical methods have been used to characterize and quantify the degree of amorphicity of the milled powders in previous studies. Calorimetric analysis such as differential scanning calorimetry and isothermal microcalorimetry are the most widespread methods mainly because of their sensitivity lower than 1% w/w of the amorphous material and the low mass of sample required. However, data interpretation and method design are critical for successful characterization. Near-Infrared spectroscopy (NIR), Raman spectroscopy and solid-state NMR offer an evaluation of the sample at the intramolecular level. They are quick and non-invasive methods detecting amorphous content of 1% w/w. Some of the drawbacks for these methods are the need for suitable reference spectra of the characterized samples, local heating by the beam and complex mathematical determination of the amorphous content (Gaisford, 2012; Willart et al., 2007). Dynamic vapor sorption (DVS) and inverse-gas chromatography analyze the sample at the particulate level, and DVS can also provide information regarding the surface properties (Einfalt et al., 2013; Vollenbroek et al., 2010). A less extensively used surface characterization technique is atomic force microscopy. AFM is surface sensitive to the material mechanical properties at the nanoscale (Badal Tejedor et al., 2017; Mahlin

et al., 2004). In a recently developed method, the energy dissipation of the surface is analyzed as a property that differentiates between amorphous and crystalline surfaces of fully amorphous and crystalline lactose (Badal Tejedor et al., 2017).

In the present study a commonly used pharmaceutical excipient, α-lactose monohydrate, is used to evaluate amorphisation induced at different milling times in a ball mill. In particular, the effect of the surface mechanical are addressed to elucidate whether amorphisation during milling is a surface induced phenomenon. To this end, AFM is used to characterize the samples surface amorphicity by means of a recently developed methodology (Badal Tejedor et al., 2017). AFM measurements were performed on the very top layer of the particles; therefore other bulk measurements were used to elucidate the non-linear evolution of the particles amorphisation overtime. Analytical techniques such as differential scanning calorimetry and thermogravimetrical analysis were used in combination with BET. Thus, the nature of the mechanically amorphized material, effects of prolonged milling times and amorphous content propagation mechanisms can be suggested.

2. Experimental

2.1. Materials

The material used in this study is α-lactose monohydrate. The lactose used to prepare the milled samples was obtained from DFE Pharma (Pharmatose® 200M, Veghel, Netherlands) and the lactose used for spray drying was purchased from Merk KGaA (Darmstadt, Germany).

2.2. Milling of the powders

Ball milling of received crystalline lactose was performed in a planetary ball mill (PM 100 CM, Retsch, Germany). Crystalline lactose was stored in desiccator over P_2O_5 before use. The milling operation was carried out in a stainless steel milling jar of a volume of 12 cm^3 containing 50 balls with a diameter of 5mm of the same material and 1g of lactose, corresponding to a ball to powder mass ratio of 25:1 was used. The rotation speed of the solar disk was set to 400 rpm and the samples were milled for 1 and 20 hours. Every 20 minutes of milling was followed by a pause period of 5 minutes and the milling experiments were performed in humidity controlled room at 30±5% relative humidity and 25±3 °C.

2.3. Spray drying

A solution of a 10% solid content of lactose was spray dried in a laboratory spray dryer built at SP (Technical Research Institute of Sweden). The feed solution was pumped with a 5ml/min flow rate through a 2mm diameter orifice nozzle, and dried with an air flow of 0,8 m^3/min in a 0,75 x 0,15 m drying chamber. The dryer operates in co-current mode with a jacketed two-fluid nozzle operated with pressurized air. The jacket temperature was 20°C. The inlet and outlet temperature of the drying air flow was 150°C and 70-75°C respectively. The powder produced was collected in a cyclone, but only the powder gravitationally deposited in the attached vessel below the cyclone was used for further analysis. The spray dried powder is stored into a desiccator at room temperature and 0-5% relative humidity.

2.4. Scanning electron microscopy

The morphology of the powder materials: lactose, milled lactose and spray dried lactose, was examined by scanning electron microscopy (FEI-XL, 30 series) with an accelerated voltage of 5 kV in high vacuum. The particulate samples were sprinkled over a double-sided carbon tape mounted on an aluminium holder and blowed out with nitrogen gas to remove the excess of powder. Afterwards the samples were coated with gold (120s, 40 mA) using a Balzers SCD050 coater to allow evaluation at high magnifications without damaging the sample with the beam.

2.5. BET surface area

The surface area of the crystalline and milled lactose powders were measured by the BET gas absorption isotherm method using a surface area analyzer (Micromeritics TriStar 3000). An amount of 0,835±0,1g of sample was used to perform the adsorption of N_2 at a temperature of 77 K. Five points were collected during gas adsorption in the interval of 0,06-0,30 P/P°. The samples were previously degassed for 60 minutes at 40°C with a VacPrep Micromeritics pump. The total surface area was calculated applying the Brunauer-Emmet-Teller (BET) equations.

2.6. Atomic force microscopy

Surface nanomechanical properties of the particulate samples were measured using a Multimode 8 atomic force microscopy equipped with a Nanoscope V controller (Bruker, Santa Barbara, CA) operated in PeakForce QNM (Quantitative Nanomechanical Property Mapping) mode. Silicon nitride tip cantilevers (HQ-NSC 14/AlBS, Mikromasch (Estonia)) with radius of approx. 8nm were used to

perform the measurements. The cantilevers spring constant was calibrated using the technique of Sader (Pettersson et al., 2007; Sader et al., 1999). A set of force profiles is represented at each oscillation (normal force vs. apparent separation). This is collected from the approach and retraction paths between the tip and the sample which corresponds to the loading and unloading of a maximum force (i.e. PeakForce) of 24nN. The area between the two curves corresponds to the work of adhesion presented as the dissipation energy (eV). The scan rate used to perform the measurements was 0,5 Hz with a PeakForce tapping frequency of 2 kHz. The size of the scanned area was 2 x 2 μm from which an average dissipation value was calculated from all the force cycles collected at each pixel (512 x 512 pixels per scan). 17 scans were collected on average over at least three different areas of several particles from each one of the samples. The dissipation data corresponds to the average dissipation at each scan. Ambient conditions were controlled and kept constant under a certain temperature (25±1 °C) and relative humidity (20±2 %) in order to avoid recrystallization of the lactose during data collection.

2.7. Raman spectroscopy

The degree of apparent amorphous content of milled lactose was determined using Raman spectroscopy (Enwave Optronics Inc., SLSR-ProTT analyser, Irvine, CA, USA) equipped with TE cooled CCD detector and a laser source with an excitation wavelength at 785 nm. The experimental methodologies developed to quantify apparent amorphous content have been described in detail in elsewhere (Pazesh et al., 2016).

2.8. Differential scanning calorimetry

The differential scanning calorimeter used in this study is a Mettler Toledo DSC 1 STARe System. Approximately 4 mg of the powder sample were weighted in an aluminium pan which was sealed with a pinned lid and an empty aluminium pan was used as a reference. The sample was held for 2 minutes at 20°C before the temperature was increased up to 240°C with a heating rate of 10 °C/min under a N_2 flow of 50 ml/min. All the measurements were run in duplicate.

2.9. Thermogravimetric analysis

Thermogravimetric analyses were carried out in a Mettler Toledo thermogravimetric analyzer, TGA2. The temperature was increased from 25°C to 240°C with a rate of 20°C/min. The sample was held during 1 min at the initial temperature and during 5 min at the final temperature. The N_2 gas flow was set to 20 ml/min.

3. Results and Discussion

The morphologies of the particles used for evaluation are displayed in the SEM images (Fig. 1). The unmilled α-lactose monohydrate shows larger particles with a polyhedral shape and smooth surfaces which are revealed at larger magnification (Fig. 1a and 1a'). The particles size is reduced when the lactose is milled during 1h and 20h (Fig. 1b and 1c, Table 1). The particle size was smaller at 1 h milling than at 20 h milling which may be due to reagglomeration where small particles stick to each other to form aggregates or to the larger particles in the powder. A larger magnification shows morphological differences at the particle surface between the two processed batches: The surface of the lactose particles milled during 1h combines smooth areas with areas that show an agglomeration of broken and mechanically deformed pieces originating from breakage of the original lactose particles (Fig. 1b'). As for the 20h milled lactose particles, they present a surface composed of rounded protuberances of the order of 100nm and material agglomeration at the micron level (Fig. 1c'). Topographical changes at the particle surface after short and longer milling time suggest changes of the particles mechanical properties. The spray dried lactose particles are significantly smaller than any of the other lactose particles, displaying a spherical shape and smooth surface (Fig. 1d and 1d').

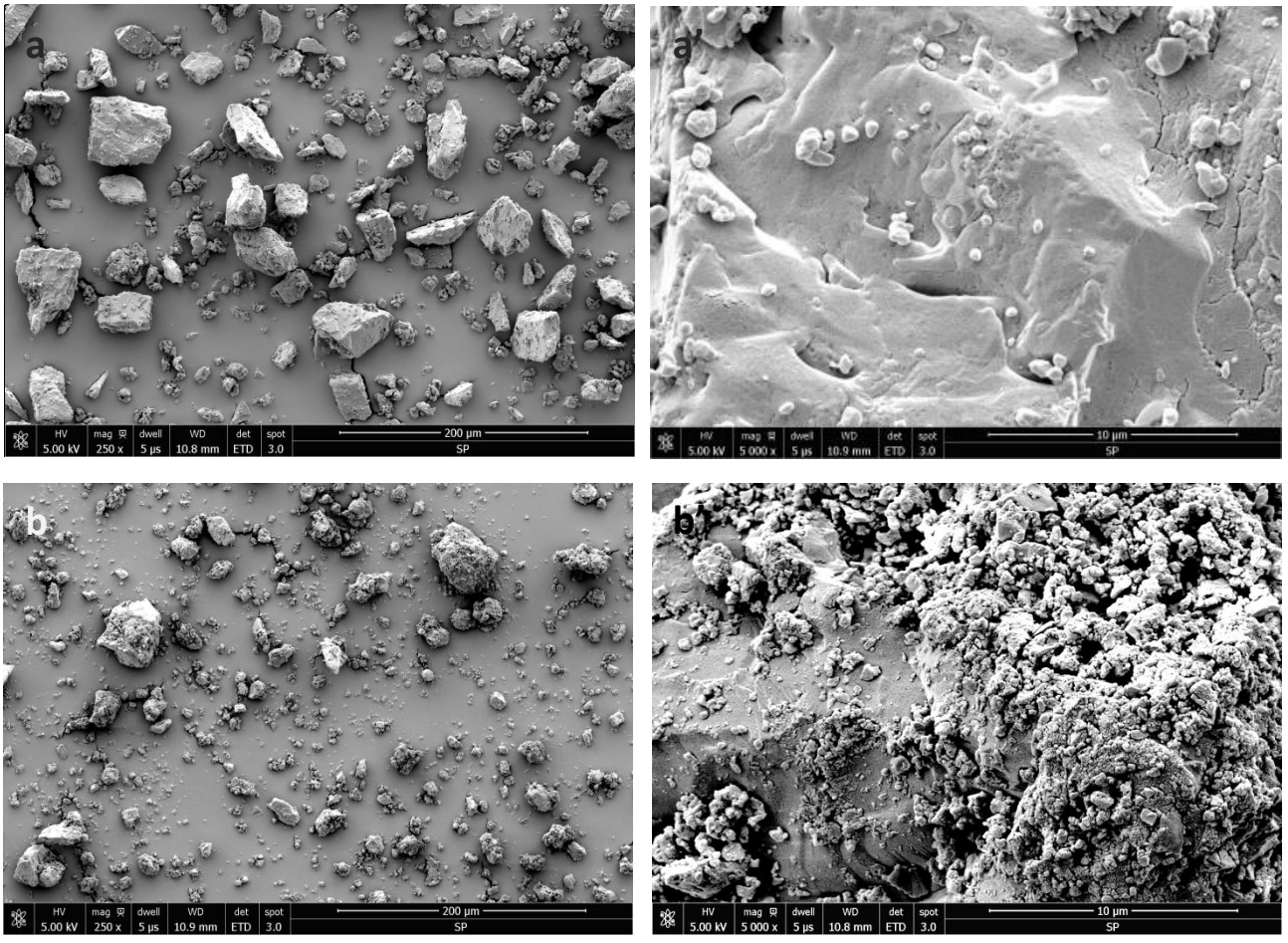

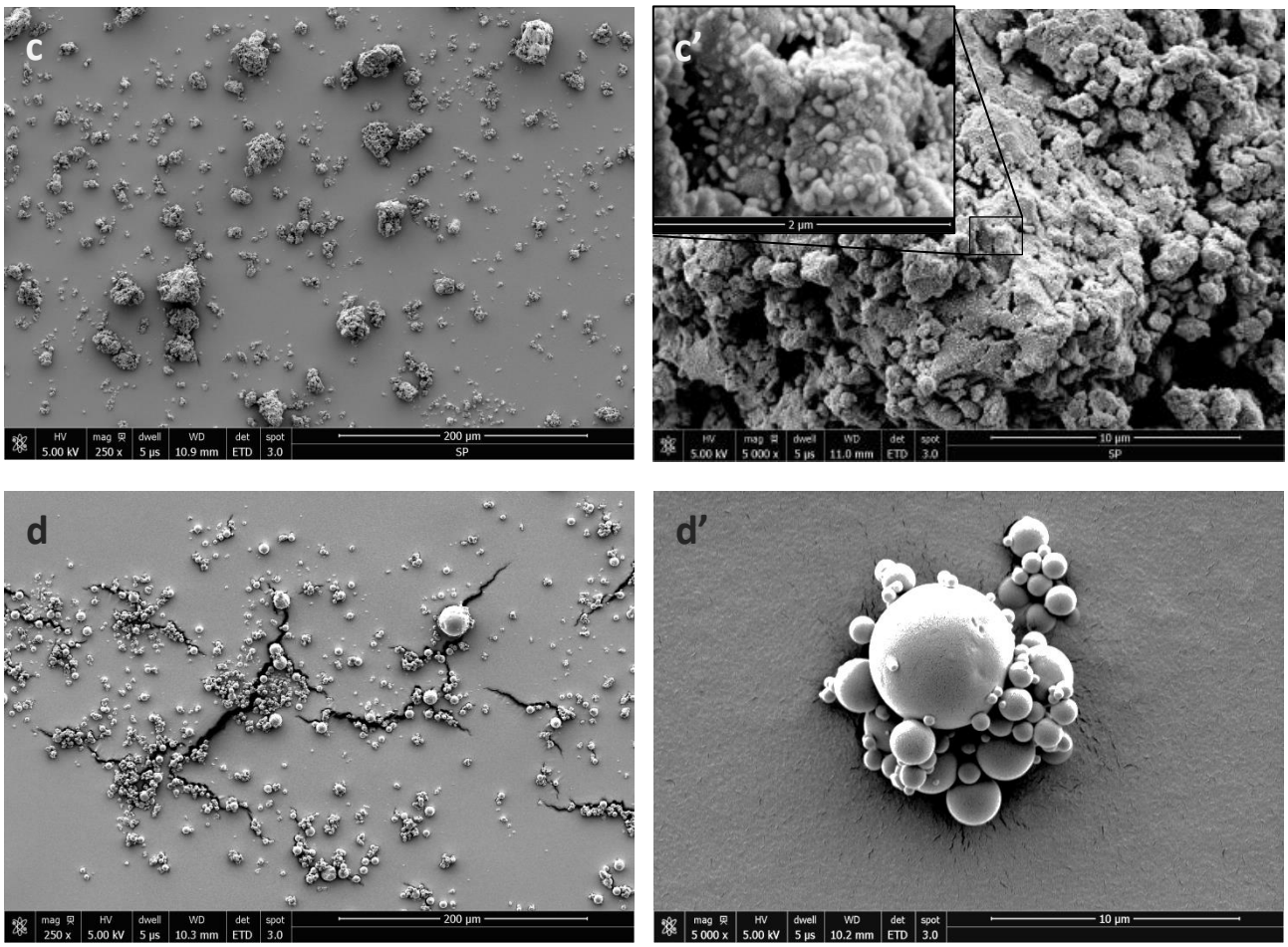

Figure 1. SEM images of α-lactose monohydrate: (a-a') unmilled (b-b') after 1h milling (c-c') after 20h milling (d-d') spray dried. All micrographs are shown at two different magnifications with a scale bar of 200µm and 10µm. As for the magnification inserted in 1c', it is five times larger than its original one with a scale bar of 2µm.

Particle size reduction usually has implications for the powder's surface area. The extension of the surface area for the unmilled lactose and the 1h and 20h milled lactose is measured with BET analysis (Table 1). As a result of the reduction in particle size a larger surface area was measured for the milled samples. The available surface area of the milled samples was increased by a factor of eight in comparison to the unmilled lactose. Even though an apparently smaller size reduction was observed in the SEM images and particle size measurements for the 20h milled lactose sample (Fig. 1, Table 1), BET analysis show no significant difference in surface area between the 1h and 20h milled lactose. The measured particle size difference implies that the specific surface area of the 20 h milled samples would be about six times smaller than the 1 h milled samples, assuming spherical particles. This suggests that the small protuberances observed with SEM (Fig. 1c') at a larger magnification for the 20h milled lactose contribute substantially to the enlargement of the surface area.

Table 1. BET surface area of the unmilled, 1h milled and 20h milled lactose powder sample; compared to particle size measurements from reference [a] performed by light scattering analysis. Apparent amorphicity is shown from reference[b].

Sample	BET Surface Area (m^2/g)	Particle size (μm)[a]	Apparent amorphicity (%)
Unmilled lactose	0,5	30,2	0[b]
1h milled lactose	4	7,5	9,70±1,98
20h milled lactose	4,2	13,8	82,36±0,81[b]

[a](Pazesh and Alderborn, 2017), [b](Pazesh et al., 2016)

The modifications in particle size and surface features during the milling process could easily induce surface-bulk propagation of the material phase transformations (from crystalline to amorphous) having implications in the material mechanical properties (Zhang et al., 2004). The surface mechanical properties and topographical features of the samples at the nanoscale can be measured and imaged in parallel with AFM using PeakForce QNM mode (Badal Tejedor et al., 2017). Fig. 2 shows a representative AFM image for each of the evaluated samples; unmilled, spray dried, 1h milled and 20h milled lactose. The 3D plot representation corresponds to the topographical features which are overlayed by a color map that displays the differences in mechanical properties measured in terms of energy dissipation which is related to the viscoelastic response of the surface. Lower energy dissipation is represented by darker colors while brighter colors show larger energy dissipation.

The topographical features at the nanoscale observed in the 3D plot (Fig. 2) appeared similar to the features evaluated with SEM although the higher resolution in AFM displays more details of the topography. Unmilled lactose presented a smooth surface of varying topographic changes (Fig. 2a) while a flat and very smooth surface was observed for the spray dried lactose (Fig. 2b). 1h milled lactose showed a rougher surface with small features on top (Fig. 2c); as for the 20h milled lactose a much rougher surface was observed where the small protuberances observed with SEM were also detected (Fig. 2d).

By measuring surface energy dissipation it is possible to estimate the state of the material (Badal Tejedor et al., 2017) since the mechanical properties of the crystalline and the amorphous lactose differ from each other. The organized arrangement of lactose molecules in its crystalline structure gives a very limited degree of mobility to the molecules and to the intermolecular water, which is incorporated in the crystal lattice (Hourigan et al., 2013). In the amorphous lactose the molecules form a random structure having certain freedom for reorganization. The water content in the amorphous material will also contribute to increase the degree of mobility of the molecules, acting as a plasticizing agent (Hancock and Zografi, 1994). Therefore crystalline lactose will respond as a stiffer material under an applied pressure while amorphous lactose will present a more viscous behavior. Consequently, stiffer materials are less deformable under an applied pressure dissipating less of the applied energy while softer materials will be more deformable dissipating a larger amount of energy (Hancock and Zografi, 1997; Hoffmann et al.,

2001). Based on that, unmilled lactose and spray dried lactose were used as reference samples for the crystalline and the amorphous phase of the lactose respectively. The measured dissipation on the unmilled lactose showed significantly lower values than the spray dried lactose sample (Fig. 2a and 2b) and reference (Badal Tejedor et al., 2017). Nonetheless, some small areas in the unmilled lactose maps could show higher dissipation values; similarly lower dissipation values can be encountered in smaller areas on the spray dried lactose maps. This is due to the presence of portions of amorphous or crystalline material in the predominantly crystalline or amorphous matrix, or potentially different amorphous populations. Both phases may coexist in pharmaceutical solids (Bates et al., 2006; Shalaev and Zografi, 2002) and reflects the importance of considering a large number of images and pixels. For simplicity, in this work the dissipation values are assumed to reflect a fully crystalline material and a fully amorphous material for the unmilled and spray dried lactose. The 1h milled lactose sample presents an intermediate behavior between the crystalline and the amorphous material displaying both low and high dissipation values distributed in well-defined areas across the map. These were comparable to the ones measured for the unmilled and spray dried lactose, indicating a partially induced surface amorphisation during 1h of milling. After 20h milling time, both low and high dissipation values appeared more evenly distributed along the mapped area, in small defined areas corresponding to the small protuberances observed in the topographical map and in Fig 1c.

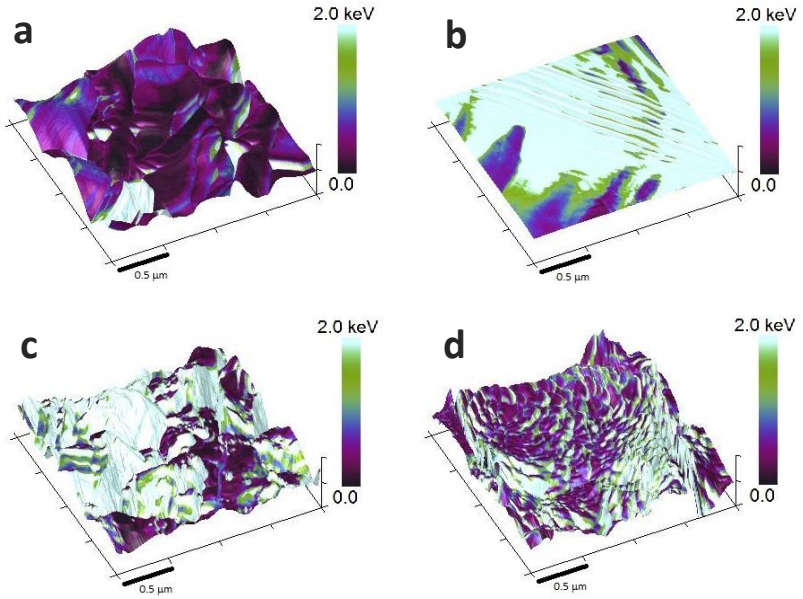

Figure 2. AFM PeakForce QNM dissipation maps overlap the 3D plot representation of the AFM surface topography: (a) unmilled lactose (b) SD lactose (c) 1h milled lactose (d) 20h milled lactose.

The complete set of all the average dissipation values measured at different areas for each sample is represented in a cumulative plot in Fig. 3. The data is divided in bins of 250eV width and the corresponding cumulative percentage in relation to the total number of scans for each sample is plotted vs. the binned dissipation. Crystalline lactose and spray dried lactose show "opposite" cumulative trends. The majority of the data for the crystalline lactose accumulates at low dissipation values (e.g. 80% of the scanned areas show an average dissipation equal or lower than 1000eV) while the spray dried lactose data increases steeply only at higher dissipation values and reflects a similar fraction with more than 1000eV. As expected, the 1h and 20h milled lactose samples display a cumulative increase of the dissipation data which lies between the two extremes of crystalline and amorphous behavior. Interestingly, the shorter milling time sample displays a trend more similar to spray dried lactose indicating almost full surface amorphisation of the particles. In contrast, prolonged milling of the lactose shows a cumulative trend closer to that of crystalline lactose. This result is unexpected and indicates an evolution of the state of the material, that reduces the initially induced extensive surface amorphisation. Therefore this observation suggests that recrystallization may occur at the surface. Note that for the bulk material the amorphicity of the 20h milled sample is higher than for the 1h milled sample, quantified with Raman spectroscopy and reported elsewhere for the same set of samples (Table 1, (Pazesh et al., 2016)).

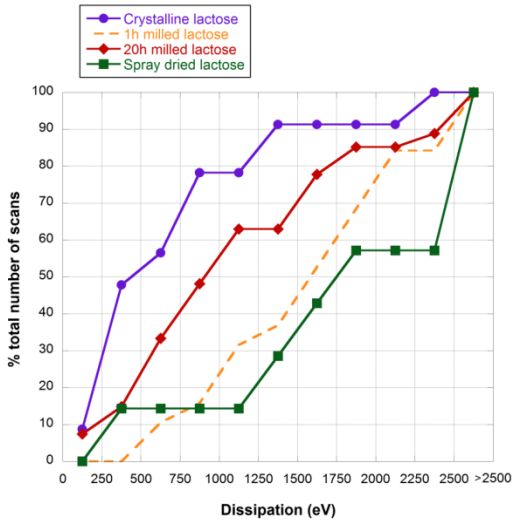

Figure 3. Cumulative distribution of the AFM scanned areas in function of the scan average dissipation values for unmilled α-lactose monohydrate, 1h milled, 20h milled and SD lactose particles.

Bulk crystallinity or amorphicity of the lactose can also be evaluated by measuring the thermal response of the material upon heating using DSC. The thermal profiles of the lactose samples are presented in Fig. 4. It is informative to also analyze the loss of moisture from the samples, since α-lactose occurs as the crystalline monohydrate and the amorphous form typically contains some less strongly bound water. Thus, weight loss profiles from the thermogravimetric analysis are shown in Fig.4 together with the

corresponding DSC profiles. In the DSC analysis and TGA analysis the samples were heated from room temperature to 240°C showing different thermal and weight profiles. The unmilled lactose (Fig. 4a) presented two main thermal events; an endothermic peak at 148°C which corresponds to the loss of the water bound in the crystalline lattice and the melting peak at 217°C, both of which are in line with literature data. The loss of crystal water occurs in the temperature range 120-160°C, with the most rapid loss occurring between 150°C and 160°C. The total water loss was 5%, which corresponds to the crystal water in α-lactose monohydrate. The fully amorphous spray dried lactose (Fig. 4b) shows a glass transition at 70°C and recrystallization at 184°C, and finally melting of α-lactose at 217°C. The water loss occurs gradually from 60°C ending at 120°C, with a total weight loss of 3%. 1h milled lactose (Fig. 4c) showed a remaining crystalline structure represented by the loss of crystal water at 149°C and the melting point at the same temperature as the unmilled lactose (217°C), but with a smaller peak area indicating a partially crystalline state of the sample. Three additional endothermic events were observed; a change associated with water loss in the range 100-140°C, a possible recrystallization event at 172°C, and a second melting peak at 225°C. Finally, the 20h milled sample (Fig. 4d) shows a thermal profile similar to that of spray dried lactose with a glass transition at 70°C and a single melting peak, although occurring at 224°C, and with an additional transition at 120°C, which may correspond to loss of structurally bound water. This is corroborated by the weight loss profile from TGA, where a second water loss ramp is observed in the same temperature range. These differences indicate that the milling induces changes in the crystalline structure, where a large portion of the water is less strongly bound than crystal water, but still desorbs at higher temperature than for the spray dried amorphous sample.

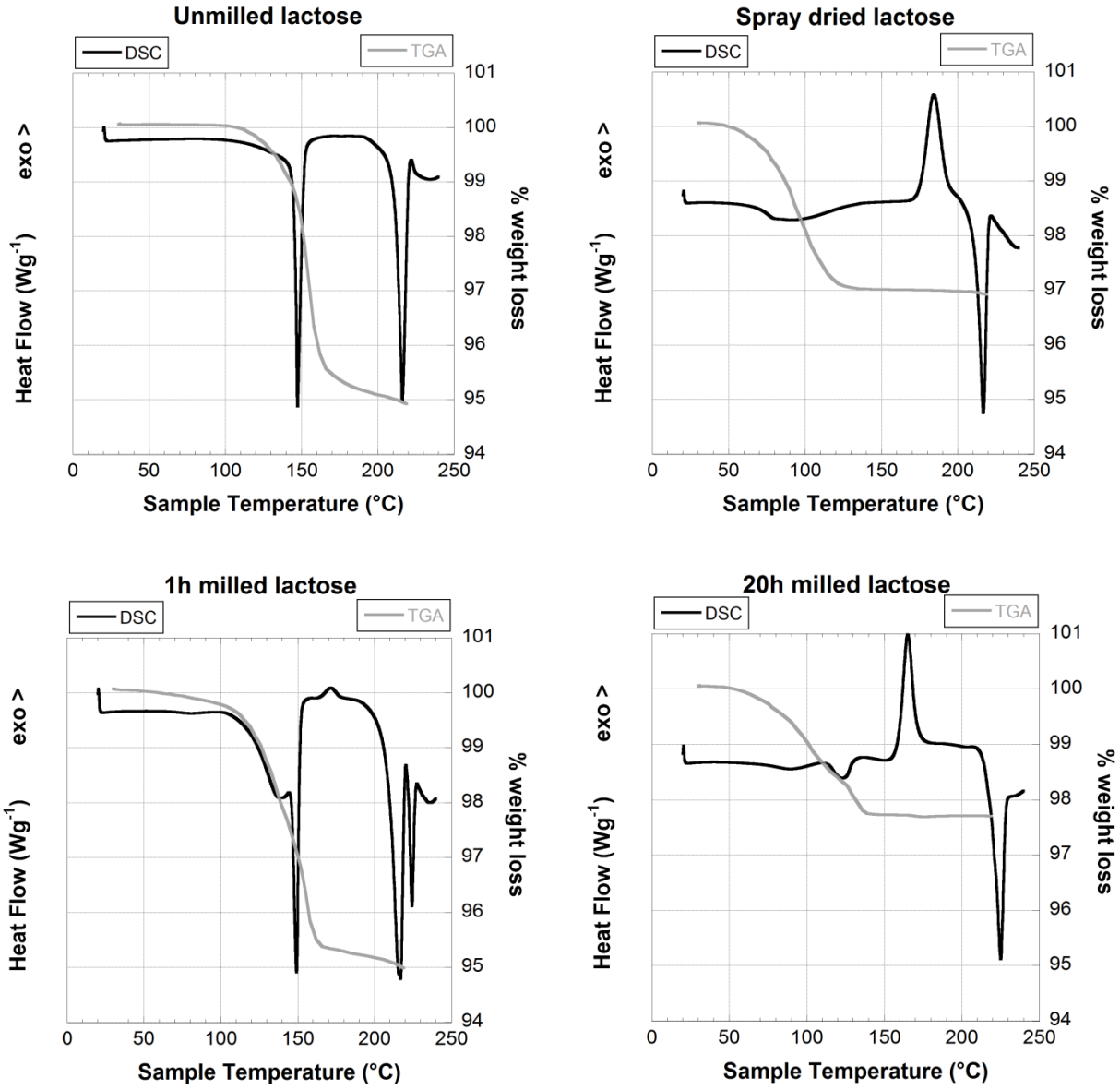

Figure 4. DSC thermal profiles and TGA weight loss profiles for (a) unmilled lactose, (b) spray dried lactose, (c) 1h milled lactose and (d) 20h milled lactose.

The differences in thermal profiles upon milling indicate that bulk material modifications of the lactose occur. The differences of the thermal pattern from the unmilled lactose after 1h milling showed the induced modifications of the material during milling (Irwin and Iqbal, 1991). The DSC analysis shows a transition of the material from the crystalline to mainly the amorphous state after prolonged milling, which is also confirmed by earlier x-ray diffraction and Raman spectroscopy studies (Pazesh et al, 2016). Part of the initial crystalline structure remains in 1h milled lactose in combination with the mechanically disrupted structure, which is observed as loss of water not bound in the crystal lattice as well as loss of crystal water and a second melting point at the same temperature as the 20h milling lactose melting peak. A full transition to the amorphous state upon 20h milling time is observed in DSC (i.e., loss of crystal

water is not observed), although the heating during the analysis may prevent observation of low levels of crystalline material in the mainly amorphous material. Thus, this observation is not in contradiction with the X-ray diffraction and Raman spectroscopy analyses of the crystallinity of the sample.

An intriguing observation is that the recrystallization and melting peaks occur at different temperatures compared to the fully amorphous lactose reference (Spray dried lactose). This may indicate that two different amorphous structures occur with different degrees of order that evolve towards different crystal forms upon heating, which melt at different temperature (Garnier et al., 2008; Shalaev and Zografi, 2002). The narrow and well-defined endothermic peak at 227°C suggests that this is a melting transition for a crystalline material, although the melting point does not coincide with the reported melting points for α-lactose monohydrate, anhydrous α-lactose or β-lactose. Thus, this peak may represent a different crystal form. The possibility of simultaneous occurrence of α and β lactose in mechanically amorphised lactose has been presented earlier (Lerk et al., 1984a, b; Willart et al., 2007; Willart et al., 2004; Willart and Descamps, 2009). Other studies have not only reported a melting peak of the mechanically processed sample around 225°C, which lies in between the α-lactose and β-lactose melting temperatures (217°C and 237°C respectively) (Angberg, 1995), but have also supported the presence of α and β lactose after heating above 170°C with X-ray diffraction analysis. In particular, Lerk et al (1984a, b) suggest that unstable anhydrous a-lactose converts at 170-180°C into a product with crystal structure different from both α- and β-lactose. Mutarotation of melted α-lactose to form β-lactose occurs in the temperature range of 60-120°C (Willart et al, 2007), which in the present case would allow this process to occur in the amorphous portion of the sample once the temperature of the sample exceeds the glass transition temperature. The observed transition at 165°C for 20h milled lactose is lower than the transition temperature observed by Lerk et al (1984a, b), but the new melting peak at 227°C is nonetheless observed. This difference in transition temperature may be due to the higher amorphous content of this sample. No evidence of β-lactose structure was detected prior to heating in the study of (Willart et al., 2004), and in X-ray diffraction analysis and Raman analysis of the present samples also showed no evidence of β-lactose. (Pazesh et al., 2016). On the contrary, it is known that spray dried lactose contains a variable ratio of α and β structures on its amorphous form, however, the amorphous structure evolves towards a fully α-lactose structural conformation during heating showing a melting peak at the same temperature as α-lactose monohydrate (Jawad et al., 2012). The fact that this melting transition is observed for the initially completely amorphous mixture of α- and β-lactose strongly suggests that the pathways for the transitions during heating are different depending on the starting point.

DSC analysis thus corroborates the differences in the samples that are implied by the surface mechanical properties detected above with AFM. Furthermore, it also contributes to elucidate the surface-bulk propagation mechanism of the amorphization during milling. Extensive surface amorphisation measured with AFM along with the partial amorphicity of the bulk for the 1h milled sample detected with DSC suggests that amorphisation is a phenomenon that begins at the surface and propagates to the bulk, disrupting the crystalline structure. Bulk amorphicity increases with milling time as it has been shown with DSC for the 20h milled sample (Pazesh et al., 2016), however further modifications changing the mechanical properties of the surface seem to occur at prolonged milling times.

The presence of water in the sample and the way it binds to the structure influences the mobility of the lactose molecules, affecting the glass transition temperature (Bhattacharya and Suryanarayanan, 2009; Hancock and Zografi, 1994). The mobility of water bound in the crystal lattice is very small, while water molecules in the disrupted crystal structure would allow a softening of the material mechanical properties. Moreover, higher moisture content decreases the glass transition temperature closer to room temperature. This modifies the material mechanical behavior towards that of the glass transition stage (Hancock and Zografi, 1994). Therefore, the similarities in surface mechanical properties of the long term milled lactose to those of the unmilled lactose may be due to the loss in water content reducing the molecular mobility, thus, the viscoelastic response of the amorphous material, as well as to the presence of a crystalline surface layer. The 1 h milled sample has the same water content as the starting material (5%), which would suggest that the surface layer has a higher moisture content and hence a lower glass transition temperature and a more viscoelastic character. However, during milling for longer time a loss of water in the material is observed (Fig 4d), and a calculation based on the measured water content of α-lactose monohydrate and milled lactose, the chamber volume and the chamber temperature of 30°C indicates that the relative humidity in the chamber is as high as 90%. At such high relative humidity recrystallisation of lactose occurs rapidly at the surface, i.e. within 65 minutes (Mahlin et al., 2004), which would alter the properties of the surface layer of the particles. The dissipation of energy observed here (Fig 3) suggests that on average the material properties of the 20h milled sample are somewhat more viscoelastic than the fully crystalline material. However, combining these observations with the topographic structure and energy dissipation map in fig 2d suggests that the surface is composed of small protuberances which are crystalline (low energy dissipation) on the top but amorphous material (high energy dissipation) may be found between these structure. These small structures may thus be the origins of recrystallization of the material, which occurs over time when exposed to higher relative humidity (Badal Tejedor et al, 2017).

4. Conclusion

While milling of lactose does indeed reduce the particle size for short times (of the order of one hour) continued milling can in fact be counter-productive in this regard. While the available surface area increases slightly, the particle size actually increases again at longer milling times suggesting that there is significant reagglomeration - but that the smaller particles retain their shape during the agglomeration. This leads to a significantly different morphology of the particles after milling with a protuberant structure of nanoscale proportions.

The milling induced amorphisation of the lactose follows a similar trend. Dissipation measurements using AFM clearly indicate extensive amorphisation at shorter times, but at longer times the surface displays a much "harder" response, which is more characteristic of a crystalline material. This unexpected behaviour is reflected in the calorimetric response of the samples – the less milled samples display significant amorphous behaviour followed by crystal melting mainly typical of alpha lactose and thus follow "normal behaviour" .The longer milled samples however show very different behaviour to the amorphous reference, and the well-defined crystalline melting peak is characteristic of neither pure alpha- nor beta-lactose. It is speculated that the structural conformation of the mechanically induced "amorphicity" thus differs significantly from that formed during spray drying. This different structure appears to be intimately connected to the water content since a much lower water content was found for the almost fully amorphized lactose in comparison to the spray dried lactose. This reduction of water, probably lost during the almost complete disruption of the crystalline structure while milling, might explain the hardening of the particle surface. Thus, the mechanical behavior at the surface of highly milled lactose is more similar to unprocessed lactose even though the particulate structure is fully amorphous. An alternative hypothesis for particle surface hardening after long term milling is the possibility of surface recrystallization, which might reasonably be due to the increase of relative humidity in the sealed milling chamber associated with the expulsion of water from the crystalline lactose. In either case it is clear that upon heating, this anomalous surface structure leads to a different crystallization pathway for the amorphous material.

Milling times are thus crucial not only for particle size, but also for the final bulk and surface properties of the milled material. The milling time will also strongly affect the subsequent behaviour of the material in terms of adhesion, water uptake and recrystallization.

References

Angberg, M., 1995. Lactose and thermal analysis with special emphasis on microcalorimetry. Thermochimica Acta 248, 161-176.

Badal Tejedor, M., Nordgren, N., Schuleit, M., Pazesh, S., Alderborn, G., Millqvist-Fureby, A., Rutland, M.W., 2017. Determination of Interfacial Amorphicity in Functional Powders. Langmuir.

Badal Tejedor, M., Nordgren, N., Schuleit, M., Rutland, M.W., Millqvist-Fureby, A., 2015. Tablet mechanics depend on nano and micro scale adhesion, lubrication and structure. International Journal of Pharmaceutics 486, 315-323.

Bates, S., Zografi, G., Engers, D., Morris, K., Crowley, K., Newman, A., 2006. Analysis of Amorphous and Nanocrystalline Solids from Their X-Ray Diffraction Patterns. Pharm Res 23, 2333-2349.

Bhattacharya, S., Suryanarayanan, R., 2009. Local mobility in amorphous pharmaceuticals—characterization and implications on stability, Hoboken, pp. 2935-2953.

Caron, V., Hu, Y., Tajber, L., Erxleben, A., Corrigan, O., McArdle, P., Healy, A., 2013. Amorphous Solid Dispersions of Sulfonamide/Soluplus® and Sulfonamide/PVP Prepared by Ball Milling. AAPS PharmSciTech 14, 464-474.

Caron, V., Willart, J.-F., Lefort, R., Derollez, P., Danède, F., Descamps, M., 2011. Solid state amorphization kinetic of alpha lactose upon mechanical milling. Carbohydrate Research 346, 2622-2628.

Çelik, M., 2011. Pharmaceutical Powder Compaction Technology, Second Edition, 2 ed.

Curtin, V., Amharar, Y., Gallagher, K.H., Corcoran, S., Tajber, L., Corrigan, O.I., Healy, A.M., 2013. Reducing mechanical activation-induced amorphisation of salbutamol sulphate by co-processing with selected carboxylic acids. International journal of pharmaceutics 18, 508-516.

Einfalt, T., Planinšek, O., Hrovat, K., 2013. Methods of amorphization and investigation of the amorphous state. Acta pharmaceutica 63, 305-334.

Fitzpatrick, J.J., Hodnett, M., Twomey, M., Cerqueira, P.S.M., O'Flynn, J., Roos, Y.H., 2007. Glass transition and the flowability and caking of powders containing amorphous lactose. Powder Technology 178, 119.

Gaisford, S., 2012. Isothermal microcalorimetry for quantifying amorphous content in processed pharmaceuticals. Advanced Drug Delivery Reviews 64, 431-439.

Garnier, S., Petit, S., Mallet, F., Petit, M.N., Lemarchand, D., Coste, S., Lefebvre, J., Coquerel, G., 2008. Influence of ageing, grinding and preheating on the thermal behaviour of α-lactose monohydrate. International Journal of Pharmaceutics 361, 131-140.

Hancock, B.C., Zografi, G., 1994. The Relationship Between the Glass Transition Temperature and the Water Content of Amorphous Pharmaceutical Solids. Pharm Res 11, 471-477.

Hancock, B.C., Zografi, G., 1997. Characteristics and significance of the amorphous state in pharmaceutical systems, Journal of pharmaceutical sciences, pp. 1-12.

Hckerfelt, M.H., Nystrm, C., Alderborn, G., 2009. Dry mixing transformed micro-particles of a drug from a highly crystalline to a highly amorphous state. Pharmaceutical Development and Technology, 2009, Vol.14(3), p.233-239 14, 233-239.

Hoffmann, P.M., Jeffery, S., Pethica, J.B., Özer, H.Ö., Oral, A., 2001. Energy dissipation in atomic force microscopy and atomic loss processes. Physical review letters 87, 265502.

Hourigan, J.A., Lifran, E.V., Vu, L.T.T., Listiohadi, Y., Sleigh, R.W., 2013. Lactose: Chemistry, Processing, and Utilization. Oxford, UK: Wiley-Blackwell, Oxford, UK.

Hüttenrauch, R., Fricke, S., Zielke, P., 1985. Mechanical Activation of Pharmaceutical Systems. Pharm Res 2, 302-306.

Irwin, W.J., Iqbal, M., 1991. Solid-state stability: the effect of grinding solvated excipients. International Journal of Pharmaceutics 75, 211-218.

Jawad, R., Elleman, C., Vermeer, L., Drake, A.F., Woodhead, B., Martin, G.P., Royall, P.G., 2012. The Measurement of the β/α Anomer Composition Within Amorphous Lactose Prepared by Spray and Freeze Drying Using a Simple 1H-NMR Method. Pharm Res 29, 511-524.

Kawabata, Y., Wada, K., Nakatani, M., Yamada, S., Onoue, S., 2011. Formulation design for poorly water-soluble drugs based on biopharmaceutics classification system: Basic approaches and practical applications. International Journal of Pharmaceutics 420, 1-10.
Lei, L., Carvajal, T., Koslowski, M., 2012. Defect-induced solid state amorphization of molecular crystals. Journal of Applied Physics 111, 073505.
Lerk, C., Andreae, A., De Boer, A., De Hoog, P., Kussendrager, K., Van Leverink, J., 1984a. Alterations of α-lactose during differential scanning calorimetry. Journal of pharmaceutical sciences 73, 856-857.
Lerk, C., Andreae, A., De Boer, A., De Hoog, P., Kussendrager, K., Van Leverink, J., 1984b. Transitions of lactoses by mechanical and thermal treatment. Journal of pharmaceutical sciences 73, 857-859.
Mahlin, D., Berggren, J., Alderborn, G., Engström, S., 2004. Moisture-Induced Surface Crystallization of Spray-Dried Amorphous Lactose Particles Studied by Atomic Force Microscopy. Journal of Pharmaceutical Sciences 93, 29-37.
Paterson, A.H.J., Brooks, G.F., Bronlund, J.E., Foster, K.D., 2005. Development of stickiness in amorphous lactose at constant T−Tg levels. International Dairy Journal 15, 513-519.
Pazesh, S., Alderborn, G., 2017. Comminution-amorphisation relationships during ball milling of lactose at different stress European Journal of Pharmaceutics and Biopharmaceutics. Submitted.
Pazesh, S., Höckerfelt, M.H., Berggren, J., Bramer, T., Alderborn, G., 2013. Mechanism of Amorphisation of Micro-Particles of Griseofulvin During Powder Flow in a Mixer. Journal of Pharmaceutical Sciences 102, 4036-4045.
Pazesh, S., Lazorova, L., Berggren, J., Alderborn, G., Gråsjö, J., 2016. Considerations on the quantitative analysis of apparent amorphicity of milled lactose by Raman spectroscopy. International Journal of Pharmaceutics 511, 488-504.
Pettersson, T., Nordgren, N., Rutland, M.W., Feiler, A., 2007. Comparison of different methods to calibrate torsional spring constant and photodetector for atomic force microscopy friction measurements in air and liquid. The Review of scientific instruments 78, 093702.
Prescott, J.K., Barnum, R.A., 2000. On powder flowability. Pharmaceutical technology 24, 60-85.
Sader, J.E., Chon, J.W.M., Mulvaney, P., 1999. Calibration of rectangular atomic force microscope cantilevers. Review of Scientific Instruments 70, 3967-3969.
Shalaev, E., Zografi, G., 2002. The concept of 'structure' in amorphous solids from the perspective of the pharmaceutical sciences, in: Levine, H. (Ed.), Amorphous Food and Pharmaceutical Systems. The Royal Society of Chemistry, pp. 11-30.
Trasi, N., Boerrigter, S., Byrn, S., 2010. Investigation of the Milling-Induced Thermal Behavior of Crystalline and Amorphous Griseofulvin. Pharm Res 27, 1377-1389.
Willart, J.F., Caron, V., Descamps, M., 2007. Transformations of crystalline sugars upon milling. J Therm Anal Calorim 90, 125.
Willart, J.F., Caron, V., Lefort, R., Danède, F., Prévost, D., Descamps, M., 2004. Athermal character of the solid state amorphization of lactose induced by ball milling. Solid State Communications 132, 693-696.
Willart, J.F., Descamps, M., 2009. Solid State Amorphization of Pharmaceuticals. Molecular Pharmaceutics 5, 905-920.
Vollenbroek, J., Hebbink, G.A., Ziffels, S., Steckel, H., 2010. Determination of low levels of amorphous content in inhalation grade lactose by moisture sorption isotherms. International Journal of Pharmaceutics 395, 62-70.
Vromans, H., Bolhuis, G.K., Lerk, C.F., van de Biggelaar, H., Bosch, H., 1987. Studies on tableting properties of lactose. VII. The effect of variations in primary particle size and percentage of amorphous lactose in spray dried lactose products. International Journal of Pharmaceutics 35, 29-37.
Zhang, G.G.Z., Law, D., Schmitt, E.A., Qiu, Y., 2004. Phase transformation considerations during process development and manufacture of solid oral dosage forms. Advanced Drug Delivery Reviews 56, 371-390.

Paper III

International Journal of Pharmaceutics 486 (2015) 315–323

Contents lists available at ScienceDirect

International Journal of Pharmaceutics

journal homepage: www.elsevier.com/locate/ijpharm

Tablet mechanics depend on nano and micro scale adhesion, lubrication and structure

Maria Badal Tejedor [a,b], Niklas Nordgren [a], Michael Schuleit [c], Mark W. Rutland [a,b], Anna Millqvist-Fureby [a,*]

[a] SP, Technical Research Institute of Sweden, Box 5607, SE-114 86 Stockholm, Sweden
[b] KTH Royal Institute of Technology, Division of Surface and Corrosion Science, Drottning Kristinas väg 51, SE-100 44 Stockholm, Sweden
[c] Novartis Pharma AG, Novartis Institutes for Biomedical Research, GDC, Novartis Campus, 4002 Basel, Switzerland

ARTICLE INFO

Article history:
Received 19 December 2014
Received in revised form 20 March 2015
Accepted 21 March 2015
Available online 1 April 2015

Keywords:
Tableting
Excipients
Adhesion
Atomic force microscopy
Profilometry
Surface roughness

ABSTRACT

Tablets are the most convenient form for drug administration. However, despite the ease of manufacturing problems such as powder adhesion occur during the production process. This study presents surface and structural characterization of tablets formulated with commonly used excipients (microcrystalline cellulose (MCC), lactose, mannitol, magnesium (Mg) stearate) pressed under different compaction conditions. Tablet surface analyses were performed with scanning electron microscopy (SEM), profilometry and atomic force microscopy (AFM). The mechanical properties of the tablets were evaluated with a tablet hardness test. Local adhesion detected by AFM decreased when Mg stearate was present in the formulation. Moreover, the tablet strength of plastically deformable excipients such as MCC was significantly decreased after addition of Mg stearate. Combined these facts indicate that Mg stearate affects the particle–particle bonding and thus elastic recovery. The MCC excipient also displayed the highest hardness which is characteristic for a highly cohesive material. This is discussed in the view of the relatively high adhesion found between MCC and a hydrophilic probe at the nanoscale using AFM. In contrast, the tablet strength of brittle materials like lactose and mannitol is unaffected by Mg stearate. Thus fracture occurs within the excipient particles and not at particle boundaries, creating new surfaces not previously exposed to Mg stearate. Such uncoated surfaces may well promote adhesive interactions with tools during manufacture.

© 2015 Elsevier B.V. All rights reserved.

1. Introduction

Oral solid dosage is one of the most popular forms of drug delivery due to ease of handling and administration. The production process is furthermore relatively simple as are distribution and storage (Aleksovski et al., 2015; Kaur, 2012). A tablet is constituted of a wide range of particulate materials that are bound together under pressure to be delivered as a unit. Processing conditions as well as the physical and chemical nature of the particulate excipients and the active drug compound are both important for the binding of the blend and, consequently, the tablet properties (Hamad et al., 2010; Hoag, 2008b; Jain, 1999). However, the contribution of the excipients properties to the manufacturing process is not yet fully understood; especially, the role of the surface properties of the excipients and their contribution to the complex behavior of the formulation during tableting.

Several studies have been conducted to evaluate the compactibility and compressibility of different excipients. The approaches for evaluation are diverse since both powder properties and processing parameters can affect tableting and the resulting tablet properties. (Sinka et al., 2009; Sun, 2011; van Veen et al., 2000). The formation of bonding bridges between the single powder particles during tableting is an important factor that causes particle–particle adhesion contributing to the overall tablet cohesion. The formation of particle–particle bonds is driven by intermolecular forces and promoted by an enlargement of the contact area under pressure. These forces are mostly Van der Waals and hydrogen bonding interactions which become stronger at short range (Patel et al., 2006). Therefore the probability of bonding formation increases when the interparticulate distance is reduced. Other forces such as electrostatic interactions are also relevant to the particle–particle bond formation acting over a longer range. However the mechanisms by which the formation of bonding sites

* Corresponding author. Tel.: +46 768640046.
E-mail address: Anna.Fureby@sp.se (A. Millqvist-Fureby).

http://dx.doi.org/10.1016/j.ijpharm.2015.03.049
0378-5173/© 2015 Elsevier B.V. All rights reserved.

is promoted depends on the behavior of the excipients under pressure. Plastic materials reduce their interparticle distance by irreversible deformation while brittle materials increase the area of contact through fracture and/or particle rearrangement. After the release of the compaction force a decrease of the contact area might occur if the materials exhibit an elastic component. The recovery of the deformation after removal of the compaction force will diminish the interparticle adhesion forces affecting the tablet strength and the overall tableting performance of the excipients (Amidon et al., 2009; Nyström et al., 1993). When surface interactions are evaluated between particles at the nanoscale, particle surface roughness influences the effective contact area between particles, thus affecting the overall magnitude of the intermolecular forces (Jallo et al., 2011). Additionally, processing parameters can modify the mechanical behavior of the excipients and particle surface interactions: the operating range of temperature and relative humidity can affect the powders depending on their viscoelastic and hygroscopic properties (Harding et al., 2008). However, a certain level of humidity is desired since water can act as a binder and as a plasticizer in the formulation (Doelker, 1993). Tableting parameters such as applied load and its duration are also adjusted and optimized as a function of the mechanical behavior and binding strength of the excipients in order to obtain consistent tablets (van Veen et al., 2000).

During powder tableting, the individual particles are not only in contact with each other but also with the surface of the tools. The physical interaction between the particles and the tool surfaces is influenced by friction and adhesion which arise from a possible combination of different intermolecular Van der Waals forces, electrostatic forces, electrical double layer formation and capillary forces (Saniocki, 2014). These phenomena also have an impact on the powder bulk microstructure during the tableting process and affect the tablet hardness. Consequently, the degree of adherence of the particles to the tools is strongly influenced by the level of adhesion and cohesion forces between and within the materials that comprise the powder blend. In some cases, a poor performance of the formulation can cause adhesion of the powders to the tools leading to imperfect tablet surfaces, commonly known as 'sticking'. Thus, in order to improve tableting performance avoiding particle-tool adhesion and friction forces, a small amount of lubricant (typically Mg stearate) is usually added to the formulation (Moody et al., 1981; Wang et al., 2010). During blending Mg stearate spreads over the surface of the particles forming at least a partial monolayer and filling the cavities on the surface of the particles (Roblot-Treupel and Puisieux, 1986). Despite the relatively thin coating, the effect on tablet properties can be significant.

Today, the performance of the excipients and active drug compounds during tableting can be predicted by the acquired knowledge of their mechanical and chemical properties together with tableting operation experience (Hamad et al., 2010; Toyoshima et al., 1988). However, this approach has not proved to be sufficient to solve all the problems arising during tableting (Matero et al., 2013). There is a lack of fundamental understanding regarding the particulate surface and interfacial properties in relation to the conformation of the tablet structure. A deeper study to better understand the interfacial processes occurring at the nanoscale level is needed, as well as their impact on the particle adhesion and material cohesion. Therefore, the development of analytical methods and new protocols to improve material characterization is essential.

The aim of this work is to study tablet surface properties in relation to the internal tablet structure and formulation using different tablet components and process parameters. The excipients selected for the present study are microcrystalline cellulose (MCC), lactose, mannitol and Mg stearate as a lubricant agent. They are all commonly used pharmaceutical excipients and they constitute a large percentage of the total weight of the tablet formulation, except Mg stearate, which is present in a very low amount. Comparative observations will be conducted since the excipients have shown different behaviors during tablet processing; lactose and mannitol are associated with tableting adhesion problems although mannitol has shown to be more problematic than lactose (Alderborn and Nyström, 1996). On the contrary, MCC is well-known as a non-sticky and easily compressible excipient (Alderborn and Nystrom, 1996; Doelker, 1993). In order to characterize and evaluate the tablets and the corresponding powders, a set of analytical tools has been used. Evaluation of tablet surface roughness and interfacial adhesion has been performed utilizing atomic force microscopy (AFM) a highly versatile tool employed by some of the authors over the last decade for studying a wide range of interfacial and contact phenomena at the nanoscale (Feiler et al., 2005, 2007; Mizuno et al., 2010; Nordgren and Rutland, 2009; Ralston et al., 2005; Rathje et al., 2014; Wang et al., 2003). Other complementary techniques, i.e., scanning electron microscopy (SEM) and profilometry have been used for macroscopic surface roughness and tablet morphology evaluation. As to link the surface properties of the tablet with their structural properties, a tablet hardness test was used to establish the tablet binding strength.

2. Experimental

2.1. Materials

The materials used in this study are common pharmaceutical excipients: microcrystalline cellulose (Cellulose Microcr. PH200, FMC), lactose (Lactose spray dried, Meggle), mannitol (Mannitol 200SD, Merck) and magnesium stearate (Magnesium stearate Pharma, FACI); the excipients were provided in powder form.

2.2. Preparation of tablets

One-, two- and three-component formulations were prepared (Table 1). Single component formulations consisted of pure excipients (MCC, lactose or mannitol). Two component formulations consisted of MCC blended with either lactose or mannitol in a 1:1 mass ratio. Mg stearate was used as a lubricant in a proportion of 1% of the total weight of the blend. Both single components and two components formulations were lubricated with Mg stearate obtaining a three component formulation.

When the tablet formulation consisted of more than one excipient, the mixing of the blend was performed with a vortex mixer which provided a homogeneous and mechanical mixing of

Table 1
Schematic figure depicting the different tablet formulations used; one, two and three component systems. The composition of the formulations consisting of two components (in boxes) was equal to 1:1 mass ratio. The case where a total amount of 1% of MgSt was added to the pure excipient and two component formulations was also studied.

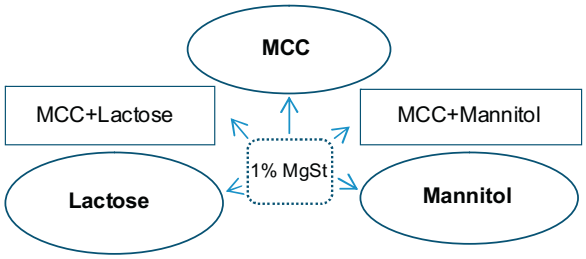

the particles. A total amount of 400 mg for each tablet was separately weighed into a 10 ml vial and shaken with the help of a vortex mixer during 30 s. For this purpose the speed of the vortex mixer (Ika, USA) was set to 1400 rpm. The powder blend was pressed into tablets using a laboratory press (Specac, England) equipped with two flat punches of stainless steel, each with a diameter of 13 mm. The punches together with the powder blend were held within a die. The die was fitted between the two plates into the manual press where the load was manually ramped by pulling the lever over a period of 40 s and released approximately 1 s after reaching the target load, which we refer to as a compression time of 1 s. Two different applied loads were employed–75 MPa (1 t) and 380 MPa (5 t). A third set of samples was obtained using an applied load of 75 MPa maintained during 30 s after reaching the target load. These three different sets of compaction conditions were applied to each formulation. They are thus referred to as 75 MPa 1 s, 75 MPa 30 s and 380 MPa 1 s.

The reproducibility of the method for sample preparation was controlled by measuring the thickness of the tablets which shows a variation of ±0,02 mm within the same set of samples. A minimum number of seven samples for each formulation and compaction condition were pressed for evaluation. No visual defects or shape variations were observed among the tablets for a given set of samples during the tablet preparation.

2.3. Scanning electron microscopy

The powder excipients, surface topography and the cross-section of the tablets were examined using scanning electron microscopy (Philips XL30 environmental scanning electron microscope) with an accelerating voltage of 20 kV. Both backscatter and a mix of backscatter and secondary electron detectors were used to analyze the features of the surface of the tablet. Before analysis, the samples were coated with gold (120 s, 40 mA) using a Balzers SCD050 coater.

2.4. Atomic force microscopy

Nanoscale information of the surface topography, surface roughness and adhesion was obtained for the tablets using a Multimode 8 atomic force microscope equipped with a Nanoscope V controller (Bruker, Santa Barbara, CA) operated with PeakForce QNM (Quantitative Nanomechanical Property Mapping) mode (see for example Ref. (Duner et al., 2012)). A silicon nitride tip cantilever, HQ-NSC 14/AIBs, Mikromasch (Estonia), with a radius of approximately 8 nm was used for evaluation of the excipients before and after addition of Mg stearate. The cantilever spring constants were calibrated using the technique of Sader et al. (1999) (Pettersson et al. (2007)). The size of the scans was set to 50 × 50 μm and the images were captured using a scan rate of 0.326 Hz in an environment of 23 °C and 47% ± 5% relative humidity. During Peakforce imaging the sample surface oscillates at 2 kHz while the cantilever tracks the surface topography. In each individual cycle the surface approaches the cantilever and retracts after the set load of 24 nN has been applied. Each time the silicon probe and the tablet surface are brought into contact and retracted, a force curve is generated from which an adhesion value is obtained. The same number of force curves was obtained in each scan. The adhesion value obtained for one full scan is the average value of the adhesion at each pixel in the scanned area, consisting of 512 × 512 pixels. At least seven scans at different areas of the tablet were measured and the average adhesion calculated.

2.5. Profilometry

Surface roughness of the tablets was also evaluated using a non-contact profilometry method based on white light interferometry (Zygo New View 5010, Middlefield, CT, USA). The objective used was a 20× Mirau interference objective (Zygo) with a 0.8× zoom which provide an image of 440 × 330 μm. The measurements were done at three different spots for each sample under ambient conditions. The parameters considered for data evaluation were obtained from Advance Texture Metropro™ Application software (Middlefield, CT, USA). The test data are filtered digitally and broken down into waviness and roughness which corresponds to a low filter and higher filter respectively. Root-mean-square of waviness and roughness (Wq, Rq) were compared.

2.6. Measurements of tablet hardness

The fracture strength of the tablets was measured with a tablet hardness tester (Holland Tablet Hardness Tester C50). The tablets were placed between two metal jaws and subjected to a diametrical pressure with a speed of 6 mm/min until fracture occurred. The tests were performed on five tablets from each formulation at ambient conditions. The standard deviation was calculated for each set of samples.

3. Results and discussion

The morphology and particle size of the excipients in their powder form prior to compression are illustrated in the SEM images in Fig. 1. MCC shows a uniform size distribution, and mannitol presents a similar particle size but broader size distribution, while lactose powder is formed by smaller units with less homogenous particle size distribution. The MCC particles seem to be constituted of elongated units forming a consistent fiber-like structure containing large voids. Smaller voids are observed at the surface of mannitol which displays a more closely packed structure. The lactose particles, appear to be formed of smaller units. Mg stearate has a large surface area due its composition of small, thin platelets. Knowledge of the initial size and physical structure of the particulate excipients is prerequisite to understand the behavior of the powder under pressure which would affect the formation of a coherent tablet structure (Amidon et al., 2009).

Visual inspection of the surface of the pressed tablets was also carried out with SEM. Fig. 2 shows the surface of MCC tablets respectively pressed at 75 MPa during 1 s (a), 380 MPa during 1 s (b) and 75 MPa during 30 s (c). The same set of experiments was conducted for the rest of the formulations. When comparing the tablet surface morphology of the samples pressed at different compaction loads, a closely packed surface structure is clearly observed at a higher applied load. A less smooth and less compact structure is always observed when the tablets were pressed at a lower applied load and no structural difference is perceived when the lower applied load (75 MPa) is maintained for 30 s instead of 1 s; the same observations are made for all the formulations (Supplementary material related to this article found, in the online version, at http://dx.doi.org/10.1016/j.ijpharm.2015.03.049). The manner in which the particles rearrange under pressure is observed at the tablet surface and likely represents how they are organized at an internal level within the tablet structure. When the applied load is higher, the plastically deformable excipients undergo larger particle deformation and brittle excipients are subjected to more extensive fracture. Therefore, a larger contact area between the particles is created and a more closely packed structure is achieved, displaying fewer voids at the surface of the tablet. In order to obtain good tablet cohesion, it is important to create a large contact area between the particles that promotes the formation of binding sites (Alderborn and Nystrom, 1996). However, the strength of the binding sites depends on the bonding mechanism between the particles, which can vary as a function of the intermolecular forces, surface tension and any

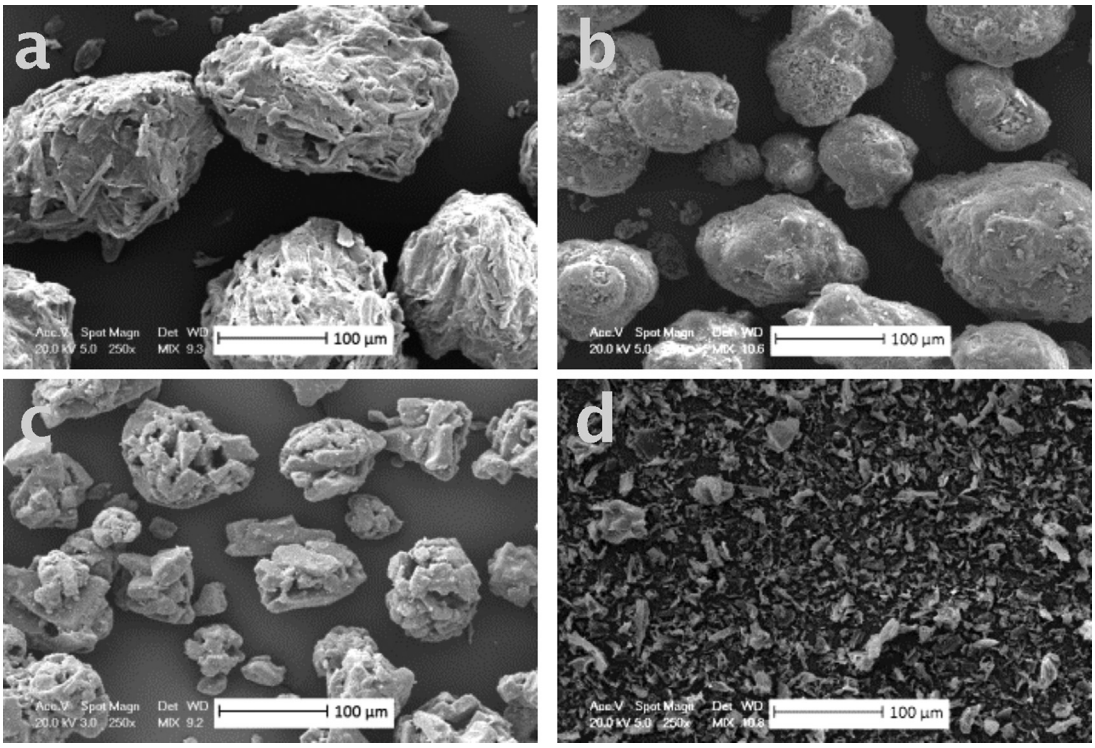

Fig. 1. SEM images of the excipients in their particulate form: (a) MCC, (b) mannitol, (c) lactose and (d) Mg stearate. All the images were taken at the same magnification and have a scale bar of 100 µm length.

electrostatic forces between the particles (Patel et al., 2006). Thus the overall tablet structure is defined by the excipients' chemical interactions and their mechanical behavior under pressure.

In order to further characterize the surface of the tablet, atomic force microscopy (AFM) was used to measure the surface topography of the tablet and the adhesion between the tablet surface and a sharp tip. The adhesion values should not be seen as absolute, since the measured values are strictly dependent on the tip geometry. Tips of comparable radius were chosen and their spring constants precisely measured. Thus the adhesion values, measured with the same tip, are most useful as comparative values, since the geometry is constant. This allows direct comparison of adhesion values. The measurements were performed for one component tablets composed of MCC, lactose and mannitol; and also for the same excipients when formulated with 1% Mg stearate. The samples chosen for these measurements were pressed with an applied load of 380 MPa during 1 s.

Topography maps of the tablet surfaces are shown in Fig. 3. Of the pure excipients, MCC showed larger and sharper features in comparison with lactose and mannitol. This observation is linked to the structure of the powder particles (Fig. 1) that constitute the tablets, since the fiber structure in MCC is unlikely to be broken up during compression. The same general trend on the topography is observed for the case with added Mg stearate. However, the many small asperities that were observed on lactose (Fig. 3b) disappeared when Mg stearate was added (Fig. 3e).

The distribution of adhesion is overlayed on the 3D topographical images for the different excipients without (Fig. 4a–c) and with (Fig. 4d–f) Mg stearate. The pure MCC displays a considerably higher and more uniform adhesion than the other excipients, which show adhesion variation over the surfaces as the color scale reveals. The effect of Mg stearate is to significantly reduce the adhesion of the MCC, and to render the adhesion both somewhat lower, but mainly more uniform on lactose and mannitol.

This decrease in adhesion for the tablets containing Mg stearate indicates that a large portion of the surface is covered by Mg stearate; Mg stearate is located on the surface of the particles during mixing covering the surface area to a large extent (Hussain et al., 1988). The lubricating properties of the Mg stearate also

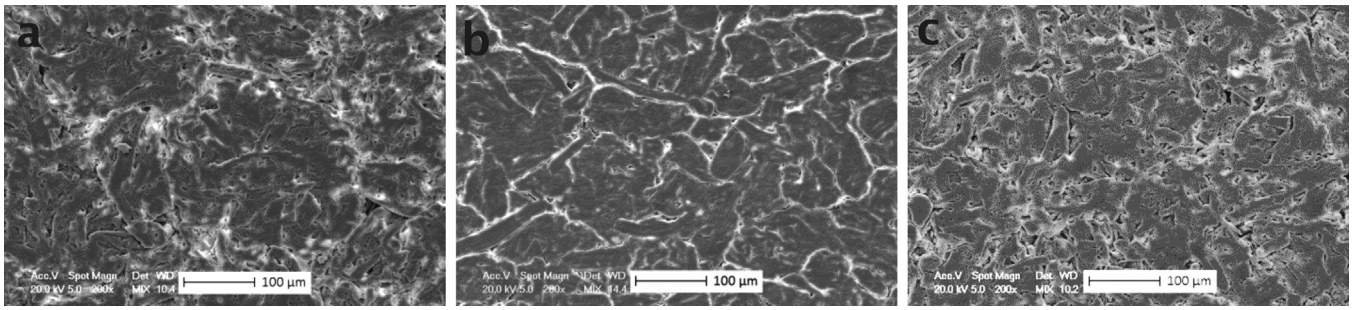

Fig. 2. SEM images of the gold sputtered MCC tablet surface pressed under different compaction conditions: (a) 75 MPa–1 s, (b) 380 MPa–1 s (c) 75 MPa–30 s. All the images were taken at the same magnification and have a scale bar of 100 µm length.

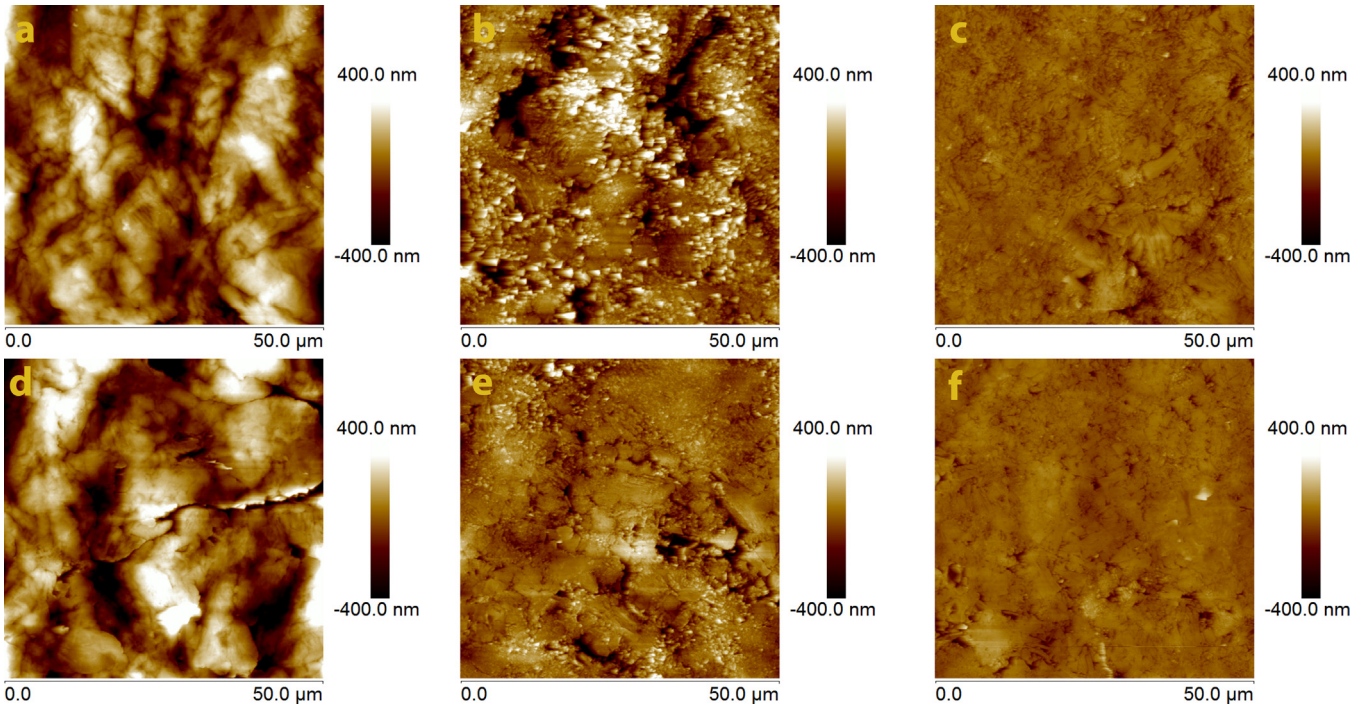

Fig. 3. AFM topography images of the surface of tablets formulated with pure excipients: (a) MCC, (b) lactose, (c) mannitol and the excipients lubricated with Mg stearate: (d) MCC + MgSt, (e) lactose + MgSt, (f) mannitol + MgSt.

diminish the force needed to retract the cantilever from the surface of the tablet resulting in a lower adhesion force on average.

Fig. 5 summarizes the adhesion between the AFM tip and the excipient surface by taking the average of the average values of at least seven different scans of 50 × 50 μm. Adhesion values for pure MCC were clearly highest, whereas pure lactose and mannitol were comparable. In the lubricated samples a significant decrease in adhesion is observed in all cases, however, the adhesion values of the lubricated excipients follow the same trend as the non-lubricated ones. The adhesion is more homogeneous in the latter case as indicated by much smaller error bars which might imply that the addition of Mg stearate into the formulations contributes

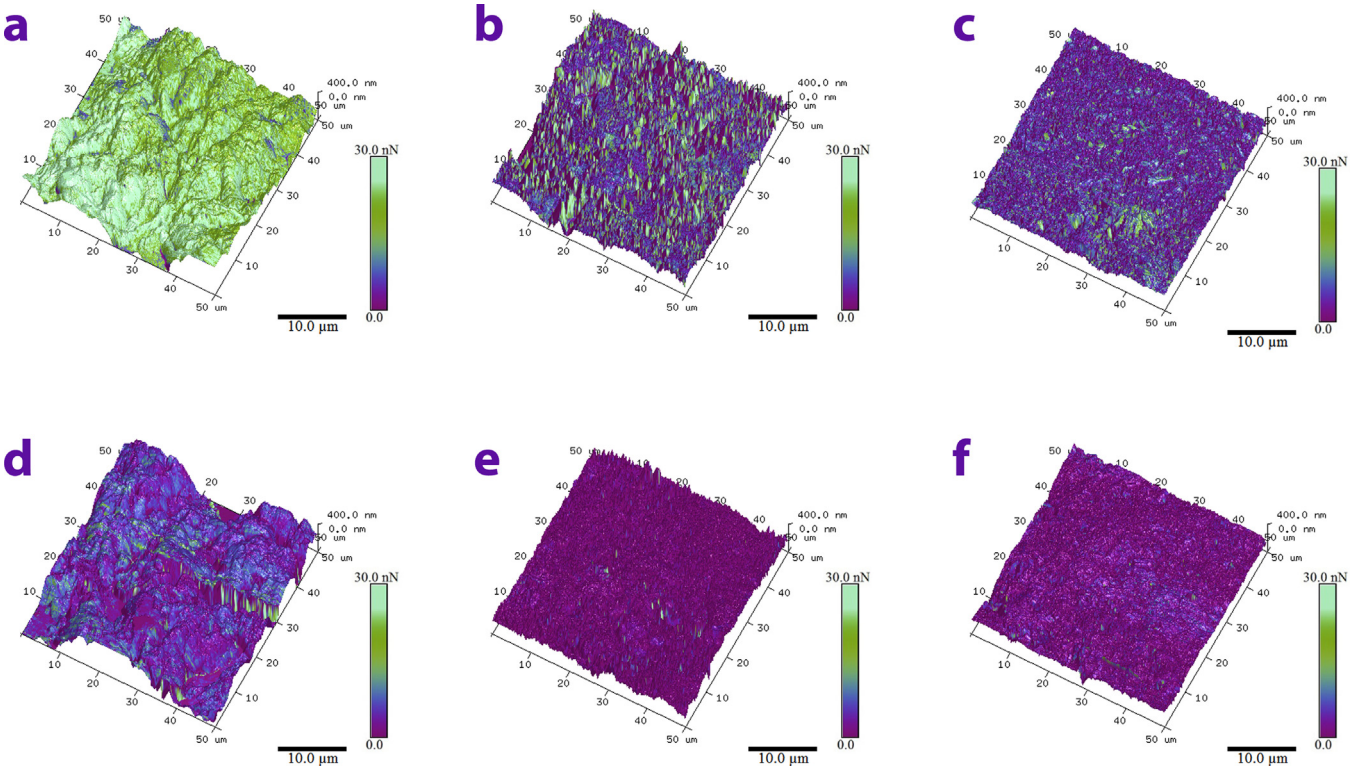

Fig. 4. The adhesion maps overlap the 3D plot representation of the AFM surface topography (Fig. 3). The adhesion level at each point is represented by the color scale where the brighter color corresponds to the higher adhesion. The measurements were performed over tablets formulated with pure excipients: (a) MCC, (b) lactose, (c) mannitol, and the excipients lubricated with Mg stearate: (d) MCC + MgSt, (e) lactose + MgSt, (f) mannitol + MgSt.

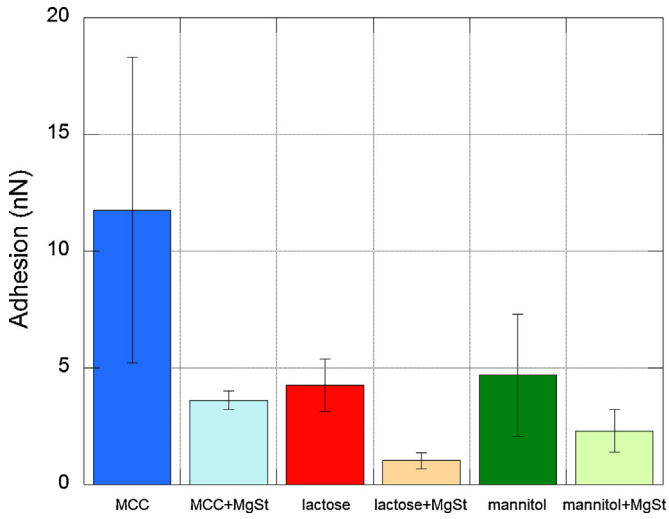

Fig. 5. AFM adhesion measurements on the surface of the tablets of pure and lubricated excipients when pressed under a compaction load of 380 MPa during 1 s. The results shown are the average of the main adhesion values obtained from each of the at least seven scans of 50 × 50 μm measured over the sample.

to evening out the characteristics of the surface of the tablet.

The adhesion with an AFM tip, which is hydrophilic, gives an indication of the magnitude of the intermolecular forces with which the materials can interact. It would be easy to consider that a high adhesion should be associated with a higher sticking propensity–in this case one could see the tip as being a model for the stamp. However this would be an oversimplification. A large adhesion against the tip is also indicative of larger cohesive forces and this might, somewhat counterintuitively, actually be the explanation for the lower propensity for sticking of MCC. If sticking is a result of cohesive failure then the high cohesion of cellulose may be the decisive factor for the non-sticking properties usually found during tableting (Alderborn and Nystrom, 1996). Both silicon nitride (tip) and cellulose are hydrophilic so there may also be an element of capillary condensation on the adhesive contribution. The reduction in the adhesion in the presence of Mg stearate indicates that in fact cohesive failure would be easier between particles coated in Mg stearate.

Considering the mechanical properties of these excipients, MCC is a plastically deformable material with an elastic component which makes the particles recover partially after the applied load is released (Doelker, 1993). This elastic recovery of the particles on the surface after compression might contribute to the irregular and non-homogeneous MCC tablet surface properties, resulting in higher local adhesion values and the larger spread in the data. A lower elastic recovery is expected from lactose and mannitol which is translated into a more even tablet surface topography and more uniform properties, such as the adhesion.

In the case of MCC, a large decrease in surface roughness is observed with profilometer when Mg stearate is added into the formulation; see Fig. 6. The profilometer is sensitive to roughness on a larger scale than the AFM, and thus these major (more microscopic than nano-scopic) changes are not appreciated when comparing surface roughness average values obtained with AFM at 50 μm scans (Supplementary material related to this article found, in the online version, at http://dx.doi.org/10.1016/j.ijpharm.2015.03.049). The two techniques are used on different scales, the images area in profilometry is almost sixty times larger than in AFM. Therefore, topographic features that extend beyond the size of the fibres in MCC have a large influence on roughness determined in profilometry images. In fact, the gross features that can be observed in Fig. 6 are of the same size as the MCC particles in Fig. 1. Thus, the addition of Mg stearate to the MCC may not only modify the tablet on the surface but it seems also to affect the mechanical behavior of the MCC under pressure, by partially removing its elastic recovery after compression. Thus a more level surface is obtained. This in turn strongly implies that the elasticity of the materials arises from a large adhesion and static friction contribution acting at the contacts between the MCC particles, which is reduced in the presence of Mg stearate and allows sliding at the contacts and thus a more plastic response.

The structural integrity of the tablet depends on the strength of the internal cohesive and adhesive forces and the balance between these and the adhesion forces created between the powders and the punch surfaces under compression (Li et al., 2004). In order to evaluate the internal tablet strength a tablet hardness test was carried out. Fig. 7 shows the results of the tablet hardness test for all the formulations pressed under all the previously mentioned conditions.

Regardless of the components of the tablet the figure shows that the tablets pressed at a higher compaction pressure presented higher tablet hardness values; consider that for MCC the force needed to fracture the sample pressed at 380 MPa exceeded the force limits of the tablet hardness tester. Therefore all that can be said is that the tablet hardness for that sample is above 500 N. In contrast, the tablets pressed at a lower compaction pressure showed lower tablet hardness values which for MCC and lactose were also independent of the duration of the applied pressure. In the case of mannitol increasing the compaction time resulted in a very slight increase in hardness. Thus, an increase on the applied load over the powder bed promotes the formation of binding sites by reducing to a large extent the voids among the particles which leads to a significant increase of the hardness of the tablet.

Irrespective of the compaction conditions, pure excipients show different tablet hardness depending on the characteristics of the material. MCC tablet hardness is significantly higher than the tablet hardness for lactose and mannitol which values are very similar to each other. The strength of the binding and the extension of the contact area achieved under pressure are attributed to the

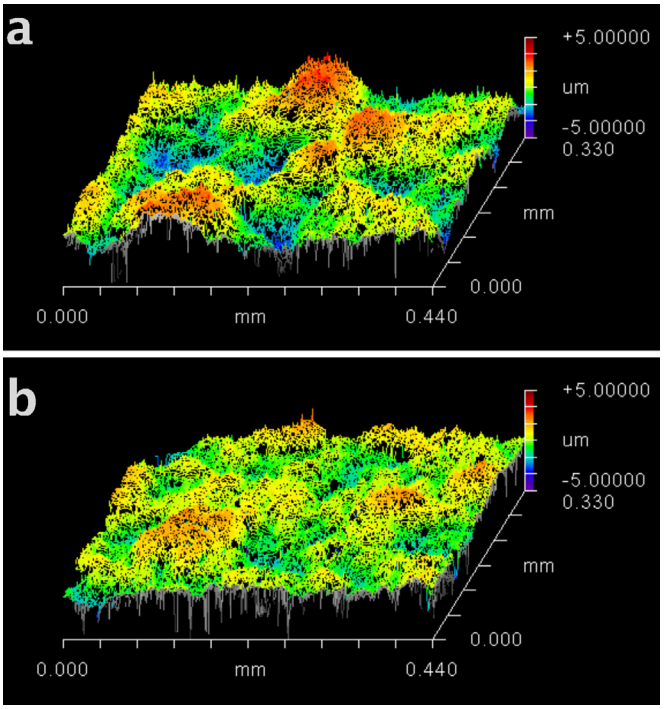

Fig. 6. Profilometry profiles of (a) pure MCC and (b) MCC lubricated with 1% Mg stearate tablets. Both tablets were pressed at 380 MPa during 1 s.

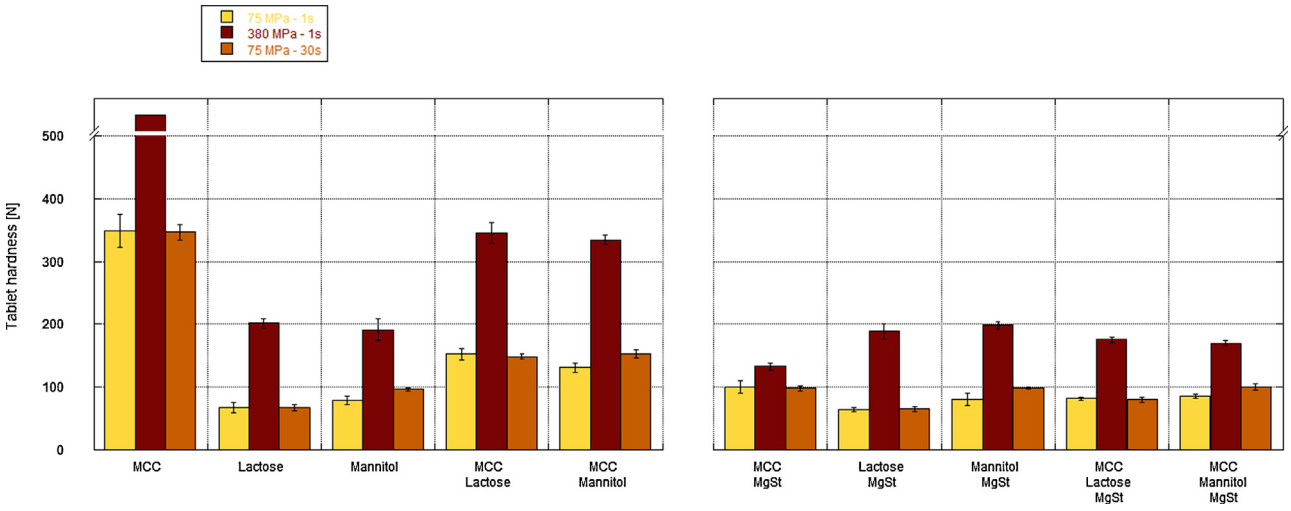

Fig. 7. Tablet hardness test was carried out for all the formulations pressed under the three defined sets of compaction conditions.

different compaction mechanisms and physical structure of the excipients. Plastic and brittle materials behave differently under pressure (Alderborn and Frenning, 2008). Materials that exhibit a more brittle behavior such as lactose and mannitol will fracture within the aggregate particles, forming smaller units and creating a large number of interparticulate contact points. However, plastically and elastically deformable materials such as MCC will mostly undergo deformation bringing the surface of the particles closer and increasing the probability of more bonding zones (Doelker, 1993; Zhang et al., 2003). The ability of the adhesive bridges to shift and deform without breaking is also a contributing factor to the increased tablet strength. The fiber-like structure of the MCC particles could contribute to the strength of the tablet creating an interlocking structure during compression which remains after decompression when limited elastic recovery occurs (Picker-Freyer, 2007).

When MCC is formulated with either lactose or mannitol, the tablet hardness combines the properties of the two materials. The resulting tablet hardness is somewhat less than the arithmetic mean of the pure excipient values. Thus, both lactose and mannitol have a slightly larger influence on the tablet strength when in mixtures with MCC, suggesting that the fracture mechanisms of lactose and mannitol dominate over those of MCC.

Tablet hardness of the pure and formulated excipients is affected in different ways when Mg stearate is added into the formulation. A material that presents a high fragmentation propensity will show a limited change in compactibility after the addition of the lubricant (Hoag, 2008a); whereas a ductile material that mostly undergoes plastic deformation during compression is significantly weakened by the addition of the lubricant. The previous statements can be supported by the significant decrease in tablet hardness when Mg stearate is added to the formulations that contain MCC. Significantly, no change in tablet hardness is noticeable for lactose and mannitol when Mg stearate is added to the formulation. This confirms that the fracture mechanism is within the excipient particles, rather than failure of the adhesive contacts between them.

Mg stearate belongs to the group of lubricants that consist of a two fatty acid chain bound to a metallic atom. These types of lubricants are very widely used in formulations for tablet compression. Mg stearate is a crystalline material formed by thin platelets which are potentially spread on the surface of other particles to create the lubricous layer. There are several studies that have attempted to explain the lubrication mechanisms of Mg stearate (Roblot-Treupel and Puisieux, 1986; van der Watt, 1987). When Mg stearate is mixed with particulate excipients, its distribution on the surface of the particles occurs either by the formation of a monomolecular film, a “monoparticulate layer” or filling of superficial cavities followed by film formation of variable thickness. In previous work, the last two hypotheses have been the ones mostly supported by the authors (Perrault et al., 2010; Roblot-Treupel and Puisieux, 1986). Depending on the Mg stearate lubrication mechanism and the compaction mechanism of the particles, tablet hardness can be significantly affected by Mg stearate.

By inspecting the cross-section of the tablets after fracture, differences in the internal structure can be observed with and without lubrication. Fig. 8 illustrates the influence of Mg stearate on MCC and lactose internal structure. The cross-section of a pure MCC tablet does not show a defined particle organization while an organized layered structure with defined boundaries is appreciated at the cross-section of the lubricated MCC sample. The layers are parallel to the tablet surface. This same observation applies for the three different sets of compaction conditions (Supplementary material related to this article found, in the online version, at http://dx.doi.org/10.1016/j.ijpharm.2015.03.049). Mg stearate can be assumed to be located around the particles forming a thin layer of lubricant that allows the particles to slip with respect to each other when they deform under pressure (Alderborn and Nystrom, 1996). The disruption of the MCC tablet strength by Mg stearate can be linked to this significantly different internal tablet structure. The structure is a result of the ability of the adhesive contacts to slide and deform, which may also be the direct cause of the tablet weakening. Thus it is difficult (and probably unnecessary) to determine to what extent the change of structure is responsible for the reduced tablet strength. The presence of Mg stearate could also affect the MCC mechanical behavior by reducing the particle interlocking, which may be created by the MCC particles fiber-like structure during rearrangement and elastic recovery. When the diametrical force is applied during the hardness tablet test, the MCC tablet structure does not collapse since it is a material that can deform plastically. The tablet breaks through its weakest points located at the particles interfaces where Mg stearate may be located during lubrication, weakening the MCC particles bonding strength.

A similar organized cross-section structure is not observed either for the lactose (Fig. 8c and d) or for the mannitol (Supplementary material related to this article found, in the online version, at http://dx.doi.org/10.1016/j.ijpharm.2015.03.049) when these are lubricated with Mg stearate. The internal structure

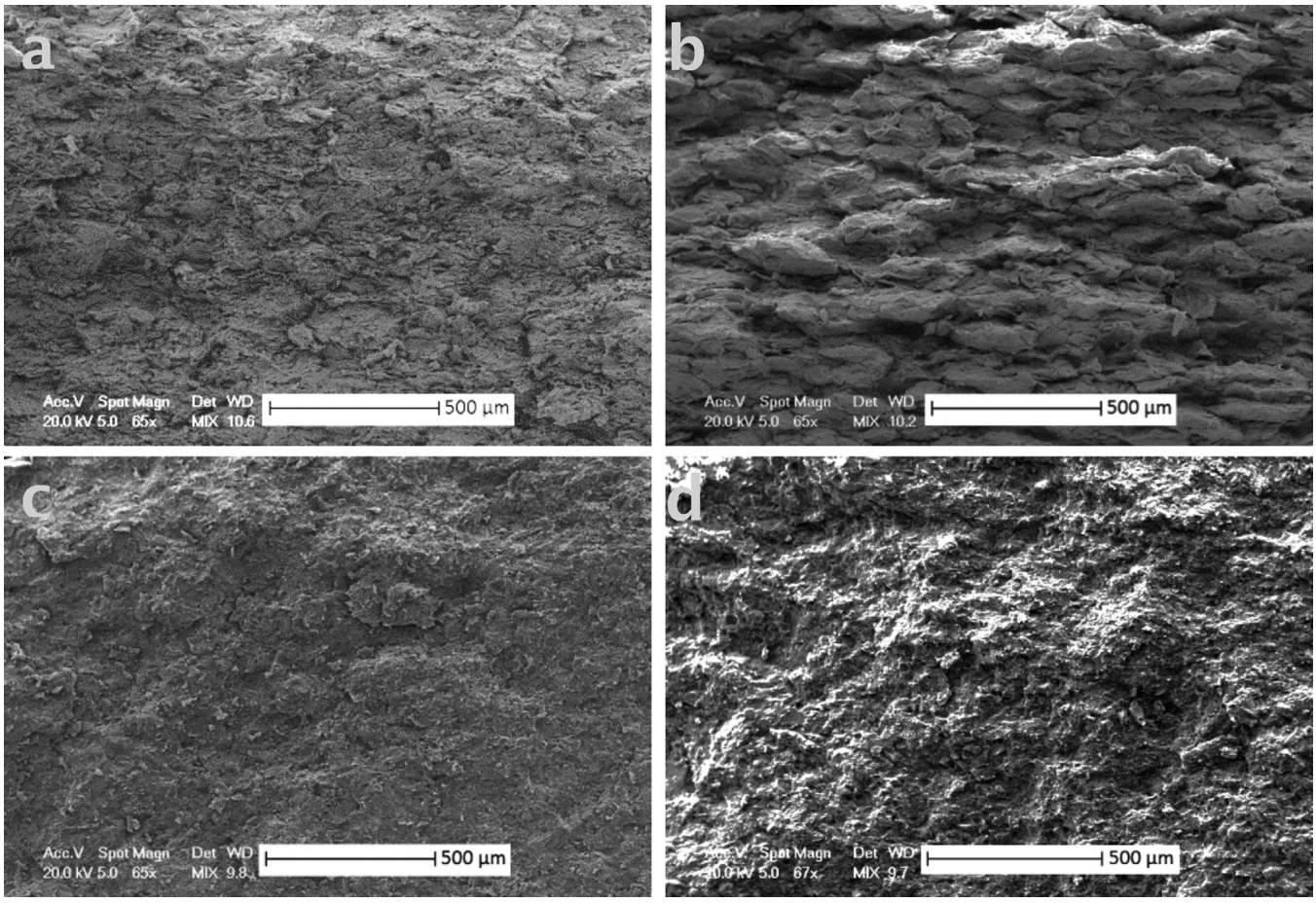

Fig. 8. SEM images of the cross-section of the tablets (a) MCC, (b) MCC + MgSt, (c) lactose and (d) lactose + MgSt. The tablets were pressed at 380 MPa during 1 s. The compression direction is vertical in the images. All the images have the same magnification and a scale bar of 500 μm size.

at the cross-section of the lubricated formulation of lactose or mannitol is distinguishable to that of the pure excipients (see Fig. 8), but the differences appear to be limited to small changes in the roughness, largely due to the presence (pure) or absence (with Mg stearate) of very fine fragments. The cohesion of a tablet comprised of pure brittle materials like lactose and mannitol is not substantially affected by the addition of a lubricant. This is a result of the fragmentation that brittle materials experience under pressure, with fracture within the particulate material, rather than at the contacts between the particles, creating new surface areas not previously exposed to Mg stearate during blending. In this case, the fracture observed on the tablet when the diametrical pressure is applied is a brittle one. The tablet breaks apart in several pieces when the pressure reaches its threshold.

4. Conclusion

Tableting performance of a formulation is affected by bulk and surface properties of the powder bed and processing parameters; the tablet surface properties are largely determined by the bulk properties of the formulation.

Synthesis of the information obtained from the tablet surfaces, their cross sections and the tablet hardness tests allows a coherent picture to develop. Firstly, mannitol and lactose can be broadly considered to behave in the same way, while MCC behaves significantly differently. The powder aggregates of MCC are much larger initially (of the order of 100 s of μm) but after tableting the roughness is more limited to being defined by the fibrous constituents, but nonetheless requires both AFM and profilometry to study the roughness over all scales. The larger roughness of the MCC tablet surfaces is evidence of the elastic recovery after compression, which reflects both the properties of the fibers as well as the nature of the interparticle bonds.

From AFM images we extract not only topographical information but also the fact that the MCC is significantly more adhesive towards polar material–which in turn necessarily means that it will have higher cohesive interactions than the other two materials. The AFM also clearly reveals that the effect of Mg stearate is to provide a thin coating over at least parts of the surface which significantly reduces the adhesion with the AFM tip in all cases. In identical fashion the Mg stearate may coat the internal surfaces, and reduce the adhesion between the particle contacts. The elastic recovery of the MCC can therefore also be directly related to the elasticity of the adhesive bonds between the particles–when Mg stearate is added this elastic recovery disappears as evidenced by the much more even surfaces observed in profilometry. This is due to lubrication by the Mg stearate–the adhesive bonds are not lost, but instead of deforming, slide, precluding recovery. The SEM pictures of the cross section reveal this sliding as a dramatic layering feature, seen in none of the other tablets.

The notable difference in behavior of the tablet strength toward Mg stearate can also be rationalized with the above to understand the different fracture mechanisms. Neither the lactose nor the mannitol tablet strength was remotely affected by the addition of Mg stearate, despite the fact that the AFM reveals that the Mg stearate reduces the strength of adhesion. This clearly indicates that failure in the case of mannitol and lactose is not at the bonds between the particles, but within the particles themselves, and this

fracture and failure therefore exposes new surface area which is not coated with Mg stearate. MCC on the other hand shows a dramatic reduction in tablet strength consistent with a fracture mechanism related to failure at the greatly weakened and lubricated bonds between interlocking fiber particles.

An interesting observation is that for mixed excipients systems the tablet robustness appears to reflect some sort of average value of the constituents, but this is not a linear function, the average appears to be always weighted slightly in favor of the mannitol/lactose component irrespective of whether Mg stearate is present. This is significant because in the presence of Mg stearate the "pure" lactose/mannitol excipient is harder than the equivalent MCC tablet, in its absence it is weaker. Thus it should be concluded that the slight favoring of the non-MCC component is related to the smaller particles size and the greater number of contacts associated with such particles.

The combination of AFM and profilometry with SEM and traditional tablet hardness measurements is crucial for providing a coherent mechanistic picture of the tablet structure and strength and its dependence upon excipient properties.

Finally we speculate that the phenomena of picking in tableting can be explained by the arguments made above. The fracture of mannitol and lactose exposes fresh surface, which is much more adhesive than that which is coated with Mg stearate and this may have the tendency to stick to the punch surface, whereas the interlocked, coated MCC cannot.

References

Augsburger, Larry L., and Hoag, Stephen W., eds. Pharmaceutical Dosage Forms: Tablets, Volume 3: Manufacture and Process Control (3rd ed.). New York, NY, USA: CRC Press, 2008. ProQuest ebrary. Web. 3 April 2015. Alderborn, G., Frenning, G., 2008. Chapter 7: Mechanical strength of tablets.

Alderborn, G., Nystrom, C., 1996. Pharmaceutical Powder Compaction Technology. Marcel Dekker, Inc..

Aleksovski, A., Dreu, R., Gaperlin, M., Planinek, O., 2015. Mini-tablets: a contemporary system for oral drug delivery in targeted patient groups. Exp. Opin. Drug Deliv. 12 (1), 65–84 p. 65-84 12.

Amidon, G.E., Secreast, P.J., Mudie, D., 2009. Chapter 8–Particle, powder, and compact characterization. In: Qin, Y., Chen, Y., G.G.Z, Liu L., Porter, W.R. (Eds.), Developing Solid Oral Dosage Forms. Academic Press, San Diego, pp. 163–186.

Doelker, E., 1993. Comparative compaction properties of various microcrystalline cellulose types and generic products. Drug Dev. Ind. Pharm. 19, 2399–2471.

Duner, G., Thormann, E., Dedinaite, A., Claesson, P.M., Matyjaszewski, K., Tilton, R.D., 2012. Nanomechanical mapping of a high curvature polymer brush grafted from a rigid nanoparticle. Soft Matter. 8, 8312–8320.

Feiler, A., Jenkins, P., Rutland, M., 2005. Effect of relative humidity on adhesion and frictional properties of micro- and nano-scopic contacts. J. Adhes. Sci. Technol. 19, 165–179.

Feiler, A.A., Stiernstedt, J., Theander, K., Jenkins, P., Rutland, M.W., 2007. Effect of capillary condensation on friction force and adhesion. Langmuir: ACS J. Surf. Colloids 23, 517.

Hamad, M.L., Bowman, K., Smith, N., Sheng, X., Morris, K.R., 2010. Multi-scale pharmaceutical process understanding: from particle to powder to dosage form. Chem. Eng. Sci. 65, 5625–5638.

Harding, L.J., Reading, M., Craig, D.Q.M., 2008. The development of thermally assisted particle manipulation and thermal nanointeraction studies as a means of investigating drug-polymer interactions. J. Pharm. Sci. 97, 1551–1563.

Hoag, S.W., 2008a. Pharmaceutical dosage forms: tablets, 3rd ed. Manufacture and Process Control, vol. 3. Informa Healthcare.

Hoag, S.W., 2008b. Pharmaceutical dosage forms: tablets, 3rd ed. Rational Design and Formulation, vol. 2. Informa Healthcare.

Hussain, M.S.H., York, P., Timmins, P., 1988. A study of the formation of magnesium stearate film on sodium chloride using energy-dispersive X-ray analysis. Int. J. Pharm. 42, 89–95.

Jain, S., 1999. Mechanical properties of powders for compaction and tableting: an overview. Pharm. Sci. Technol. Today 2, 20–31.

Jallo, L.J., Chen, Y., Bowen, J., Etzler, F., Dave, R., 2011. Prediction of inter-particle adhesion force from surface energy and surface roughness. J. Adhes. Sci. Technol. 25, 367–384.

Kaur, H., 2012. Processing technologies for pharmaceutical tablets: a review. Int. Res. J. Pharm. 3, 20.

Li, Q., Rudolph, V., Weigl, B., Earl, A., 2004. Interparticle van der Waals force in powder flowability and compactibility. Int. J. Pharm. 280, 77–93.

Matero, S., Den Berg, F.v., Poutiainen, S., Rantanen, J., Pajander, J., 2013. Towards better process understanding: chemometrics and multivariate measurements in manufacturing of solid dosage forms. J. Pharm. Sci. 102, 1385–1403.

Mizuno, H., Luengo, G.S., Rutland, M.W., 2010. Interactions between crossed hair fibers at the nanoscale. Langmuir 26, 18909–18915.

Moody, G., Rubinstein, M.H., FitzSimmons, R.A., 1981. Tablet lubricants I: theory and modes of action. Int. J. Pharm. 9, 75–80.

Nordgren, N., Rutland, M.W., 2009. Tunable nanolubrication between dual-responsive polyionic grafts. Nano Lett. 9, 2984.

Nyström, C., Alderborn, G., Duberg, M., Karehill, P.-g., 1993. Bonding surface area and bonding mechanism-two important factors for the understanding of powder comparability. Drug Dev. Ind. Pharm. 19, 2143–2196.

Patel, S., Kaushal, A.M., Bansal, A.K., 2006. Compression physics in the formulation development of tablets. Critic. Rev. Ther. Drug Carrier Syst. 23, 1–65.

Perrault, M., Bertrand, F., Chaouki, J., 2010. An investigation of magnesium stearate mixing in a V-blender through gamma-ray detection. Powder Technol. 200, 234–245.

Pettersson, T., Nordgren, N., Rutland, M.W., Feiler, A., 2007. Comparison of different methods to calibrate torsional spring constant and photodetector for atomic force microscopy friction measurements in air and liquid. Rev. Sci. Instrum. 78, 093702.

Picker-Freyer, K., 2007. An insight into the process of tablet formation of microcrystalline cellulose. J. Therm. Anal. Calorim. 89, 745–748.

Ralston, J., Larson, I., Rutland, M.W., Feiler, A.A., Kleijn, M., 2005. Atomic force microscopy and direct surface force measurements (IUPAC technical report). Pure Appl. Chem. 77, 2149–2170.

Rathje, L.-S.Z., Nordgren, N., Pettersson, T., Rönnlund, D., Widengren, J., Aspenström, P., Gad, A.K.B., 2014. Oncogenes induce a vimentin filament collapse mediated by HDAC6 that is linked to cell stiffness. Proc. Natl. Acad. Sci. U. S. A. 111, 1515.

Roblot-Treupel, L., Puisieux, F., 1986. Distribution of magnesium stearate on the surface of lubricated particles. Int. J. Pharm. 31, 131–136.

Sader, J.E., Chon, J.W.M., Mulvaney, P., 1999. Calibration of rectangular atomic force microscope cantilevers. Rev. Sci. Instrum. 70, 3967–3969.

Saniocki, I., 2014. Characterization and quantification of sticking to punch surfaces during tablet manufacture by direct compaction. Dissertation., Staats- und Universitätsbibliothek Hamburg, Hamburg.

Sinka, I.C., Motazedian, F., Cocks, A.C.F., Pitt, K.G., 2009. The effect of processing parameters on pharmaceutical tablet properties. Powder Technol. 189, 276–284.

Sun, C.C., 2011. Decoding powder tabletability: roles of particle adhesion and plasticity. J. Adhes. Sci. Technol. 25, 483–499.

Toyoshima, K., Yasumura, M., Ohnishi, N., Ueda, Y., 1988. Quantitative evaluation of tablet sticking by surface roughness measurement. Int. J. Pharm. 46, 211–215.

van der Watt, J.G., 1987. The effect of the particle size of microcrystalline cellulose on tablet properties in mixtures with magnesium stearate. Int. J. Pharm. 36, 51–54.

van Veen, B., van der Voort Maarschalk, K., Bolhuis, G.K., Zuurman, K., Frijlink, H.W., 2000. Tensile strength of tablets containing two materials with a different compaction behaviour. Int. J. Pharm. 203, 71–79.

Wang, J., Wen, H., Desai, D., 2010. Lubrication in tablet formulations. Eur. J. Pharm. Biopharm. 75, 1–15.

Wang, J.J., Li, T., Bateman, S.D., Erck, R., Morris, K.R., 2003. Modeling of adhesion in tablet compression—I. Atomic force microscopy and molecular simulation. J. Pharm. Sci. 92, 798–814.

Zhang, Y., Law, Y., Chakrabarti, S., 2003. Physical properties and compact analysis of commonly used direct compression binders. AAPS PharmSciTech 4, 489–499.

Tablet mechanics depend on nano and micro scale adhesion, lubrication and structure.

Maria Badal Tejedor[a,b], Niklas Nordgren[a], Michael Schuleit[c], Mark W. Rutland[a,b], Anna Millqvist-Fureby*[a].

[a]SP, Technical Research Institute of Sweden, Box 5607, SE-114 86 Stockholm, Sweden
Anna.Fureby@sp.se; Mobile: +46 768640082
[b]KTH Royal Institute of Technology, Division of Surface and Corrosion Science, Drottning Kristinas väg 51, SE-100 44 Stockholm, Sweden.
[c]Novartis Pharma AG, Novartis Institutes for Biomedical Research, GDC, Novartis Campus, 4002 Basel, Switzerland.

SUPPORTING INFORMATION

The SEM micrographs in figures S 1-9 show the tablet surfaces of all the formulations when pressed at 75 MPa 1s, 380 MPa 1s and 75 MPa 30s. All the samples showed a more compact structure when the applied load was of 380 MPa. A less compact structure was observed under a lower applied load while no structural difference was noticed when the lower applied load was hold for 30s.

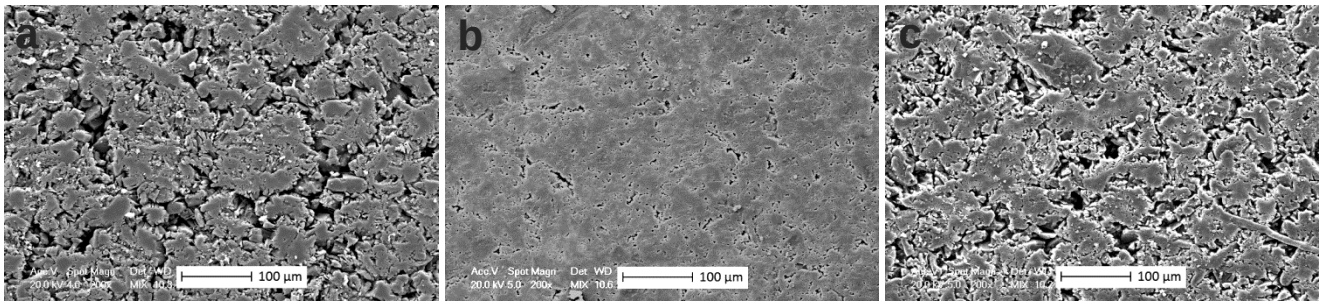

Figure S1. SEM images of the gold sputtered *lactose* tablet surface pressed under different compaction conditions: (a) 75 MPa – 1s, (b) 380 MPa – 1s, (c) 75 MPa – 30s. All the images were taken at the same magnification and have a scale bar of 100 µm length.

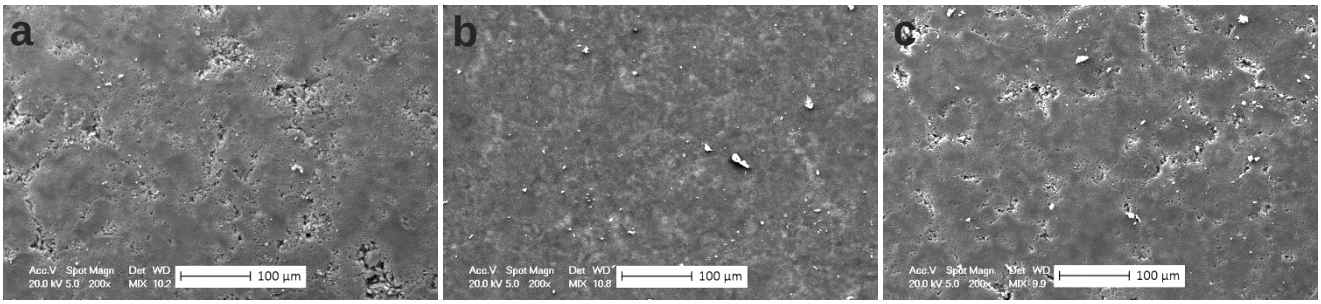

Figure S2. SEM images of the gold sputtered *mannitol* tablet surface pressed under different compaction conditions: (a) 75 MPa – 1s, (b) 380 MPa – 1s, (c) 75 MPa – 30s. All the images were taken at the same magnification and have a scale bar of 100 µm length.

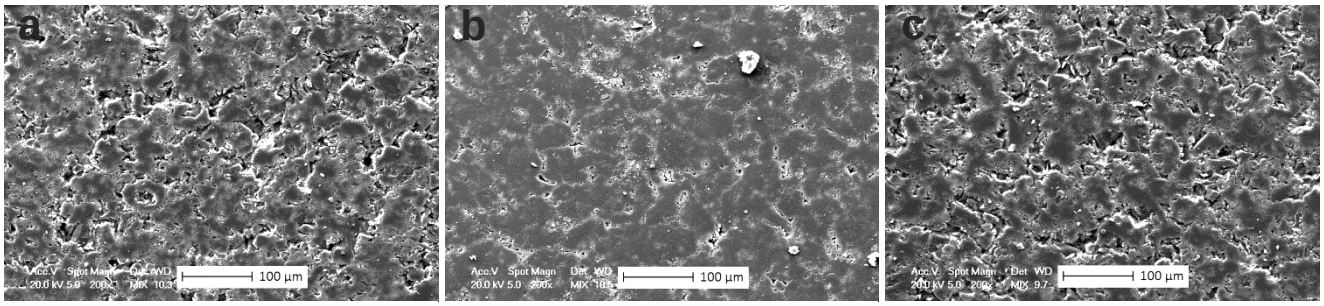

Figure S3. SEM images of the gold sputtered lactose+MgSt tablet surface pressed under different compaction conditions: (a) 75 MPa – 1s, (b) 380 MPa – 1s, (c) 75 MPa – 30s. All the images were taken at the same magnification and have a scale bar of 100 µm length.

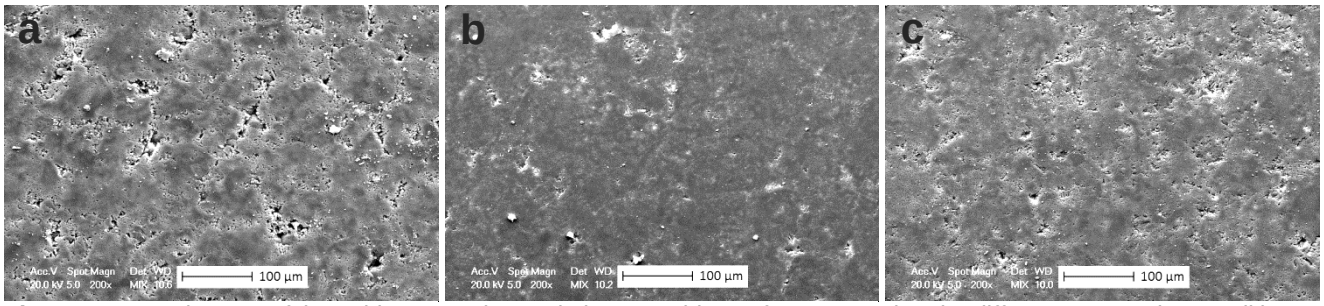

Figure S4. SEM images of the gold sputtered *mannitol+MgSt* tablet surface pressed under different compaction conditions: (a) 75 MPa – 1s, (b) 380 MPa – 1s, (c) 75 MPa – 30s. All the images were taken at the same magnification and have a scale bar of 100 µm length.

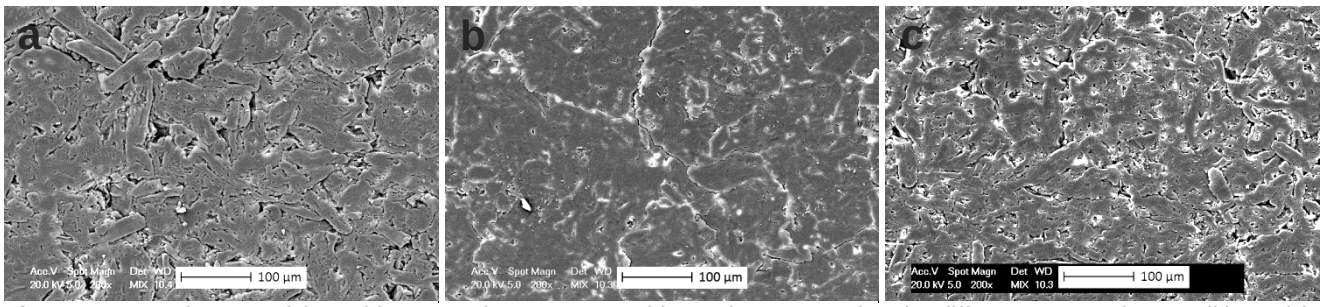

Figure S5. SEM images of the gold sputtered *MCC+MgSt* tablet surface pressed under different compaction conditions: (a) 75 MPa – 1s, (b) 380 MPa – 1s, (c) 75 MPa – 30s. All the images were taken at the same magnification and have a scale bar of 100 µm length.

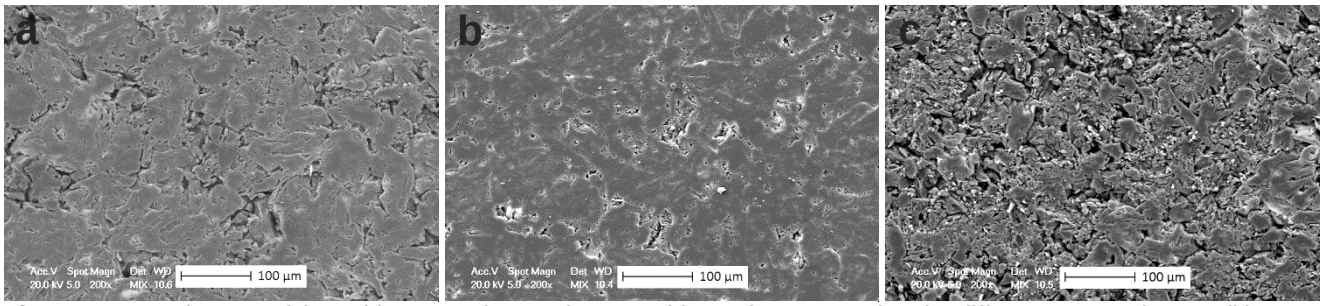

Figure S6. SEM images of the gold sputtered *MCC+lactose* tablet surface pressed under different compaction conditions: (a) 75 MPa – 1s, (b) 380 MPa – 1s, (c) 75 MPa – 30s. All the images were taken at the same magnification and have a scale bar of 100 µm length.

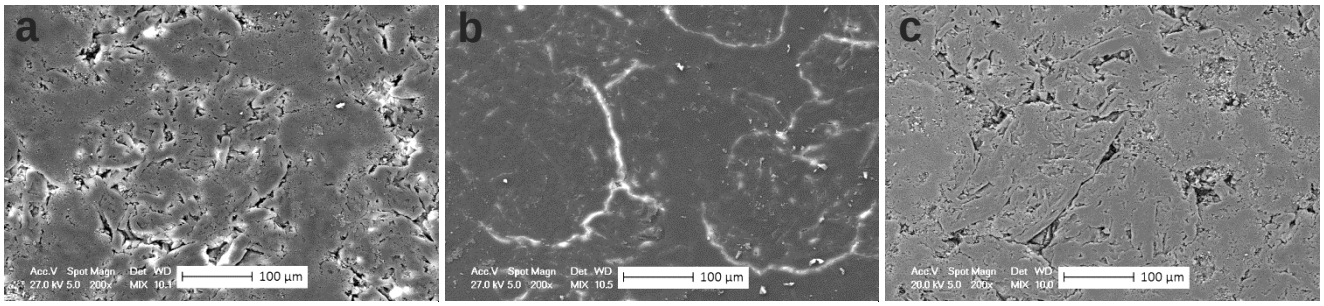

Figure S7. SEM images of the gold sputtered *MCC+mannitol* tablet surface pressed under different compaction conditions: (a) 75 MPa – 1s, (b) 380 MPa – 1s, (c) 75 MPa – 30s. All the images were taken at the same magnification and have a scale bar of 100 µm length.

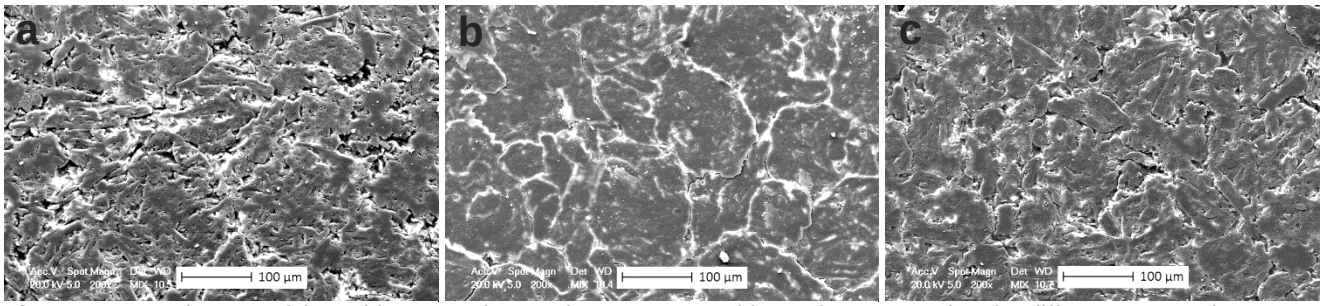

Figure S8. SEM images of the gold sputtered *MCC+lactose+MgSt* tablet surface pressed under different compaction conditions: (a) 75 MPa – 1s, (b) 380 MPa – 1s, (c) 75 MPa – 30s. All the images were taken at the same magnification and have a scale bar of 100 µm length.

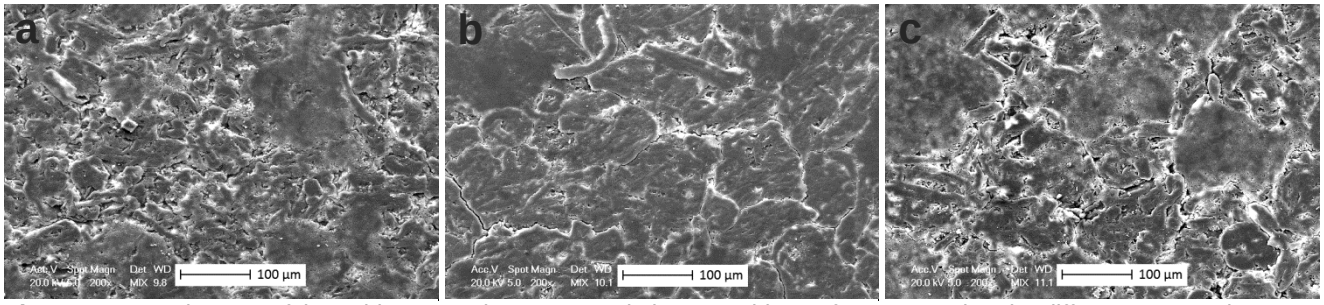

Figure S9. SEM images of the gold sputtered *MCC+mannitol+MgSt* tablet surface pressed under different compaction conditions: (a) 75 MPa – 1s, (b) 380 MPa – 1s, (c) 75 MPa – 30s. All the images were taken at the same magnification and have a scale bar of 100 µm length.

Surface roughness information from the AFM topographical images is summarized in Table 1. The values are an average from the average surface roughness data provided by AFM software for each 50x50um scan. A number of at least seven scans were performed at different areas over the tablets of pure MCC, lactose and mannitol; and also for the same excipients when formulated with 1% Mg stearate. The tablets used for these measurements were pressed at 380 MPa during 1s.

Of the pure excipients MCC showed the largest surface roughness whereas lactose surface roughness was lower. Mannitol presented the flattest tablet surface with a roughness value much lower than those for MCC and lactose. After addition of Mg stearate to the pure excipients, the tablet surface roughness values did not vary significantly. The excipient with a largest difference in roughness between the pure and lubricated tablet was mannitol, which also showed a larger standard deviation for the average value of the lubricated sample. The size of the studied areas was 50x50um which might be rather small to evaluate tablet surface roughness and the possible changes induced by addition of Mg stearate.

	Roughness (Rq)		
Single components	***MCC***	***Lactose***	***Mannitol***
AFM (nm)	182	159	47
StdDev	31,79	34,33	14,92
Two components	***MCC+MgSt***	***La+MgSt***	***Ma+MgSt***
AFM (nm)	196	149	93
StdDev	26,94	40,52	111,51

Table S1. Surface roughness data collected from the 50x50um AFM topographical images of pure excipients: MCC, lactose and mannitol; and these lubricated with 1% Mg stearate. The tablets were pressed at 380 MPa during 1s.

In order to evaluate changes in roughness induced by lubrication of the pure excipients with Mg stearate, profilometry measurements were carried out. Table 2 shows the average data collected from the measurements performed on a 440x330 μm area over the tablets of pure excipients (MCC, lactose and mannitol) and those after addition of Mg stearate. The tablets were pressed at 380 MPa during 1s. Three different measurements were performed on each sample.

Of the pure excipients MCC showed the largest surface roughness while mannitol presented the lowest one. When Mg stearate was added to the pure excipients, MCC showed a decreased in surface roughness compared to the pure tablet. This did not occur in case of lactose and mannitol where no significant differences were observed on the surface roughness data between the pure and the lubricated samples.

	Roughness (Rq)			Waviness (Wq)		
Single components	***MCC***	***Lactose***	***Mannitol***	***MCC***	***Lactose***	***Mannitol***
Profilometer (nm)	1355	387	162	1100	210	130
StdDev	295,53	26,9	11,67	264,46	10,69	15,01
Two components	***MCC+MgSt***	***La+MgSt***	***Ma+MgSt***	***MCC+MgSt***	***La+MgSt***	***Ma+MgSt***
Profilometer (nm)	998	433	162	710	260	100
StdDev	121,18	70,68	31,53	87,9	31,53	9,71

Table S2. Surface roughness data as measured by profilometry for tablets of pure excipients: MCC, lactose and mannitol; and these lubricated with 1% Mg stearate. The tablets were pressed at 380 MPa during 1s.

The data for the surface roughness obtained with AFM and profilometry agreed on the tablet surface roughness trend for the three different excipients both lubricated and non-lubricated. As for the changes induced by lubrication AFM did not provide with any relevant information while profilometry showed a significant decrease in surface roughness for the lubricated MCC sample. However, surface roughness data may vary depending on the size of the analyzed area in a non-homogeneous and rough sample such as the tablets. Profilometer provides data of a larger area of the tablet surface. Therefore, it is possible to conclude that Mg stearate induces changes on the MCC tablet surface roughness while lactose and mannitol are not significantly affected. This effect can also be observed visually at the Profilometer images in the publication.

The micrographs shown in figure S10 are the tablet cross-section of the MCC and MCC with MgSt formulations when pressed at 75 MPa for 1s and 30s. An organized particle arrangement is observed at the internal structure of the MCC tablet when MgSt is present in the formulation.

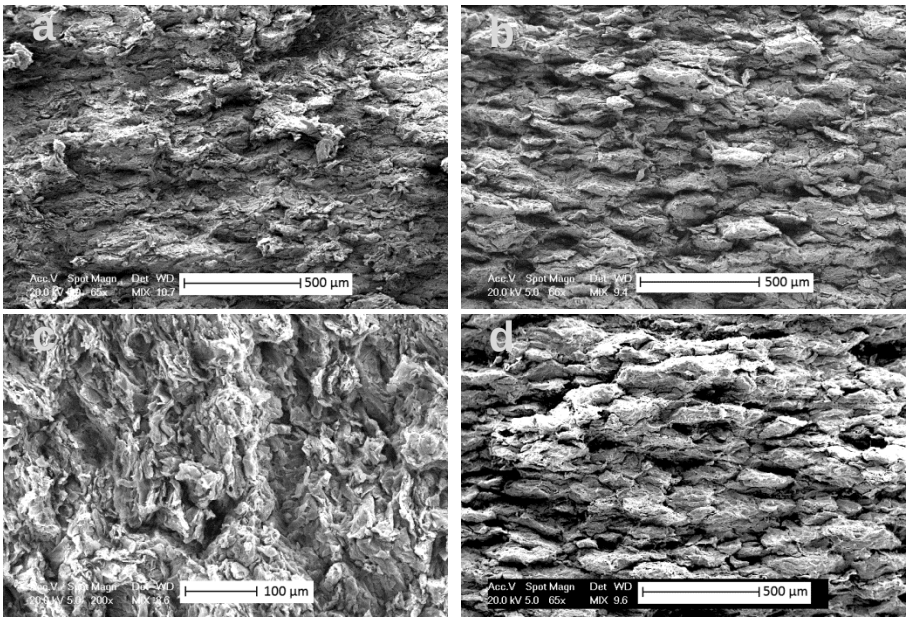

Figure S10. SEM images of the cross-section of the (a) MCC and (b) MCC+MgSt tablets pressed at 75 MPa during 1s and the (c) MCC and (d) MCC+MgSt tablets pressed at 75 MPa during 30s. The compression direction is vertical in the images, except for image c which is diagonally applied. All the images have the same magnification and a scale bar of 500 µm size, except for image c which scale bar is of 100 µm size.

The SEM images in figure S11 show the cross section of the tablet of mannitol without and with Mg stearate. The internal structure of the tablets does not present a parallel layer organization of the particles as it was observed for the MCC when Mg stearate was present in the formulation.

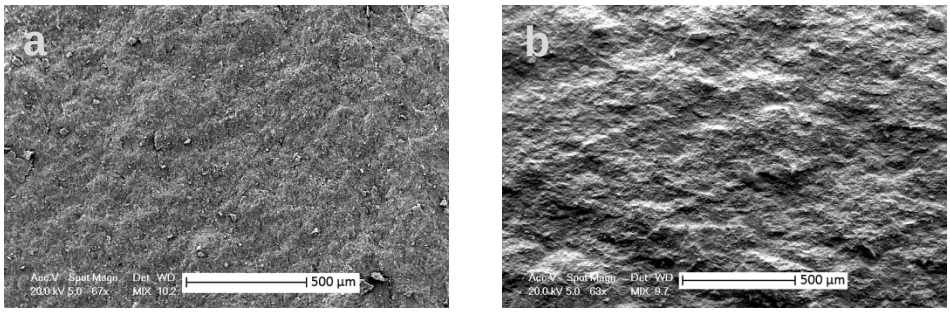

Figure S11. SEM images of the cross-section of the tablets pressed at 380 MPa 1s of (a) mannitol and (b) mannitol+MgSt. The compression direction is vertical in the images. All the images have the same magnification and a scale bar of 500 µm size.

Another observation made on the tablet surface for two of the studied binary formulations is presented in figure S12, which illustrates the surface of the MCC+lactose and MCC+mannitol tablets. The surface of the MCC+mannitol tablet showed granules segregation under the SEM, but this was not observed for MCC+lactose tablets. Granule separation could be simply attributed to different behavior of the excipients under compression; mannitol particles are constituted by smaller units than lactose particles which may do not lead to an extensive breakage and consequent particle reorganization under pressure. Further, there is a possibility that the granule separation is well observed for MCC+mannitol since these materials are more different in their properties compared to MCC+lactose.

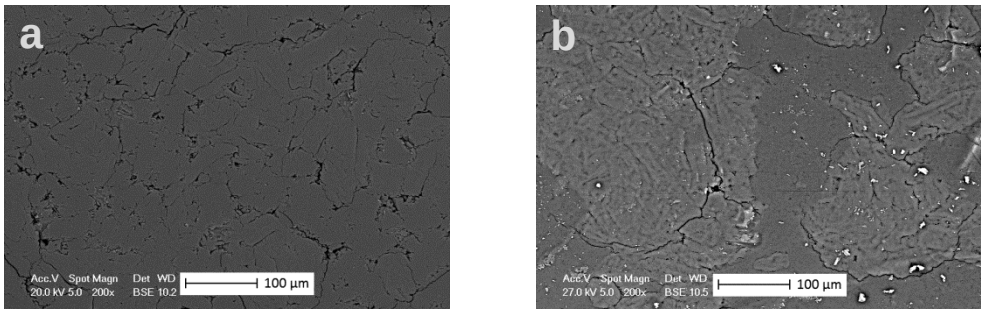

Figure S12. SEM images of the tablet surface of (a) MCC+lactose and (b) MCC+mannitol in a relation of 1:1 weight. The analyzed tablets were pressed at 380 MPa during 1s.

Paper IV

AFM colloidal probe measurements to mimic punch-particle surface interactions during tableting

Maria Badal Tejedor[a,b], Niklas Nordgren[a], Michael Schuleit[c], Anna Millqvist-Fureby[a], Mark W. Rutland[a,b]*.

[a]SP Technical Research Institute of Sweden, SP Chemistry, Materials and Surfaces, Box 5607, SE-114 86 Stockholm, Sweden
[b]KTH Royal Institute of Technology, Division of Surface and Corrosion Science, Drottning Kristinas väg 51, SE-100 44 Stockholm, Sweden
mark@kth.se; Mobile: +46768640081
[c]Novartis Pharma AG, Novartis Institutes for Biomedical Research, GDC, Novartis Campus, 4002 Basel, Switzerland

Abstract

Adhesion of the powders to the punches is a common issue during tableting. This phenomenon is known as *sticking* and affects the quality of the manufactured tablets. Defective tablets increase the cost of the manufacturing process. Thus the ability to predict the tableting performance of the formulation blend before the process is scaled-up is important. The adhesive propensity of the powder to the tableting tools is mostly governed by the surface-surface adhesive interactions. AFM colloid probe is a surface characterization technique that allows measurement of the adhesive interactions between two materials of interest. In this study, AFM steel colloidal probe measurements were performed on Ibuprofen, MCC, α-lactose monohydrate and spray dried lactose particles as an approach to modeling the punch-particle surface interactions during tableting. The excipients showed constant, small, attractive and adhesive forces towards the steel surface after repeated number of contacts. In comparison, Ibuprofen displayed a much larger attractive and adhesive interaction increasing over time both in magnitude and jump-in/jump-out separation distance. The type of interaction acting in the excipients-steel interface can be related to a Lifshitz force, relatively weak and short ranged. In contrast, the Ibuprofen-steel interaction is described by a capillary force profile. Even though Ibuprofen is not highly hydrophilic, the relatively smooth surfaces of the crystals allow "contact flooding" upon contact with the steel probe. Capillary forces increase due to "harvesting" of moisture - due to fast condensation kinetics- leaving a residual condensate that contributes to increase the interaction force after each consecutive contact. Local asperity contacts on the more hydrophilic surface of the excipients prevent flooding of the contact zone and there is no such adhesive effect under the same ambient conditions. The markedly different behavior detected by force measurements clearly shows the sticky and non-sticky propensity of the materials and allows a mechanistic description.

(Keywords: surface characterization, excipients, atomic force microscopy, colloid probe, tableting, ibuprofen.)

1. Introduction

Sticking is a common problem during tablet manufacturing in the pharmaceutical industry. It refers to the adhesion of the powders to the tablet punch and consequent buildup of a particulate layer on the surface of the punch. This leads to tablet defects which renders them unfit for sale, and the speed of the tableting process is such that a large number of tablets can be faulty. Hence, productivity levels decrease which leads to increasing manufacturing costs. Despite the fact that tablet sticking has been widely studied and documented[1-3], it remains poorly understood due to the complexity of this phenomenon. Multiple key factors could potentially contribute to the sticking phenomenon making the evaluation of the problem more difficult. Some examples are physicochemical properties of the powders, particle size and shape, surface energy, water content and fragmentation mechanisms under pressure[4]; all these parameters contribute to the formation of the tablet as a unit. It is important to keep a positive balance between internal tablet cohesion and tool/powder surface interactions to prevent stickiness. As batch sizes are increased, tool/powder surface interactions become more affected by the manufacturing conditions which may lead to sticking at later stages of the manufacturing process. Due to the difficulty at this stage of modifying the formulation, the solutions implemented to reduce stickiness are thus adjustments of the manufacturing conditions. Decreasing tableting speed and increasing the applied compaction force tends to mitigate the sticking issue [5,6]. Tool replacement with others of a different coating material and surface roughness might also alleviate the problem[7]. Furthermore, temperature and humidity conditions of the working environment affect material surface properties which in turn influence the tableting performance. Hence, it is essential to establish a good correlation between material properties, processing conditions and sticking propensity in order to assure good performance of the formulation from an early stage.

A rough evaluation of sticking is usually done by visual inspection of the tablets or the surface of the punches[8,9]. A precise quantification and assessment of the powder adhered to the punch can be achieved with liquid chromatography (HPLC), however this methodology requires expensive equipment and it is time consuming[10]. The impact of physicochemical properties of the materials, processing and ambient conditions during tableting has been studied by evaluating tablet quality parameters such tensile strength. Tablet tensile strength is directly associated with the strength of bonding adhesion/cohesion forces that arise during compaction. In successful tableting, these forces overcome the adhesion between the powder and tools, and prevent tablet defects[4]. Therefore tablet strength can be used to indirectly predict the sticking propensity of the powders. The so called pull-off force needed for tablet ejection or punch retraction has also been measured to elucidate the strength of the tool-powder interaction of different tablet ingredients or under various applied processing conditions. The aforementioned approaches for

sticking evaluation are however macroscopic. In fact sticking results from the contribution of all the individual particle-tool adhesive interactions at the nanoscale. Thus it is equally relevant to investigate the force interactions at the nanoscopic level that initiate and promote the sticking event.

Atomic force microscopy is a technique that has proved to be very useful in the field of surface force measurements. It has been widely used in pharmaceutical research due to the relevance of surface interactions in fundamental manufacturing processes[11,12]. The possibility of attaching a particle of interest at the very end of the AFM cantilever is offered by the so called colloidal probe technique[13,14]. Thus single particle force interactions can be measured as a function of separation (force-distance curves). The adhesive force minimum and type of force interaction are analyzed from the converted force-distance curves from the raw data, usually normalized by the radius of the probe. A well-defined area of contact is preferred, and spherical probes are ideal to allow data from different experiments to be compared. Various types of interactions can be distinguished, such as van der Waals, electrostatic and capillary forces[15-17]. The colloidal probe technique has been employed extensively during the last two decades by some of the authors to study different surface interactions and phenomena at the nanoscale[18-21].

As an approach to better understand the problem with sticking, the adhesion forces between a steel colloidal probe and some widely used excipients in tablet formulation i.e. crystalline and spray dried lactose and microcrystalline cellulose, along with a well-known sticking active drug: Ibuprofen, have been measured with AFM. The aim of the study is to elucidate the type of interaction and the magnitude of the force generated upon contact between the surface of the particles and the tools under realistic manufacturing conditions of humidity and temperature. The experimental approach was used to mimic continuous punch/particle interactions at the nanoscale in order to better understand their role during large scale tableting production.

2. Experimental

2.1. Materials

The materials used in the present study are microcrystalline cellulose (Cellulose Microcr. PH200, FMC), α-lactose monohydrate (KGaA, Merck), spray dried lactose and Ibuprofen (Ibuprofen 70, BASF).

2.1.1. Spray drying

Spray dried lactose powder was prepared in a laboratory spray dryer built at SP (Technical Research Institute of Sweden). A feed solution of a 10% solid content of α-lactose monohydrate was pumped at a flow rate of 5ml/min through a 2mm diameter orifice nozzle. The sprayed solution was dried in a 0.75 x 0.15 m drying chamber with an air flow of 0.8 m^3/min. The dryer operates in co-current mode with a jacketed two-fluid nozzle operated with pressurized air at 20 °C. The inlet temperature was set to 150 °C while the outlet temperature was 70-75 °C. The powder flowed through a cyclone and was collected by gravitational deposition in a vessel attached below the cyclone. The spray dried powder was stored into a desiccator under 0-5 % relative humidity at room temperature.

2.2. Scanning electron microscopy

Before imaging the powder samples were sprinkled on a double-sided tape adhered on an aluminium holder. The excess of powder was blown out with pressurized air. In order to obtain images at large magnifications without burning the samples with the electron beam, the particles were gold coated (120 s, 40 mA) with a Balzers SCD050 coater. Scanning electron microscopy was performed using a FEI-XL, 30 series in high vacuum with a voltage of 5 kV.

2.3. Atomic force microscopy

Force measurements were performed using a MultiMode Picoforce atomic force microscope with a Nanoscope V controller (Bruker, Santa Barbara, CA). The colloidal probe technique[13] was employed using steel functionalized probes (Fig. 1)[22]. Spherical steel particles of approximately 18 to 23 μm diameters were glued to the end of uncoated tip-less cantilevers (HQ-NSC12-35/No Al, Mikromasch (Estonia)) with a very small amount of epoxy resin by using a micromanipulator (Eppendorf 5171, Hamburg) under an optical microscope. The cantilever spring constant was obtained using the calibration technique of Sader[23,24]. Several colloid probes were used and their size was rather consistent. For the setup of the measurement, the cantilever was placed in a holder above the powder sample. The powder sample was prepared by sprinkling the powder on a double sided sticky tape mounted on a metallic holder. The excess of powder was then removed with pressurized air. The selection of the particle and the approach of the cantilever to the particle were facilitated using an optical microscope. Due to optical reasons during the approach of the probe to the particle surface, the

particles selected were larger than 50 μm in size. The measurements were performed over a total number of nine spots across the surface of the different particles for statistical analysis. At least three different spots (a, b, c) on a minimum of three particles (1, 2, 3) per sample were evaluated. A set of 20 single force measurements were performed at each spot with a ramp size of 1 μm at a rate of 0,501 Hz. The maximum loading force was set to 24 nN. In order to verify that the colloidal probe had not been contaminated during contact with the samples force measurements on a clean mica surface were conducted before and after the measurements on each of the different materials. For one of the probes it was possible to perform measurements on all of the materials with documented "contamination free" status each time, so for comparison purposes all data is shown for this probe.

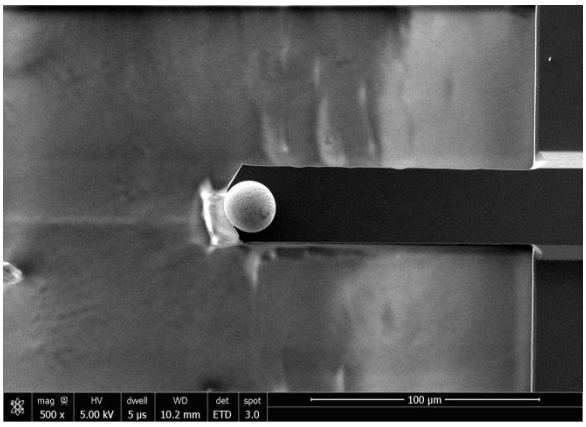

Figure 1. SEM image of the steel colloidal probe mounted on a tipless cantilever used to perform the force measurements.

AFM force IT v2.5.4 software (ForceIT, Sweden) was used for the evaluation of the force curves and to extract the corresponding relevant information. The deflection of the cantilever is monitored via the photodiode signal and voltage converted to meters by using the so called constant compliance region[13] from the force measurements performed on a hard reference such mica[25]. The deflection of the cantilever is converted into force units by using Hooke's law and the calibrated spring constant[22], and then plotted as a function of the separation distance. In order to collect an adhesion value at each contact, the depth of the adhesive minimum was extracted from each constructed force curve and normalized with the radius of the probe according to Derjaguin's approximation[26].

The data for the adhesive minimum depth were plotted as an average for each set of force measurements. The minimum depth of adhesion for each set of measurements was also represented in a sequential order (see supporting information) for evaluation of the evolution of the adhesion over time after repeated contacts. The measurements were performed at ambient conditions (24±2 °C and relative humidity of 45±5%).

3. Results and discussion

A sticky model drug, Ibuprofen, and excipients that are known to experience a different tabletability behavior were used in this study[27,28]. A readily compressible excipient such as MCC, and lactose in both crystalline and amorphous form which tend to be more problematic during compression, were all firstly evaluated with SEM. Images of the topographical features found across the excipients and Ibuprofen are displayed in Figure 2. MCC particles show a relatively round shape with a rough fiber-like surface structure (Fig. 2a). The lactose particles in both the crystalline and amorphous forms show a completely different morphology. Crystalline lactose powder presents a wide particle size variation of regularly shaped particles (Fig. 2b); while spray dried lactose results in smooth, generally much smaller, spherical particles of an amorphous structure (Fig. 2c). The spheres tend to adhere to each other forming larger agglomerates. Ibuprofen particles are elongated crystals with a tetrahedral shape and flat side faces (Fig. 2d).

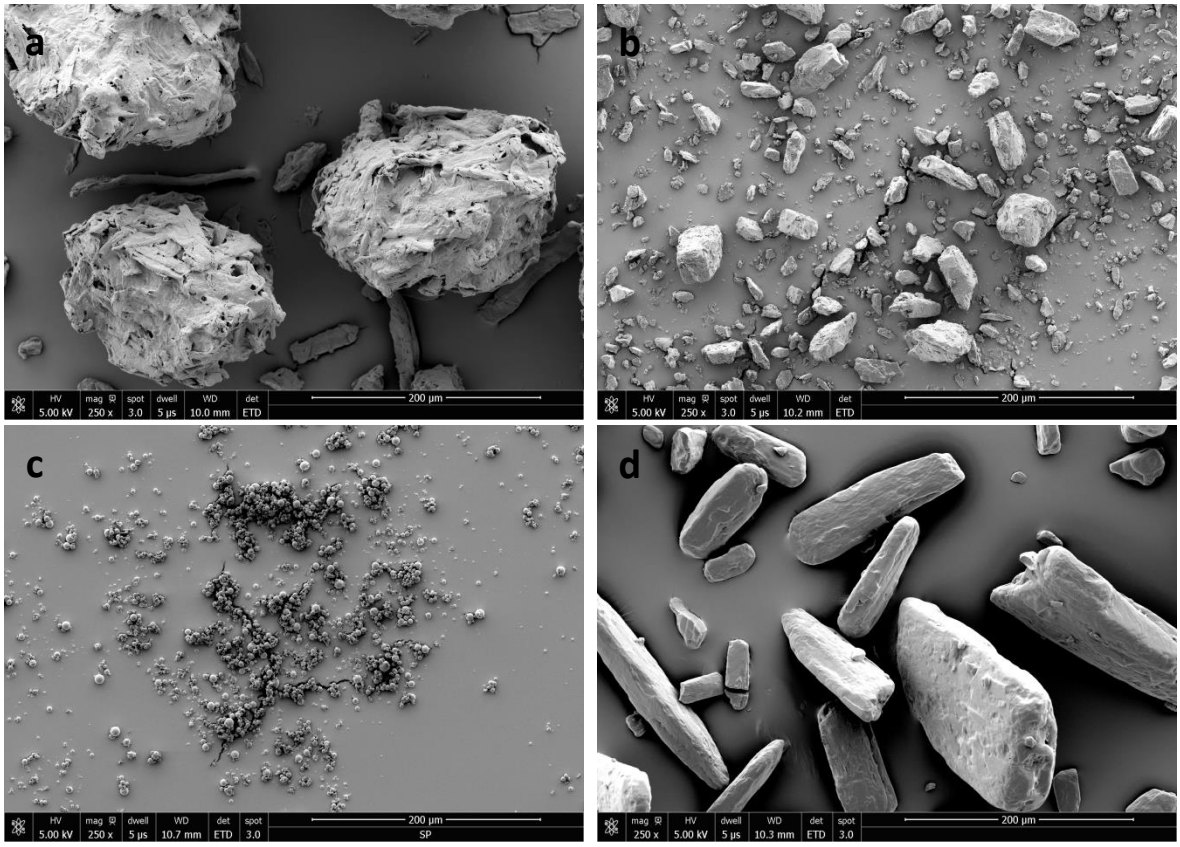

Figure 2. SEM images of the (a) MCC, (b) lactose monohydrate, (c) spray dried lactose and (d) Ibuprofen particles. Scale bar of 200 µm.

The surfaces of the particles come into direct contact with the surface of the steel punch during tableting. The probability that the surfaces adhere to each other will partially depend on the force with which these two surfaces interact. AFM force measurements were performed to evaluate the magnitude of the adhesion force between the individual particles for each of the powder samples and the steel surface. The particle selection for AFM evaluation was based on the particle size since a certain area is required to approach the particle with the colloid probe and further analyze it across the selected area. The preferred particles for MCC, crystalline lactose and Ibuprofen measurement were of a minimum size of ca 100 μm. Since the size of the spray dried lactose particles is smaller than 50 μm, the measurements were performed on the particle agglomerates. Thus it was possible for the colloidal probe to be in contact with several particles simultaneously.

Figure 3 shows typical force-separation curves for each of the evaluated samples. The normal force curves obtained can be classified into two different types: short distance/sharp retraction and long distance/extended retraction. The retraction curves classified as short distance present a jump out separation distance of about 10-20 nm. A longer jump out separation distance is denominated as a long distance retraction. Sharp retraction refers to the shape of the retraction curve in which no progressive deflection is observed between the minimum force and the non-contact position (ie. The surfaces jump apart from a well-defined point). The opposite behavior is referred to as extended retraction and in this case implies a sluggish physical separation of the surfaces, which may be due to deformation, capillary bridging, etc [16,25].

A short distance/sharp retraction is observed for MCC, lactose monohydrate and spray dried lactose (Fig. 3a, 3b, 3c) in 78% of the performed measurements. The probe jumps into contact from a separation distance of around 5nm with a low attractive force and retracts with a detachment force lower than 10 N/m. The corresponding separation distances to pull the surfaces apart are about 10-20 nm. When the pull-off force overcomes the adhesive interaction between the two surfaces, the cantilever instantly jumps out of contact for these three excipients. In contrast, Ibuprofen shows a longer distance/extended interaction during the probe-particle retraction in approximately 65% of the performed measurements. Upon approach the probe jumps into contact from around 50 nm due to a longer ranged attractive force of about 20 mN/m. As for the retraction of the probe, zero force is not achieved until a separation distance of around 150 nm. The adhesion force is of the order of 60 mN/m, six times larger than for the other evaluated excipients. The force-separation profile of Ibuprofen in Figure 3d is therefore presented on a different scale to those of the other excipients.

Several different types of forces can act at the particle-steel interface. Interactions such as Lifshitz attractive forces are relatively weak and short ranged; they are always present however, and an estimate of this force is shown in each of the graphs in figure 3 as a continuous black line. Electrostatic interactions

are strong and act over much larger distances. A fit to an electrostatic coulombic interaction is shown in figure S10 with a continuous orange line. Charge transfer may occur during the contact, depending on the state of the materials or the crystallographic structure of each face[29]. An increase of charge would clearly promote higher adhesion forces between the interacting surfaces do such an explanation is appealing, particularly in view of the apparently convincing form of the data in figure S10. On the other hand the repeat nature of the experiments means that an equally long ranged attractive force should be manifested on approach[30], which is clearly missing in figure 3d. Ambient humid conditions greatly affect the charge of the materials. Water interacts with the materials surface dissipating the charge[31]. Capillary forces may also arise if sufficient water condenses to form a water bridge between the two surfaces. This would create a quite strong adhesive interaction, but the occurrence of water bridge formation will be dependent on the hydrophilic surface properties of the materials[32] and depends strongly on topography[16,33]. Even though temperature and relative humidity conditions were kept within a constant range, (24±2 °C and 45±5% RH) capillary forces will act at the local asperity contacts of hydrophilic materials though for surface roughnesses below the Kelvin radius this does not strongly affect the adhesion[16,34]. For smooth surfaces, (roughness less than Kelvin radius) the formation of a condensate floods the contact zone and will dramatically increase adhesion[16,33,34] (see supporting information).

According to the different types of force profiles described above, the exemplified profiles shown in figure 3 measured with AFM for MCC, lactose monohydrate and spray dried lactose can be related to a conventional Lifshitz interaction. While all these materials are sufficiently hydrophilic for capillary condensation to occur, this is likely confined to the aforementioned asperities and the adhesion is thus below the flooding threshold. Ibuprofen on the other hand shows a much larger adhesive attraction towards the steel particle. The magnitude of the adhesion force (as well as its extended nature) is also consistent with a capillary force[35], Ibuprofen is not highly hydrophilic on any of its crystal faces[28] (contact angles between 45 and 70°) so it might initially seem unlikely that significant capillary condensation will occur on this material. The thermodynamics of condensation are such however that condensation is possible in symmetric systems with contact angles below 90° (see for example[36,37]). For an asymmetric system such as this the thermodynamics demand that the net decrease in surface energy associated with condensation outweighs the enthalpy penalty of condensation below the saturation vapour pressure. Given that steel has a hydrophilic oxide surface, this criterion is therefore met. (Note that presence of liquid water bridges will prevent electrostatic charging so one does not need to consider the possibility of both electrostatic and capillary mechanisms occurring simultaneously).

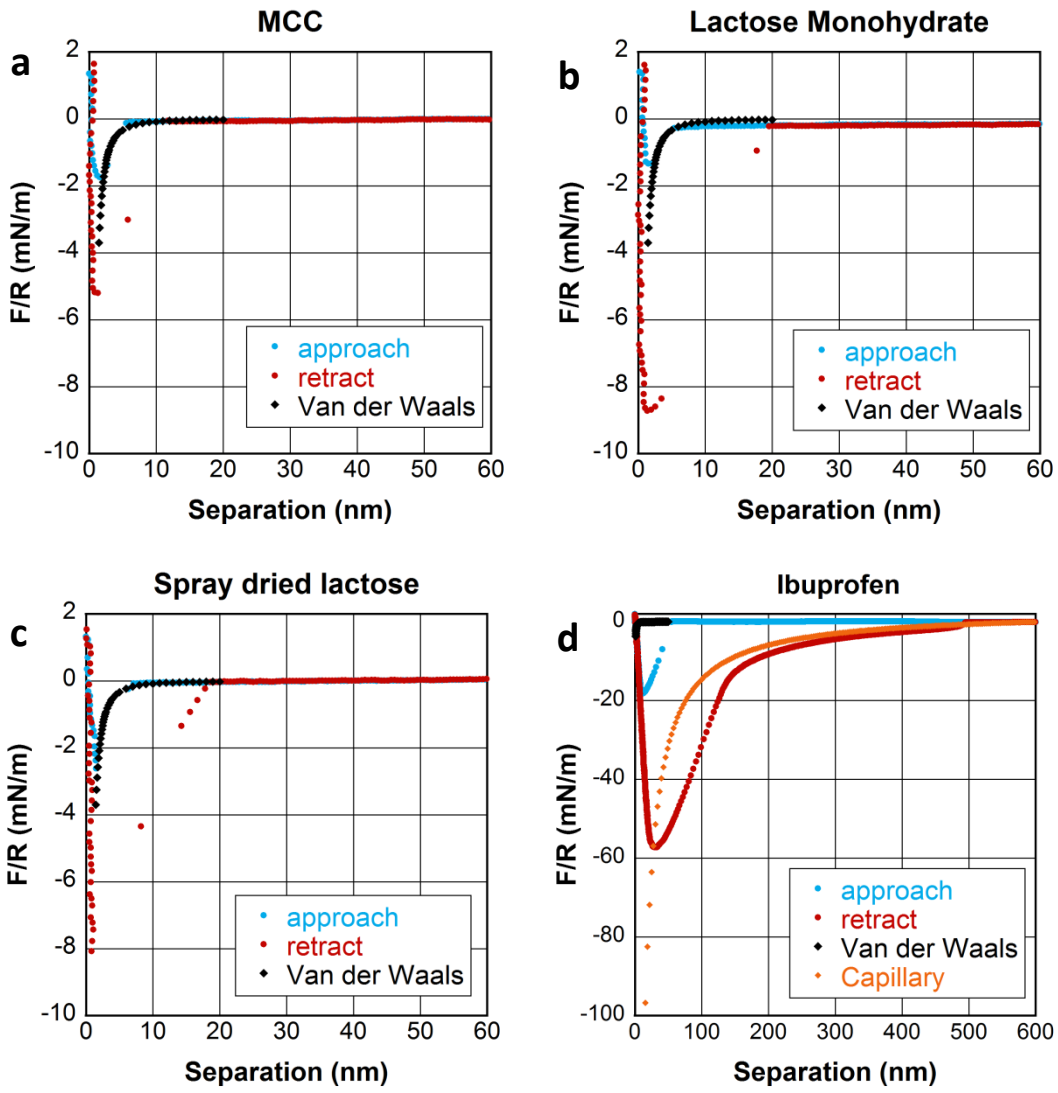

Figure 3. Representative examples of the type of force curves obtained with AFM colloidal probe for (a) MCC, (b) lactose monohydrate, (c) spray dried lactose and (d) Ibuprofen. Note that (d) Ibuprofen shows larger unit of magnitude than the other excipients. An example of the Van der Waals (black continuous line) and capillary (yellow continuous line) forces are represented in each of the graphs.

The adhesive, or pull-off force, F_{PO} arising from the Laplace pressure inside a condensate around the contact point of a spherical particle in contact with a surface of the same material is given by [35]:

$$F_{PO} = 4\pi R\,\gamma_{lv}\,\cos\theta \qquad \text{Eq. 1}$$

R is the effective radius of interaction (equal to the radius of the particle for smooth surfaces), γ_{lv} is the liquid-vapour surface tension and θ is the contact angle of the liquid on the material. (Note that these latter 2 parameters reflect the difference in the solid-liquid (γ_{SL}) and solid vapour (γ_{SV}) surface energies via the Young equation, and are not themselves explicitly important). Note also that there is an additional

adhesive term in contact and that (once again for a symmetrical system) this leads to a total adhesive force of [35]:

$$F_{PO} = 4\pi R\,(\gamma_l \cos\theta + \gamma_{sl}) = 4\pi R\,\gamma_{sv} \qquad \text{Eq. 2}$$

Where the final term is achieved via once again applying Youngs equation. The second term in the brackets reflects the work of adhesion between two solids immersed in a liquid (the condensate) once the surfaces separate and overcome the work of adhesion they are still bridged by the liquid condensate. This is clearly seen in figure 3d where there is an initial sharp separation with a damped "jump" (between approximately zero and 100 nm). The surfaces jump apart in the liquid due to a spring instability after the energy stored in the cantilever exceeds the adhesion. The jump is slow compared to a jump in air (indicated by the pint density in the linear region) due to the viscous resistance of the liquid which continues to bridge between the probe and the particle surface. For the case of a suspended capillary bridge (ie where the particles are not in physical contact) Equation 1 needs to be modified and is given by:

$$F_{PO} = \frac{4\pi R\,\gamma_{lv}\cos\theta}{(1+{}^{D}/_{d})} \qquad \text{Eq. 3}$$

Where *D* is the surface separation and *d* refers to the additional distance that the droplet projects onto the sphere[37] (see figure S1). Note that this equation assumes that the droplet is of constant volume. Biggs et al.[35] have earlier shown that this equation can be used to describe the force between two glass surfaces with a capillary condensate between them. Above about 100 nm when the spring instability has damped away it can be seen that the separation curve is quite well described by a fit to Equation 3. (Note that *d* depends on the initial condensate thickness which is unknown but can be estimated from the Kelvin equation to be of the order of 1 nm[16,33], and its variation with *D* has been crudely estimated by a linear relationship, which becomes zero at 600 nm, corresponding to the point where the droplet finally ruptures in figure 3d. Since the system is asymmetric the cosine of the contact angle is essentially a fitting parameter that describes the average surface properties). The adhesive and attractive forces on separation are thus consistent with a capillary condensate bridge.

A complete summary of the magnitude of adhesion between the steel probe and each of the evaluated particles for the different materials is therefore shown in figure 4. Average values of the adhesive minimum depth (AMD) are presented. The AMD is the lowest value measured at zero separation between the probe and the sample. The averaged values of the adhesion were obtained from each set of at least 25 force measurements performed sequentially on the same spot. The evaluated excipients (MCC, lactose monohydrate and spray dried lactose) display comparable adhesion values with similar variation. Figure 4 reinforces the snapshots of figure 3 and demonstrates that the adhesion measured for Ibuprofen is clearly

systematically much larger. The variation in adhesion of Ibuprofen particles is rather large though and occasionally values comparable to the excipients are observed. Broadly this indicates a higher affinity of the Ibuprofen to the steel surface which likely reflects sticky and adhesive behavior of the material during tableting. Since the large adhesion of the ibuprofen is consistent with a capillary bridge, it remains to explain why this is not observed on the excipients. It has earlier been shown that the capillary bridging depends strongly on the surface roughness and the relative humidity[16,33]. As mentioned above when the Kelvin radius exceeds the local roughness then the capillary condensate can flood the contact zone (see figure S3) leading to a dramatically increased adhesion[16,33]. Thus the reason for the large capillary adhesion displayed by ibuprofen lies not in its surface chemistry, but in its smoothness. The fact that it is softer also means that asperities can locally be compressed (both elastically and plastically) which also makes it easier to flood the contact. The excipients while more hydrophilic, are rougher and more rigid, so any capillary condensation will be confined to asperity contacts and the adhesion will be low. (The Laplace pressure which is responsible for capillary adhesion is also much smaller for asperity contacts, see arguments in supporting information) Thus the difference between the excipients and ibuprofen is simply explained by the presence or absence of full flooding of the contact zone (see fig. S3).

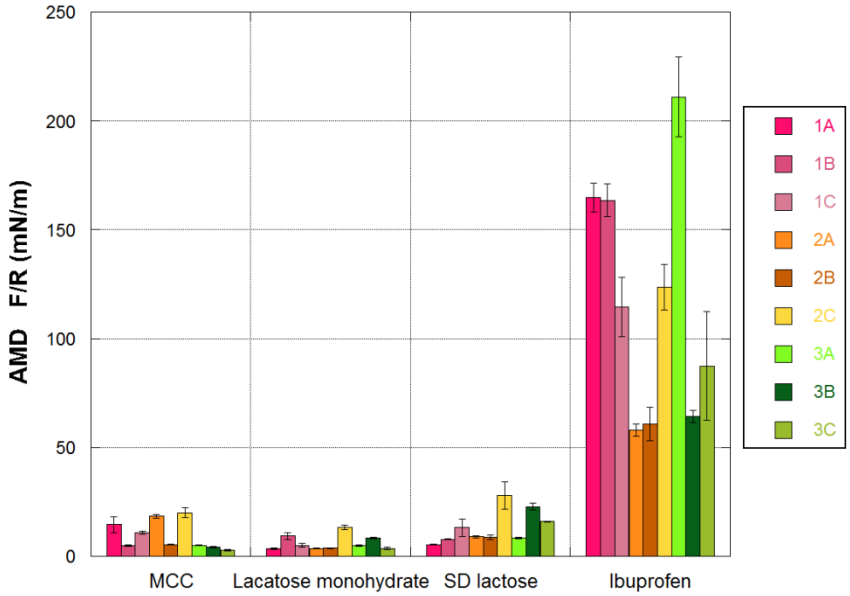

Figure 4. Average of the adhesive minimum depth (AMD) measured with AFM colloidal probe at three different spots (A, B, C) on three particles (1, 2, 3) for each of the evaluated samples.

A remarkable behavior was observed for the consecutive force-distance curve series of the Ibuprofen-steel interaction. This is shown in figure 5 with an example of one of the sets of force curves collected sequentially in one of the spots. The observation is related to an increase of the jump-in distance and the corresponding attractive forces for the inward curve, between the steel and the particle surface with increasing number of contacts. An increase of both the AMD and separation distance for the outward

curve over time is also detected. The same trend was observed for 70% of the force measurements performed on Ibuprofen. Increasing the number of contacts leads to a systematic increase of the adhesion, and thus more work is required to separate the surfaces.

There are essentially three possible explanations for a general observation of this type. Firstly, the surfaces may be systematically flattened into improved conformability with repeated contact leading to more parallel surfaces with higher real area of contact. Such a mechanism cannot be entirely ruled out though there is no evidence for deformation in the constant compliance regions of the curves which should change systematically as deformation occurs[25]. Secondly, contact electrification might occur. The higher the charge difference, the larger is the attractive force between the surfaces on both approach and separation. A repeated contact gives the opportunity for charged materials to generate a larger effective charge[38,39]. This behavior is entirely consistent with the post jump portions of the outward curves, but although the attractive contribution on approach increases with no. of contacts, there is no suggestion of a Coulombic force-distance dependence so once again we rule this out. Thirdly, it has earlier been observed that repeated contact and or sliding between surfaces can lead to "harvesting"[16,33] of moisture due to the fact that condensation kinetics are generally fast compared to evaporation[40]. As discussed above, the relative smoothness and softness of ibuprofen is consistent with such behaviour. The forces measured on approach, which preclude and electrostatic explanation, are highly consistent with a capillary condensate which remains on the surface(s) after separation and which grows with each contact. The approach is characterized by an abrupt jump-in which is much longer than the Lifshitz interaction characteristic of the excipients. As the surfaces approach the droplets(s) will deform towards one another due to Lifshitz interactions, but the AFM cantilever will not register this. Once the droplets meet each other or the opposing surface a capillary neck is formed leading to a large attractive force resulting from equation from equation 3. The gradient of this force is with distance is large compared to the cantilever spring constant so an instability occurs and the surfaces jump together from a distance determined by the size of the residual drop(s).

There are thus four separate aspects of the ibuprofen force curves that are consistent with capillary condensation effects. I) the arrested jump out, II) The long-range attractive behaviour upon separation, III) the abrupt jump in from longer separations, IV) the systematic increase in attraction and adhesion with increasing number of contacts. This is already rather irrefutable evidence for this mechanism. As a fifth supporting argument we refer to the reader to supporting information where we show frictional forces between the materials. In friction measurements the surfaces are never separated but slid continuously and harvesting effects are thus even more important[16,33]. There is evidence in the raw data for apparent negative friction coefficients, which is a clear indicator of harvesting. Briefly, the friction coefficient is the proportionality constant between friction force and load. When measuring friction with the AFM the

capillary adhesion acts as an additional load. As the *applied* load is decreased during sliding, the continuous growth of a condensate leads to a simultaneous *increase* in the *true* load, which leads to an apparently negative gradient. The friction loops in figures S4-7 show evidence of such behaviour. Note that in tableting the punch makes repeated contact with powder, but only once for each tablet. Since the steel surface is higher energy, any liquid resulting from capillary bridges is likely to remain on the steel surface. Conceivably this liquid can build up and lead to sticking. Alternatively the large adhesion towards ibuprofen can lead to attachment of ibuprofen on the steel. In general one would expect such attached material to be re-stamped into the subsequent tablet and thus removed. However for punches with embossed designs for marking the tablets, it has been shown that the local pressure is much lower adjacent to regions of height difference on the punch. Thus the probability of material stuck to the punch remaining there, or picking up more particles (due to both adhesion and moisture effects) is much larger.

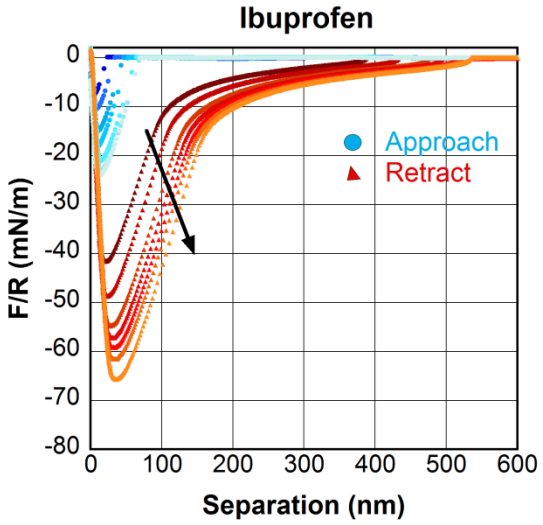

Figure 5. Several force-separation curves of Ibuprofen measured for particle 2 at spot A. The 2nd, 5th, 8th, 10th, 13th, 16th and 20th are represented out of the set of 22 curves collected at the same spot.

A summary of the adhesion dependence on repeated contacts for all the measurements on each of the materials is shown in figure 6. As a first approximation the adhesion is assumed to be a linear function of the number of contacts. The slope of each solid line is the average value of the slopes of the linear fit to each set of force measurements performed on different particles and spots on each of the materials (see supporting information). The data in figure 5 for example would provide one value, as would each of the columns represented in Figure 4. A positive gradient thus indicates that the data is consistent with a systematic increase with number of contacts, whereas a flat line would imply no dependence on number of contacts. The intercept of the linear equation is also calculated as an average of those obtained from each such "local" linear fit. The dotted lines represent the standard deviations of the gradients and intercepts and thus provide a "probability wedge". The figure demonstrates that the systematic increase with contact seen in figure 5 is in fact a general feature of all the data sets at different points on ibuprofen (while

demonstrating that the slope and absolute values do vary from point to point). In contrast, a constant adhesion over the repeated contacts is measured on MCC and lactose monohydrate indicating that there is no systemic variation. In fact a slightly decreasing linear trend is observed for spray dried lactose, but inspection shows that the probability wedge is bounded by positive and negative gradients so this is deemed not significant.

Once again, the behavior observed for an increased number of contacts over time for Ibuprofen, may well be related to tableting sticking events since this is generally observed after a large number of compaction impacts. Moisture buildup on the steel material over time could help to attract fines from the powder. This could contribute to the build-up of a particle layer on the surface of the tableting tool promoting further material to stick[1]. The different behavior over time detected between the excipients and Ibuprofen shows a clear distinction between the behaviour of sticky and non-sticky tableting components. Therefore AFM colloidal probe measurements can be useful in predicting the magnitude of adhesion between particles and tools, as well as providing mechanistic information as to the possible origin of stickiness.

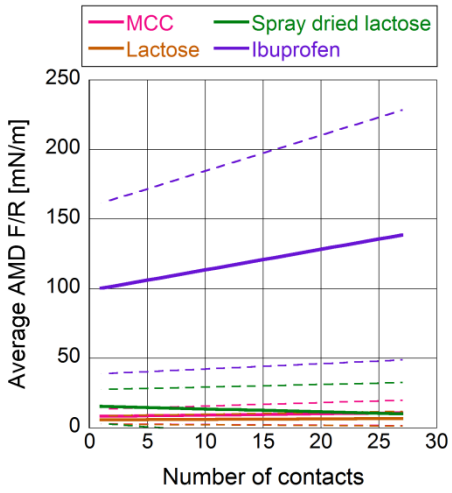

Figure 6. Relative evolution of the adhesion force for each sample as function of the increasing number of contacts performed on the same spot continuously.

In order to rule out the possibility of contamination, the probes were imaged with SEM (figure 7) after force measurement. The colloid probe used to generate the presented results is shown in figure 7a. Imaging of the probe was done after completion of all the measurements and it appeared free of any type of material residue. Material transfer after measurement on Ibuprofen is clearly observed in figure 7b for one of the steel probes used during the control experiments. The SEM image was taken after completion of the force measurements on Ibuprofen. Note that the particles are not at the contact point (12 degree tilt of cantilever) but surround it, and in some cases are rather distant. This suggests that the large adhesion detected between Ibuprofen and steel could possibly lead to material pick up and transport on a water film.

Alternatively the water formation may lead to trace amount of ibuprofen being dissolved and then it recrystallizes on evaporation. Note that the size of the crystals is much smaller than observed in SEM, which may support this latter mechanism. Translated into the tableting running cycle this could also lead to the evolution of a particulate layer over the surface of the punch which could be responsible for sticking and picking problems over time.

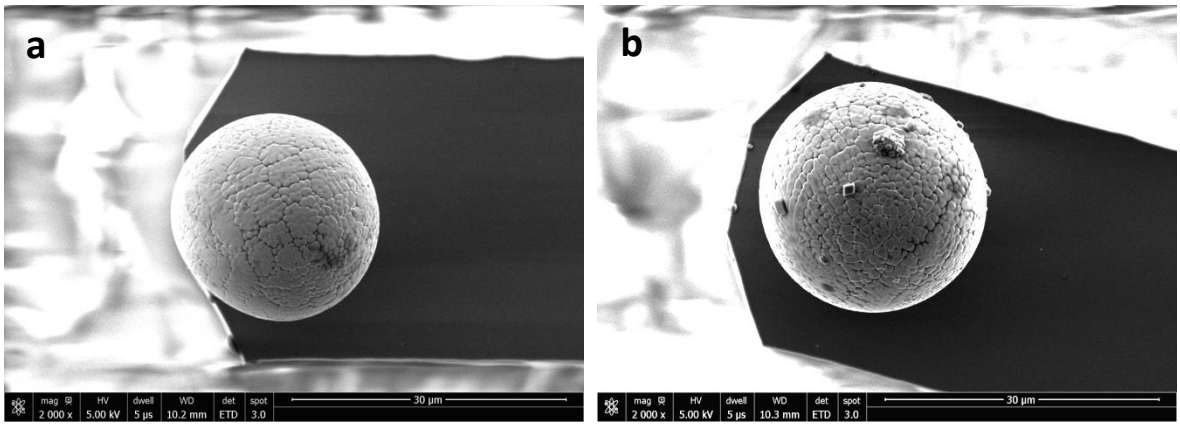

Figure 7. SEM images of (a) clean probe after measurements and (b) contaminated probe after measurements showing the possible material transfer when measuring on Ibuprofen.

4. Conclusion

The use of a steel colloid probe interacting with various tableting components allows a mechanistic description of, as well as a quantitative measurement of, particle adhesion to steel. The rather hydrophilic but rough and rigid excipients display fairly constant and rather low adhesion. The interactions are suggestive of a predominantly Lifshitz type interaction with the possibility of local asperity condensate formation. Ibuprofen on the other hand, which is known to be "sticky" in terms of causing problems with the tableting process displays a completely different adhesion behaviour. Firstly the magnitude is systematically considerably larger. This large adhesion appears to be consistent with a capillary condensation behaviour and there are no less than 5 separate indicators implicating this mechanism. This phenomenon appears to increase in magnitude with number of contacts, consistent with a harvesting mechanism. This is related to the fact that condensation is rapid but evaporation is very slow so each contact allows the capillary droplet to be "topped up". In a tableting machine the steel punch makes only a single impact with any given tablet, but since the steel is the higher energy surface the condensate is likely to prefer to remain on the steel surface.

The observation of "levitated" particles onto the steel probe and removed from the contact zone further implicates the potential hazards for sticking and it may be that fine particles stick to and are transported on the residual moisture. Alternatively there may be dissolution and recrystallization possible – this could

particularly arise as the punch heated up with time and moisture tended to evaporate. Embossing on the punches, where there are regions of low contact pressure are likely to be particularly susceptible areas for this moisture collection and associated particle adhesion.

Finally, the ability to clearly distinguish between the adhesions mechanisms and to have a physical description of the picking propensity will allow strategies to be developed to combat this unwelcome phenomenon.

References

1. Paul S, Taylor LJ, Murphy B, Krzyzaniak J, Dawson N, Mullarney MP, Meenan P, Sun CC 2016. Mechanism and Kinetics of Punch Sticking of Pharmaceuticals. Journal of Pharmaceutical Sciences.
2. Sabir A, Evans B, Jain S 2001. Formulation and process optimization to eliminate picking from market image tablets. International Journal of Pharmaceutics 215(1–2):123-135.
3. Neilly J, Vogt A, Dziki W. 2009. Characterization of Sticking Residue on Tablet Punch Faces by Scanning Electron Microscopy and X-Ray Mapping. Microsc Microanal, ed. p 18-19.
4. Badal Tejedor M, Nordgren N, Schuleit M, Rutland MW, Millqvist-Fureby A 2015. Tablet mechanics depend on nano and micro scale adhesion, lubrication and structure. International Journal of Pharmaceutics 486(1–2):315-323.
5. Aoki S, Danjo K 1998. Effect of tableting conditions on the sticking of tablet using ibuprofen. Yakugaku zasshi : Journal of the Pharmaceutical Society of Japan 118(11):511.
6. Kakimi K, Niwa T, Danjo K 2010. Influence of compression pressure and velocity on tablet sticking. Chemical & pharmaceutical bulletin 58(12):1565.
7. Bunker M, Zhang J, Blanchard R, Roberts CJ 2011. Characterising the surface adhesive behavior of tablet tooling components by atomic force microscopy. Drug development and industrial pharmacy 37(8):875-885.
8. Reed K, Davies C, Kelly K 2015. Tablet sticking: Using a 'compression toolbox' to assess multiple tooling coatings options. Powder Technology 285:103-109.
9. Mollereau G, Mazel V, Busignies V, Tchoreloff P, Mouveaux F, Rivière P 2013. Image Analysis Quantification of Sticking and Picking Events of Pharmaceutical Powders Compressed on a Rotary Tablet Press Simulator. Pharm Res 30(9):2303-2314.
10. McDermott TS, Farrenkopf J, Hlinak A, Neilly JP, Sauer D 2011. A material sparing method for quantitatively measuring tablet sticking. Powder Technology 212(1):240-252.
11. Etzler FM, Uddin MN 2013. Powder Technology and Pharmaceutical Development: Particle Size and Particle Adhesion. KONA Powder and Particle Journal 30(0):125-143.
12. Chow EHH, Buar D-k, Jones W 2012. New opportunities in crystal engineering the role of atomic force microscopy in studies of molecular crystals. Chemical Communications 48(74):9210-9226.
13. Ducker WA, Senden TJ, Pashley RM 1991. Direct measurement of colloidal forces using an atomic force microscope. Nature 353(6341):239.
14. Erath J, Schmidt S, Fery A 2010. Characterization of adhesion phenomena and contact of surfaces by soft colloidal probe AFM. Soft Matter 6(7):1432-1437.
15. Young PM, Price R, Tobyn MJ, Buttrum M, Dey F 2004. The Influence of Relative Humidity on the Cohesion Properties of Micronized Drugs Used in Inhalation Therapy. Journal of Pharmaceutical Sciences 93(3):753-761.
16. Feiler A, Jenkins P, Rutland M 2005. Effect of relative humidity on adhesion and frictional properties of micro- and nano-scopic contacts. Journal of Adhesion Science and Technology 19(3):165-179.
17. Claesson PM, Rutland MW. 2002. Measuring interactions between surfaces. ed. p 383-414.
18. Rutland MW, Carambassis A, Willing GA, Neuman RD 1997. Surface force measurements between cellulose surfaces using scanning probe microscopy. Colloids and Surfaces A: Physicochemical and Engineering Aspects 123:369-374.
19. Nordgren N, Rutland MW 2009. Tunable nanolubrication between dual-responsive polyionic grafts. Nano letters 9(8):2984.
20. Nordgren N, Carlsson L, Blomberg H, Carlmark A, Malmström E, Rutland MW 2013. Nanobiocomposite adhesion: role of graft length and temperature in a hybrid biomimetic approach. Biomacromolecules 14(4):1003.
21. Rathje L-SZ, Nordgren N, Pettersson T, Rönnlund D, Widengren J, Aspenström P, Gad AKB 2014. Oncogenes induce a vimentin filament collapse mediated by HDAC6 that is linked to cell stiffness. Proceedings of the National Academy of Sciences of the United States of America 111(4):1515.

22. Ralston J, Larson I, Rutland MW, Feiler AA, Kleijn M 2005. Atomic force microscopy and direct surface force measurements (IUPAC technical report). Pure and applied chemistry 77(12):2149-2170.
23. Sader JE, Chon JWM, Mulvaney P 1999. Calibration of rectangular atomic force microscope cantilevers. Review of Scientific Instruments 70(10):3967-3969.
24. Pettersson T, Nordgren N, Rutland MW, Feiler A 2007. Comparison of different methods to calibrate torsional spring constant and photodetector for atomic force microscopy friction measurements in air and liquid. The Review of scientific instruments 78(9):093702.
25. Rutland MW, Tyrrell JWG, Attard P 2004. Analysis of atomic force microscopy data for deformable materials. Journal of Adhesion Science and Technology 18(10):1199-1215.
26. Derjaguin B 1934. Untersuchungen über die Reibung und Adhäsion, IV. Kolloid-Zeitschrift 69(2):155-164.
27. Mousa Al-Ibraheemi Z, Anuar M, Taip F, Amin M, Tahir S, Mahdi A 2013. Deformation and Mechanical Characteristics of Compacted Binary Mixtures of Plastic (Microcrystalline Cellulose), Elastic (Sodium Starch Glycolate), and Brittle (Lactose Monohydrate) Pharmaceutical Excipients. Particulate Science and Technology 31(6):561.
28. Rasenack N, Müller BW 2002. Ibuprofen crystals with optimized properties. International Journal of Pharmaceutics 245(1):9-24.
29. Sharmistha D, David JWG 2004. Crystal structures of drugs: advances in determination, prediction and engineering. Nature Reviews Drug Discovery 3(1):42.
30. Mizuno H, Luengo GS, Rutland MW 2010. Interactions between Crossed Hair Fibers at the Nanoscale. Langmuir 26(24):18909-18915.
31. Kulvanich P, Stewart P 1988. Influence of relative humidity on the adhesive properties of a model interactive system. Journal of pharmacy and pharmacology 40(7):453-458.
32. Podczeck F, Newton JM, James MB 1997. Influence of Relative Humidity of Storage Air on the Adhesion and Autoadhesion of Micronized Particles to Particulate and Compacted Powder Surfaces. Journal of Colloid and Interface Science 187(2):484-491.
33. Feiler AA, Stiernstedt J, Theander K, Jenkins P, Rutland MW 2007. Effect of capillary condensation on friction force and adhesion. Langmuir : the ACS journal of surfaces and colloids 23(2):517.
34. Rabinovich YI, Adler JJ, Esayanur MS, Ata A, Singh RK, Moudgil BM 2002. Capillary forces between surfaces with nanoscale roughness. Advances in Colloid and Interface Science 96(1):213-230.
35. Biggs S, Cain RG, Dagastine RR, Page NW 2002. Direct measurements of the adhesion between a glass particle and a glass surface in a humid atmosphere. Journal of Adhesion Science and Technology 16(7):869-885.
36. Evans DF. 1999. The colloidal domain : where physics, chemistry, biology, and technology meet. 2. ed.. ed., New York: New York : Wiley-VCH.
37. Israelachvili JN. 2010. Intermolecular and Surface Forces. 3rd ed.. ed., Burlington: Burlington : Elsevier Science.
38. Eve JK, Patel N, Luk SY, Ebbens SJ, Roberts CJ 2002. A study of single drug particle adhesion interactions using atomic force microscopy. International Journal of Pharmaceutics 238(1):17-27.
39. Bunker M, Davies M, James M, Roberts C 2007. Direct Observation of Single Particle Electrostatic Charging by Atomic Force Microscopy. Pharm Res 24(6):1165-1169.
40. Carpick RW 1996. Variation of the interfacial shear strength and adhesion of a nanometer-sized contact. Langmuir 12(13):3334-3340.

AFM colloidal probe measurements to mimic punch-particle surface interactions during tableting

Maria Badal Tejedor[a,b], Niklas Nordgren[a], Michael Schuleit[c], Anna Millqvist-Fureby[a], Mark W. Rutland[a,b]*.

[a]SP Technical Research Institute of Sweden, SP Chemistry, Materials and Surfaces, Box 5607, SE-114 86 Stockholm, Sweden
[b]KTH Royal Institute of Technology, Division of Surface and Corrosion Science, Drottning Kristinas väg 51, SE-100 44 Stockholm, Sweden
mark@kth.se; Mobile: +46768640081
[c]Novartis Pharma AG, Novartis Institutes for Biomedical Research, GDC, Novartis Campus, 4002 Basel, Switzerland

SUPPORTING INFORMATION

Extension of the classical capillary condensate adhesion theory to small particles.*

The classical equation for capillary condensation is given by Eq. 1 in article and describes the adhesion in the following geometry.

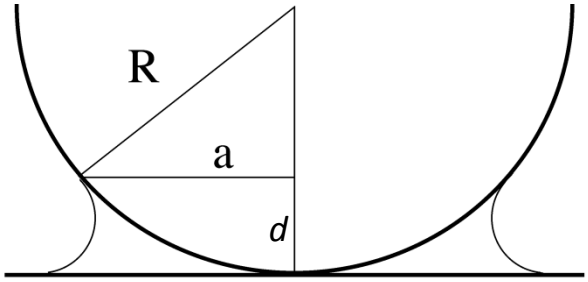

Figure S1. Capillary condensation geometry

We point out here that there are two assumptions made in the simple derivation, which render this equation less appropriate for small particles or to describe the contribution from asperity contacts. The first is that as R is reduced, the tangents of the spherical meniscus described by the Kelvin radius do not meet the two surfaces diametrically and thus the height, *d*, of the line labelled *a* is not in fact $2r_K$. The second is that the expression for the Laplace pressure used to derive equation 1 ignores the second radius of the condensate, *a*, (which has opposite sign) since *a* is considered to be generally much larger than r_K. (true for smooth surfaces with R> μm) For a Kelvin radius of 2 nm and a particle or asperity of radius 10 nm, *a* is equal to 6.3 nm, so this contribution cannot be ignored. Thus the Laplace pressure term is

$$P = \gamma \cdot \left(\frac{1}{r_K} + \frac{1}{a}\right) \qquad \text{Eq. 2}$$

Where a and r_K have opposite signs. It can simply be shown that

$$a = 2\sqrt{(R.r_K)}$$

For the case mentioned above, the capillary adhesion will be 1.8 times smaller than that where the classical equation is used. The other correction will also lead to a lower adhesion than predicted by equation 1.

Figure S2 shows how a correction factor to equation 1 looks for various values of the particle radius and as a function of the capillary radius. As a guide the Kelvin radius of a spherical drop is 10 nm at p/po = 0,9, 1.6 nm at p/po = 0,5 and 0,5 nm at p/po = 0,1.

Note that a corollary of this argument is that a nanoparticle, or a single asperity contact of low radius will NOT follow the classical equation 1 but in fact the adhesion should decrease with increasing humidity! If a sharp AFM tip were considered as a single asperity contact then the adhesion should in fact also DECREASE with increasing relative humidity.

As far as we are aware, this is the first time this correction has been made.

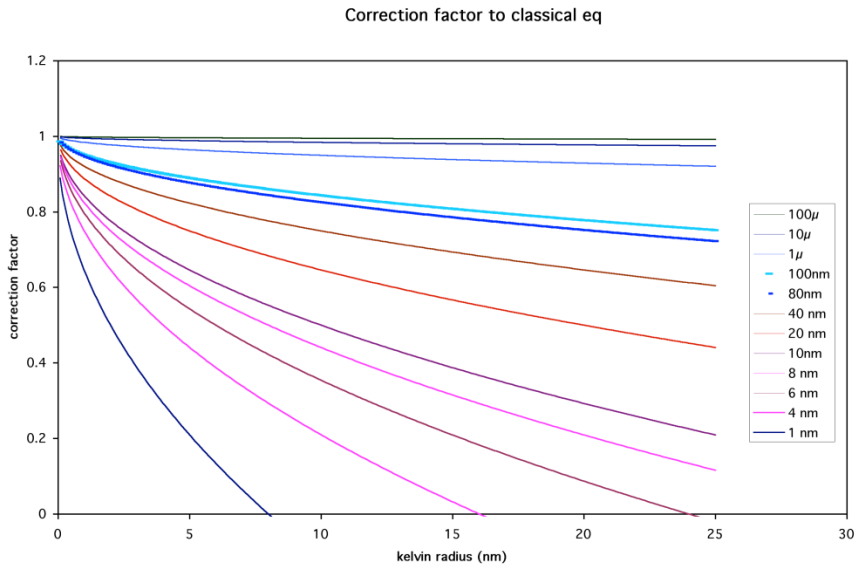

Figure S2. Correction factor taking into account the reduction in capillary condensate due to decreasing Laplace pressure with decreasing interaction radius.

This result may explain the previously apparently anomalous results in the literature where tip-surface adhesion is occasionally observed to decrease with increasing humidity, the reverse of what is generally observed.

Figure S3 indicates the difference in the nature of the capillary condensate depending on flooding or otherwise. r_K is the Kelvin radius.

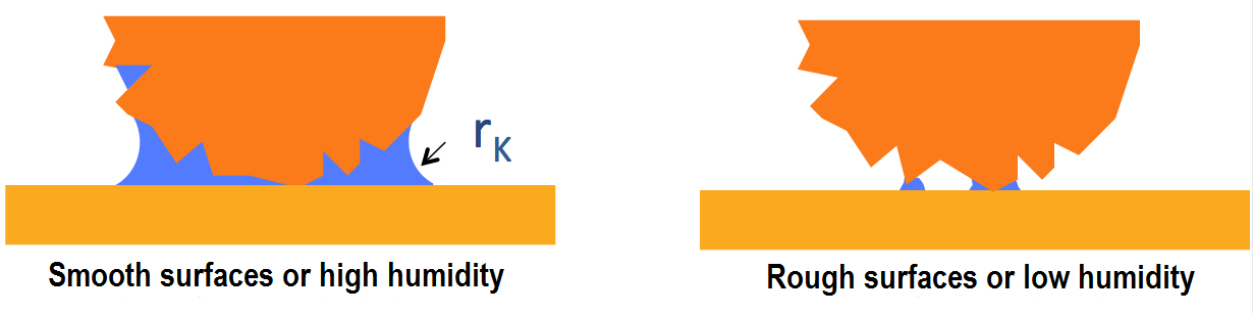

Figure S3. Capillary condensate depending on the flooding.

Friction loops

When the steel surface is brought into contact with the excipient or ibuprofen, it is possible to measure friction forces as a function of load and extract a friction coefficient. In the absence of a fully flooded capillary condensate generally a linear relation is observed according to Amontons law and the behaviour is reproducible on loading and unloading. An example of this behaviour is seen in Figure S4 for MCC against a steel tip.

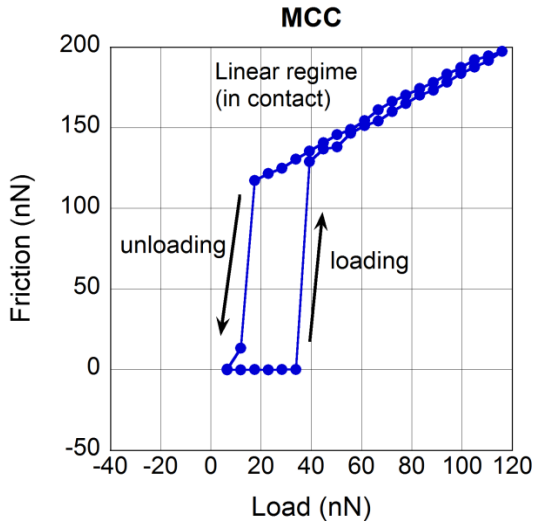

Figure S4. Friction load relationship MCC-steel. No capillary condensate evidence. Linear, anhysteretic friction-load relationship.

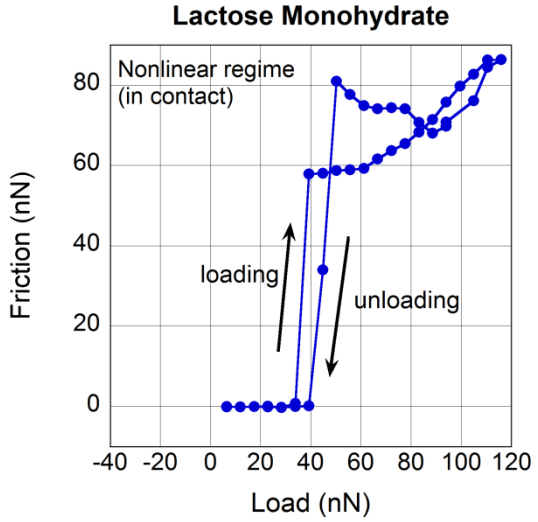

Figure S5. Lactose –steel friction data. The contact regime is non linear due to a gradual increase in adhesion contributing to the effective load as a result of harvesting at asperity contacts. When the sliding direction is reversed the harvesting continues and the adhesion increases faster than the load is decreased leading to apparent negative friction coefficients.

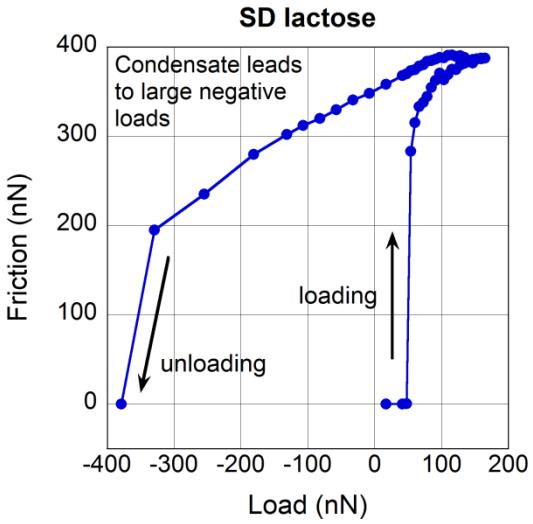

Figure S6. Spray dried lactose against steel. In this example the capillary becomes more established (closer to a flooded state) due to harvesting. The friction forces become very large due to the large extra load that builds up due to capillary adhesion. This means that upon unloading, large negative loads reflect the force required to break the condensate.

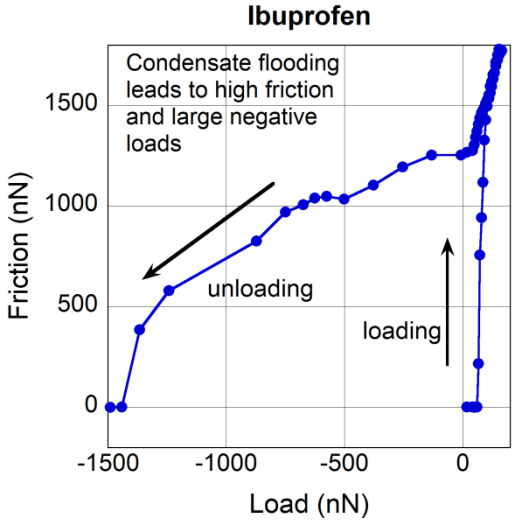

Figure S7. Ibuprofen –steel friction data. Basically as for Fig S6 but complete flooding of contact zone (Fig S3) leads to very high friction and negative loads.

Complete data of the AMD for the materials

The adhesive minimum depth (AMD) over the several contacts measured at each spot for all the evaluated areas at each sample are presented in figure S8. These four graphs are summarized in figure 6 each one represented by the average linear fit calculated from the six individual linear fits of each graph. The graphs are plotted at different scales to represent all the collected data.

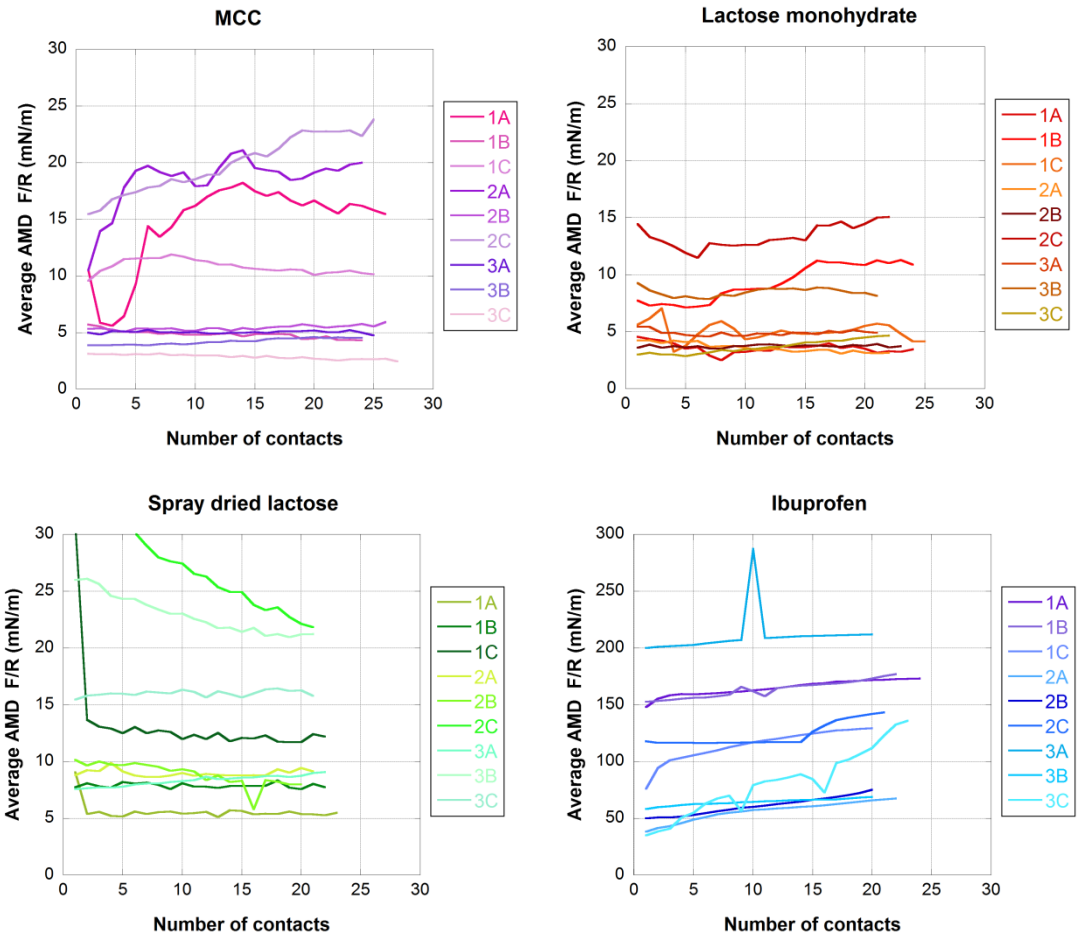

Figure S8. Evolution of the adhesion force after a continuous number of contacts for each of the evaluated contact points of each sample.

Control measurements on mica

In one occasion anomalies were detected in the reproducibility of the control force measurements on mica performed in between force measurement on Ibuprofen. This deviation of the typical force shape detected on mica, was related to material transfer to the probe. The probe was then moved laterally side to side several times on the mica surface to wipe off the possible attached material. The shape of the following force curve collected on mica was then comparable to the previous ones collected with the freshly mounted probe.

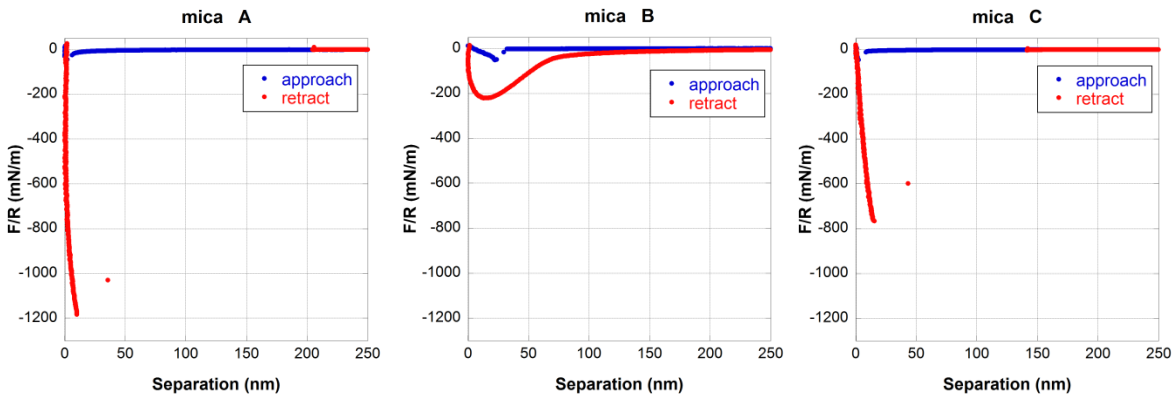

Figure S9. AFM force curves on mica (a) before measurement on Ibuprofen, (b) after measurement, (c) after lateral movement of the probe.

Ibuprofen force curve

The representative force curve for Ibuprofen is shown in figure 3d in the paper. Figure S10 shows the same force curve including the fitting for a coulombic force.

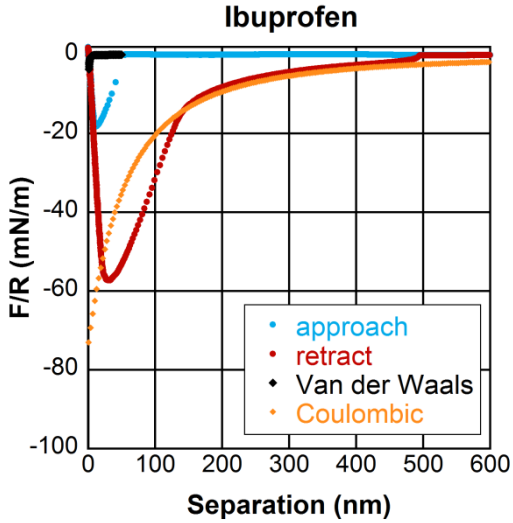

Figure S10. Representative example of the type of force curve obtained with AFM colloidal probe for Ibuprofen. An example of the Van der Waals (black continuous line) and coulombic (orange continuous line) forces are represented in the graph.

* Calculations performed by Rutland 2002.